Bucknell University
Bucknell Digital Commons

Master's Theses | Student Theses

2010

Solid-State Compatibilization of Immiscible Polymer Blends: Cryogenic Milling and Solid-State Shear Pulverization

Marc Frederick Henry
Bucknell University

Follow this and additional works at: https://digitalcommons.bucknell.edu/masters_theses

Part of the Chemical Engineering Commons

Recommended Citation
Henry, Marc Frederick, "Solid-State Compatibilization of Immiscible Polymer Blends: Cryogenic Milling and Solid-State Shear Pulverization" (2010). *Master's Theses*. 9.
https://digitalcommons.bucknell.edu/masters_theses/9

This Masters Thesis is brought to you for free and open access by the Student Theses at Bucknell Digital Commons. It has been accepted for inclusion in Master's Theses by an authorized administrator of Bucknell Digital Commons. For more information, please contact dcadmin@bucknell.edu.

SOLID-STATE COMPATIBILIZATION OF IMMISCIBLE POLYMER BLENDS: CRYOGENIC MILLING AND SOLID-STATE SHEAR PULVERIZATION

by

Marc Frederick Henry

A Thesis
Presented to the Faculty of
Bucknell University
In Partial Fulfillment of the Requirements for the Degree of
Master of Science in Chemical Engineering

Approved:

K. Wakabayashi

Katsuyuki Wakabayashi, PhD
Adviser

Timothy Raymond, PhD
Department Chairperson

Brandon Vogel, PhD
Committee Member

Michael Malusis, PhD
Committee Member

Date: May 2010

I, Marc Henry, permit my thesis to be copied.

Acknowledgements

First and foremost I would like to thank my advisor, Dr. Kat Wakabayashi, for the support, guidance, and professionalism which brought this research and I to where they are now. Despite the momentary desires for bloodshed when receiving new draft corrections, I feel honored to be part of Dr. Wakabayashi's life through considerable changes over the past two years. Monumental events occurred, including the graduation of his first Masters student, five energetic research groups, the first ChemE Cup, his marriage, and above all the rest, the oft-delayed installation and subsequent repair of the Bucknell University Solid-State Shear Pulverizer. And of course, thanks are also certainly due for the proper elucidation of the uses of each form of dash in the English language including the hyphen (-), figure dash (−), EN dash (–), EM dash (—), and horizontal bar (―) — I will use them forthwith in the most fundamentally facile fashions functionally feasible. Jokes aside, I truly appreciate the great lengths of time and effort Dr. Wakabayashi contributed to my work and personal development.

Another great deal of thanks is owed to Dr. Brandon Vogel, who, in addition to being an influential member of my committee, acted as a stand-in advisor during any periods of Kat's absence. I am very grateful of the time you spent with me in your lab and in heated discussions over models, statistics, and MATLAB.

I am very appreciative of the important questions and concerns asked of me by my third committee member, Dr. Michael Malusis. I must thank Diane Hall for always providing me with any material or equipment I needed and always being concerned for my safety and well-being. Thanks to my psychologist/stand-in mom Nancy Lamay for the oft-needed talks and assistance.

Finally, I must acknowledge and thank my friends and family who have supported me throughout my time at Bucknell and especially during this research: the other graduate students Joel Russell, Andrew Litzenberger, Renee Perry, Dave Marchese, Jeweliet Yost, and Jeffrey Stein for the company in the office over the late nights, Adrienne for always being there but also letting me go to the lab when needed, and last but certainly not least my parents and sisters, Fred, Joyce, Lauren, and Andi, for the unwavering support and constant encouragement.

"Piled Higher and Deeper" by Jorge Cham – Reproduced with Permission

Table of Contents

Acknowledgements ii
Table of Contents iv
List of Tables vii
List of Figures viii
List of Abbreviations x
Abstract xii
1. Introduction 1
2. Background 6
2.1 Polymer Blend Theory 6
2.1.1 Miscible Polymer Blends 9
2.1.2 Partially Miscible Polymer Blends 9
2.1.3 Immiscible Polymer Blends 10
2.1.4 Compatibilization of Immiscible Blends 11
2.1.5 Definition and Determination of Compatibilization 11
2.1.6 Functionalized Monomer and Discrete Species Compatibilization 14
2.1.7 Block Copolymer Compatibilization 15
2.2 Solid-State Polymer Processing 18
2.2.1 Mechanochemistry of Solids 18
2.2.2 Solid-State Batch Milling Methods 20
2.2.3 Solid-State Shear Pulverization 24
3. Materials and Methods 27
3.1 Materials 27
3.1.1 Polystyrene 27
3.1.2 High-Density Polyethylene 27
3.1.3 Pyrene-Labeled Poly(Methyl Methacrylate) 27
3.2 Sample Preparation 34
3.2.1 Processing 34
3.2.2 Post-Processing 41
3.3 Sample Analysis 44
3.3.1 Scanning Electron Microscopy 44
3.3.2 Gel Permeation Chromatography 48
3.3.3 Differential Scanning Calorimetry 49

3.3.4 Thermogravimetric Analysis 50
3.3.5 Tensile Testing 50
3.3.6 Dynamic Mechanical Analysis 52
4. Solid-State Polymer Blending via Cryogenic Milling 53
4.1 Quantitative Detection of Block Copolymer Synthesis during Cryogenic Milling 53
4.1.1 Experimental Procedure 55
4.1.2 Results and Discussion 55
4.1.3 Summary 59
4.2 Effect of Cryogenic Milling on the Static Growth of Dispersed Domains 59
4.2.1 Experimental Procedure 61
4.2.2 Results and Discussion 61
4.2.3 Summary 73
4.3 Conclusions 75
5. Optimizing Solid-State Shear Pulverization: Effects of Screw Design and Operating Conditions 76
5.1 Full-Factorial Analysis of the Solid-State Shear Pulverizer Operation 76
5.2 Experiment Design 79
5.3 Statistical Analysis 81
5.4 SSSP Operation Considerations 87
5.5 Results and Discussion 88
5.5.1 D_n and Variance Analysis 88
5.5.2 Molecular Weight Analysis 97
5.5.3 Uncoupling Contributions to Factor A and Zone Temperature Analysis ... 99
5.5.4 Combined Results 101
5.6 Summary 102
6. Correlation of Domain Size Compatibilization to Physical Properties 104
6.1 Experimental Procedure 105
6.2 Blend Analysis and Discussion 106
6.2.1 Previous Results 106
6.2.2 Thermogravimetric Analysis 106
6.2.3 Differential Scanning Calorimetry 107
6.2.4 Tensile Mechanical Testing 110
6.2.5 Dynamic Mechanical Analysis 111

6.3 Summary 112
7. Conclusions and Recommendations 114
7.1 Major Conclusions 114
7.2 Recommendations for Future Work 117
8. References 119
Appendix A. Additional Figures 126
Appendix B. Software Design, Analysis, and Code 140
Appendix C. Standard Operation Manuals 177

List of Tables

Table 1. Chemicals utilized during pyMA synthesis and supplier information 28
Table 2. Maximum peak absorbance wavelengths for pyrene-containing compounds 33
Table 3. List of available screw elements and descriptions 38
Table 4. GPC data for cryomilled PS and the PS phase of PS/HDPE blends..... 66
Table 5. The initial growth constant of PD/HDPE blends 68
Table 6. Variance analysis of PS/HDPE (80/20 wt%) cryomilled blends 72
Table 7. High and low settings for the four experimental factors 79
Table 8. List of all sample run settings for full factorial experiment 80
Table 9. Variance analysis of blends fabricated via SSSP following anneal at 204ºC..... 92
Table 10. Values generated from applying the Crist growth model to the SSSP blends.. 96
Table 11. GPC molecular weight characterization of the PS phase of the SSSP blends.. 97
Table 12. Temperature analysis of SSSP Zone 4..... 100
Table 13. Compilation of all previous analysis results on the blends selected for further analysis using common techniques.. 106
Table 14. Results of thermogravimetric analysis of blends 107
Table 15. Relevant thermal phase transition values determined during DSC analysis.. 108
Table 16. Results from tensile testing sample materials using rubber clamps 111

List of Figures

Figure 1. Generic phase diagram for miscible polymers 7
Figure 2. Polymer chains from partially miscible blends 10
Figure 3. An immiscible, phase-separated polymer blend..... 11
Figure 4. Steric compatibilizers act as both anchors for stability and repulsive springs.. 12
Figure 5. Use of block copolymers in stabilizing the interface 16
Figure 6. Free radical creation via chain scission and subsequent reaction pathways 20
Figure 7. Regions of the Northwestern University Solid-State Shear Pulverizer..... 25
Figure 8. Chemical structure of pyrene (SigmaAldrich) 28
Figure 9. Esterification reaction to form pyMA 29
Figure 10. ^{1}H 400 MHz NMR spectrum of pyMA 31
Figure 11. Ultraviolet spectra of 1-methanol pyrene, pyMA, pyPMMA, and several pure polymers over active absorbance range of pyrene 33
Figure 12. Cryomill and supporting equipment..... 35
Figure 13. Diagram of cryomill vial design and magnetic driving..... 35
Figure 14. Bucknell University's Solid-State Shear Pulverizer/Twin Screw Extruder.... 37
Figure 15. Schematic of the SSSP/TSE zone configuration with six barrel zones..... 38
Figure 16. Brabender DS28-10 Pellet Feeder 40
Figure 17. Atlas Laboratory Mixing Molder 41
Figure 18. Molds for the Atlas LMM used in the course of study..... 42
Figure 19. Carver presses used for pressing polymer sheets 43
Figure 20. Example gold-coated SEM sample tray with orientation pattern..... 45
Figure 21. A typical SEM micrograph featuring a polymer blend 46
Figure 22. High-contrast mask of Figure 21 47
Figure 23. Mask from Figure 22 imported into Particle Size Analyzer software..... 47
Figure 24. Interface of the GPC-SEC Analysis program with loaded GPC data 49
Figure 25. The Tensile Test Analyzer program with data from HDPE. 51
Figure 26. GPC-UV absorbance response of pure polystyrene and pyPMMA 56
Figure 27. GPC-UV absorbance response of the PS/pyPMMA cryomilled blend compared to neat pyPMMA..... 56
Figure 28. Enlarged response of blends from Figure 27..... 57
Figure 29. UV absorbance response of neat pyPMMA compared to pyPMMA which was cryogenically milled for fifteen cycles.. 58

Figure 30. A typical SEM micrograph of a cryomilled PS/HDPE following post-processing. 62

Figure 31. Diagram showing how hole size cannot be an accurate approximation to dispersed phase diameter 63

Figure 32. Growth of the average dispersed phase diameter following melt mixing and sustained static anneal at 204ºC 65

Figure 33. Application of the Crist growth model to the cryomilled PS/HDPE blends ... 67

Figure 34. Example of the importance of characterizing the dispersed phase distribution with regards to compatibilization..... 70

Figure 35. Inclusion of histograms allow for rapid identification of domain size distribution and growth during annealing 71

Figure 36. The SSSP screws designed for the full 2^4 factorial experiment 82

Figure 37. A segmented Gaussian probability distribution with four quantiles 84

Figure 38. A random set of data on a standard normal quantile plot..... 85

Figure 39. A standard half-normal quantile plot of the data from Figure 38..... 86

Figure 40. Temperature profiles (in °F) of the five temperature-controlled SSSP barrel zones following the introduction of pellets..... 87

Figure 41. Growth of D_n for PS/HDPE blends fabricated via SSSP after anneal..... 90

Figure 42. Half-normal plots of the effect of the experimental factors on D_n 91

Figure 43. Half-normal quantile plots of the effects of the experimental factors on the variance factor..... 94

Figure 44. Application of the Crist growth model to the "+ - - -" blend with histogram data for each anneal point 95

Figure 45. Half-normal plot of the effect of the experimental factors on the static growth constant, K 97

Figure 46. Normal quantile plot of the effect of the experimental factors on the number averaged molecular weight of blends fabricated via SSSP..... 98

Figure 47. Normal quantile plot of the effect of the experimental factors on the weight averaged molecular weight of blends fabricated via SSSP..... 99

Figure 48. DSC traces for each blend with and without anneal..... 109

Figure 49. Measurement of blend strength via dynamic mechanical analysis with a temperature ramp of 5°C/min 112

List of Abbreviations

ABS – Acrylonitrile Butadiene Styrene

AIBN – 2,2'-Azobisisobutyronitrile

ASTM – American Society for Testing and Materials

BU – Bucknell University

CFM – Cubic Feet per Minute

CMA – Cryogenic Mechanical Alloying

CMC – Critical Micelle Concentration

DCM – Dichloromethane

DMA – Dynamic Mechanical Analysis

DSC – Differential Scanning Calorimetry

FT-IR – Fourier Transform – Infrared Spectroscopy

GPC – Gel Permeation Chromatography

HDPE – High-Density Polyethylene

HPB – Hydrogenated Polybutadiene

HPLC – High Performance Liquid Chromatography

LDPE – Low-Density Polyethylene

LLDPE – Linear Low-Density Polyethylene

LMM – (Atlas) Lab Melt Mixer

LS – Light Scattering

MW – Molecular Weight

NMR – Nuclear Magnetic Resonance

NU – Northwestern University

PA – Polyamide

PC – Polycarbonate

PDI – Polydispersity Index

PE – Polyethylene

PEP – Poly(ethylene-*alt*-propylene)

PET – Polyethylene Terephthalate

PI – Polyisoprene

PMMA – Poly(methyl methacrylate)

PP – Polypropylene

PS – Polystyrene

PPO – Poly(2,6-dimethylphenylene oxide)

PSA – Particle Size Analyzer

PSI – Pounds per Square Inch

PVDF – Poly(vinylideneflouride)

PVP – Poly(2-vinylpyridine)

RI – Refractive Index

RPM – Rotations Per Minute

SAN – Styrene-Acrylonitrile copolymer

SEC – Size Exclusion Chromatography

SEI – Secondary Electron Imaging

SEM – Scanning Electron Microscopy

SSSP – Solid-State Shear Pulverization

TGA – Thermogravimetric Analysis

THF – Tetrahydrofuran

TSE – Twin Screw Extrusion

TTA – Tensile Test Analyzer

UV – Ultraviolet

Abstract

The blending of common polymers allows for the rapid and facile synthesis of new materials with highly tunable properties at a fraction of the costs of new monomer development and synthesis. Most blends of polymers, however, are completely immiscible and separate into distinct phases with minimal phase interaction, severely degrading the performance of the material. Cross-phase interactions and property enhancement can be achieved with these blends through reactive processing or compatibilizer addition. A new class of blend compatibilization relies on the mechanochemical reactions between polymer chains via solid-state, high energy processing. Two contrasting mechanochemical processing techniques are explored in this thesis: cryogenic milling and solid-state shear pulverization (SSSP). Cryogenic milling is a batch process where a milling rod rapidly impacts the blend sample while submerged within a bath of liquid nitrogen. In contrast, SSSP is a continuous process where blend components are subjected to high shear and compressive forces while progressing down a chilled twin-screw barrel.

In the cryogenic milling study, through the application of a synthesized labeled polymer, in situ formation of copolymers was observed for the first time. The microstructures of polystyrene/high-density polyethylene (PS/HDPE) blends fabricated via cryomilling followed by intimate melt-state mixing and static annealing were found to be morphologically stable over time. PS/HDPE blends fabricated via SSSP also showed compatibilization by way of ideal blend morphology through growth mechanisms with slightly different behavior compared to the cryomilled blends. The new Bucknell University SSSP instrument was carefully analyzed and optimized to produce

compatibilized polymer blends through a full-factorial experiment. Finally, blends of varying levels of compatibilization were subjected to common material tests to determine alternative means of measuring and quantifying compatibilization

1. Introduction

Polymeric materials have been rapidly evolving since the 1930s, with recent research advances in the field of polymer blends. General Electric sparked the first commercial interest in polymer blend technology in the late 1960s with the production of a poly(phenylene oxide)/polystyrene blend (under the Noryl® trade name) that offered increased tensile and impact strength while also retarding flames.[1] Industry has since realized that polymer blends offer highly tunable material properties while minimizing costs traditionally associated with customized materials.[2] New blend systems allow for rapid product development and deployment, with only a few scale-up and commercialization complications needing to be addressed. Effective blending can also impart improvements in properties, such as gas permeability and diffusivity, chemical resistance, electrical conductivity, flame resistance, and processability.[3] These synergistic interactions and adjustable material properties make the application of polymer blends attractive to mainstream industry.[2] Contemporary commercial applications of polymeric blends include elastomeric blends for automotive tires, styrene-maleic anhydride/polycarbonate blends for power tool shells and automotive trim, and polyamide blends with acrylonitrile butadiene styrene or polyolefins used in high performance consumer goods such as sporting equipment and appliances.[2, 4] Meanwhile potential future applications include improved solar panels, lithium batteries, bio-compatible materials, and fuel cells.[2]

Despite the alluring material and cost improvements provided by polymer blends, the widespread application of the majority of blends are constrained due to thermodynamic and kinetic limitations. The synergistic properties observed in currently

exploited blends are not fully understood or poorly extrapolated, preventing accurate prediction of new blend performance. In addition, most polymer blends are fully immiscible, resulting in greatly reduced mechanical properties due to poor component interaction at the interfaces. Improving the performance of immiscible blends through additional processing or the inclusion of additives has been demonstrated and is termed blend compatibilization.

Previous compatibilization methods have included functionalized monomer inclusion, reactive extrusion, and melt-phase compatibilizing agent mixing, but these all have critical application limitations. Inclusion of functionalized monomers in the polymer chain can improve secondary interactions between chains, but can only be utilized when polymerizing new polymers in an industrial reactor. Melt-mixing of a compatibilizing agent into a blend is often limited by poor dispersion, high compatibilizer cost, and a thermodynamic tendency to leach over time, reducing blend performance.[5] Reactive extrusion compatibilization is restricted primarily to polyamide-based systems in conjunction with chemically-modified copolymers featuring maleic anhydride endgroups, which increase material costs.[6] Therefore, current research in polymer compatibilization has progressed into more novel processing techniques involving solid-state mechanics and mechanochemistry.

Mechanochemistry, a science pertaining on chemical reactions initiated by mechanical forces, has been utilized for intimate metallic blending for several decades, but is starting to find applications in polymer blend systems.[7, 8] High-energy mechanical forces cause chain scission and free radical generation in solid-state polymeric systems. These radicals are reported to disproportionate between differing homopolymers when

mechanically processed together to form blend-compatibilizing block copolymers. These copolymers are hypothesized to migrate to phase boundaries upon melt-state processing and stabilize the system through steric hinderances and reductions in interfacial tension.[2] While this mechanism has been documented in some solid-state processing systems,[9] it has not been confirmed for all. Cryogenic milling (cryomilling) embrittles polymers through submersion in liquid nitrogen and causes chain scission through repeated mechanical impacts.[10, 11] Another novel technology, solid-state shear pulverization (SSSP), cools polymers while subjecting them to extreme shear forces in an industrially-scalable, twin-screw process.[12]

In this thesis, the two representative solid-state processing methods are further investigated from a fundamental mechanochemistry standpoint, with systematic experimental design and processing-structure-property correlations. Immiscible blends fabricated via cryogenic milling have been shown to produce nano-structured morphologies when compacted and/or heat pressed from powder, but have not been studied following melt-phase mixing.[13-16] The cryomilled polymer blends in this study were subjected to melt-mixing and extended heat treatment, and the morphological and property response observed. Melt-mixing is common in industrial polymer applications and the process is critical for determining commercial applicability. Additionally, the creation of compatibilizing block copolymers during cryomilling, which has not yet been confirmed, was quantitatively demonstrated. In the case of SSSP, blends have been analyzed to a great extent, but only on a single machine located at Northwestern University. The new Solid-State Shear Pulverizer at Bucknell University is an updated version of the original SSSP instrument, and thus is capable of both confirming the

results of Northwestern researchers and advancing SSSP research. Before expanding the field of SSSP polymer blending, full characterization of the operation of the apparatus and determination of the optimal blending procedure is important. Thus, this thesis confirms the Northwestern results utilizing an identical polymer blend while determining the optimal operating conditions for polymer blending on the Bucknell SSSP.

This thesis is composed of eight chapters, including this introduction. The second chapter details the history and nature of polymer blend compatibilization, current production methods, and new mechanochemical methods of production under development. Chapter 3 focuses on the materials employed in the investigation, the two means of mechanochemical processing being employed, and the equipment and procedures utilized for characterization of the resulting polymer blends. Chapter 4 reports two distinct studies from the cryomilling work. The first is a confirmation of block copolymer-creating mechanochemical reactions during cryogenic milling, while the second documents the growth of cryomilled blends when subjected to extended heat treatment following melt-state mixing. Chapter 5 presents studies involving the Bucknell University Solid-State Shear Pulverizer, the second of its kind in academia. In addition to providing operation recommendations, in this chapter a full-factorial analysis is performed on the pulverizer to determine the most significant operating conditions towards achieving compatibilized immiscible polymer blends, as defined by average dispersed domain size and growth. Chapter 6 utilized two blends created using the Solid-State Shear Pulverizer and attempts to correlate the dispersed domain size with common mechanical and thermal analysis results. Final conclusions and recommendations are

succinctly presented in the Chapter 7, while Chapter 8 contains references to all published works utilized in creating this thesis.

Three appendices accompany this thesis. The first contains additional figures and tables which support the text. The second provides detailed design documentation and code for the software created during this study. The final appendix compiles the standard operating guides created to educate new operators of the new Solid-State Shear Pulverizer and other equipment recently introduced to the Polymer Hybrid Nanotechnology Research Group.

2. Background

Forming blends from two or more polymers serves as a relatively inexpensive and facile method of achieving desired mechanical and physical properties compared to developing new monomers or exploiting alternative polymerization mechanisms and kinetics.[17] Similar to metal alloys, polymer blends can yield additive or even synergistic property improvements compared to their neat components. While most metal alloy components homogeneously mix due to similar atomic sizes and preferred crystal structures, polymeric blends feature components of very large and varying molecule sizes and structural conformations. Fundamental thermodynamic and kinetic factors due to these size and structure variances restrict polymers to more complex blending interactions. Polymer blends are referred to by several alternative classifications, including polymer alloys, toughened blends, and reinforced blends.[2, 18]

2.1 Polymer Blend Theory

Blending behaviors for mixtures rely heavily on the thermodynamics of mixing for the components. In order to facilitate spontaneous single-phase blending, polymer blends require a negative Gibbs free energy of mixing, ΔG_m, as defined in:

$$\Delta G_m = \Delta H_m - T\Delta S_m \qquad \textbf{Equation 1}$$

where ΔH_m and ΔS_m are the enthalpy and entropy of mixing, respectively, and T is temperature. Additionally, a second equation must also be satisfied across all compositions to achieve a single phase binary polymer blend:

$$\left(\frac{\partial^2 \Delta G_\mathrm{m}}{\partial {\phi_i}^2}\right)_{T,P} > 0 \qquad \textbf{Equation 2}$$

where φ_i is the component volume fraction. If ΔG_m is negative and Equation 2 does not hold, the polymer blend will phase separate into two domains enriched in one component.[2]

Figure 1 shows a generic phase diagram for polymer blend systems. The spinodal curves indicate where the partial derivative in Equation 2 equals zero. Inside these curves, the polymer blend is unstable, will promote spinodal decomposition (creating bicontinuous morphologies). Outside of these curves lie the stable and metastable regions. The transition between these two regions is the binodal curve, which is where $\Delta G_m = 0$. Blends in the metastable region will spontaneously nucleate due to composition fluctuations and separate into continuous and dispersed phases, while blends in the stable region will undergo spontaneous mixing and exhibit a single, homogenous phase.[2]

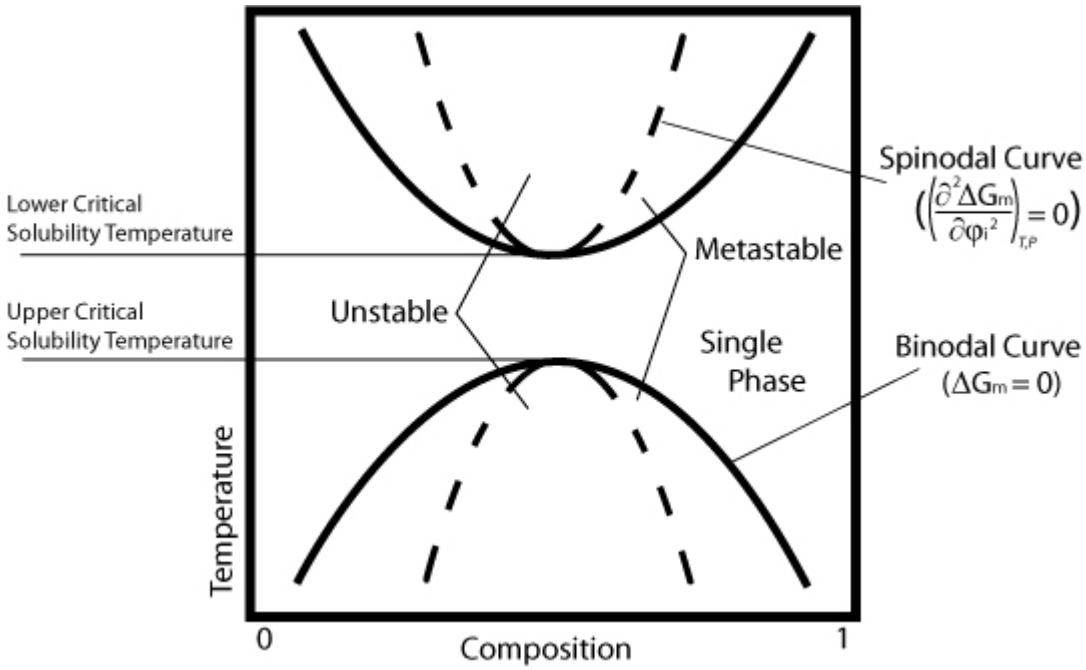

Figure 1. Generic phase diagram for miscible polymers. Note that the blend will form a single phase over a limited temperature and composition regime.

The prevailing theory to predict ΔG_m for two-component polymer blends is the Flory-Huggins expression:

$$\frac{\Delta G_m}{VRT} = \frac{\phi_1}{v_1 N_1} \ln \phi_1 + \frac{\phi_2}{v_2 N_2} \ln \phi_2 + \phi_1 \phi_2 \frac{\chi}{v} \qquad \textbf{Equation 3}$$

where V is the total sample volume, T is absolute temperature, v_i is the molar component volume of component i, N_i is the degree of polymerization of component i, φ_i is the component i volume fraction, v is a reference volume (typically set to $\sqrt{v_1 v_2}$), and χ is the Flory-Huggins interaction parameter.[19, 20] The first two terms on the right side of Equation 3 account for the $T\Delta S_m$ term in Equation 1 and are the entropic contribution of each component to mixing, while the final term on the right describes the enthalpic mixing contribution to ΔG_m.

For components of large size ($N_i > 1000$) the respective entropic term becomes negligible, allowing a critical spontaneous mixing interaction parameter, χ_c, to be defined when $\Delta G_m = 0$ as shown in:Equation 4[21]

$$\chi_c = \frac{v}{2}\left(\frac{1}{\sqrt{v_1 N_1}} + \frac{1}{\sqrt{v_2 N_2}}\right)^2 \qquad \textbf{Equation 4}$$

Equation 4 is often simplified further assuming both components have equal degrees of polymerization ($N_1=N_2$) and molecular volumes ($v_1=v_2$), yielding:

$$\chi_c N = 2 \qquad \textbf{Equation 5}$$

Comparing the χN values for different blend systems in reference to this critical $\chi_c N$ value allows for first-order determination on whether a polymer blend is fully miscible or creates a more complex two-phase system, as described further in the next three subsections.

2.1.1 Miscible Polymer Blends

Miscible blends feature a $\chi N < 2$ and can form a single, homogeneous phase due to small chain lengths (allowing the entropic terms to become significant) or favorable enthalpies of mixing, ΔH_m. Most often negative ΔH_m values are caused by complimentary intermolecular forces between side groups such as acid-base interaction, hydrogen bonds, dipoles, ionic groups, and π-orbital complexes.[2, 18, 22] For example, interaction of styrene groups allows polystyrene and poly(2,6-dimethylphenylene oxide) (PS/PPO) blends to be miscible with each other.[23] These blends exhibit improved physical properties and a single glass transition temperature — indicating the existence of only one phase.[17]

2.1.2 Partially Miscible Polymer Blends

Binary polymer blends which have a χN value of approximately 2 may be considered partially miscible. These blends are characterized by two distinct phase regions with a very large interface region separating them, as seen in Figure 2.[17] An alternative definition is a blend that phase separates into two distinct phases, but have sufficient concentrations of minority components in both phases to sufficiently modify the bulk properties.[2] Blends of polystyrene and acrylonitrile butadiene styrene (PS/ABS) are of this classification.[24-26] Blends exhibit two glass transition temperatures (T_g), with the T_g of each component being shifted slightly toward the other compared to neat polymer transitions.[17] While the impact strength of this blend is greatly increased, the separated phases restrict the deformation mechanisms of the blend, promoting irreversible

microcrazing.[27] Paul, and by extension some other literature sources, name this blending regime "compatible blends".[18]

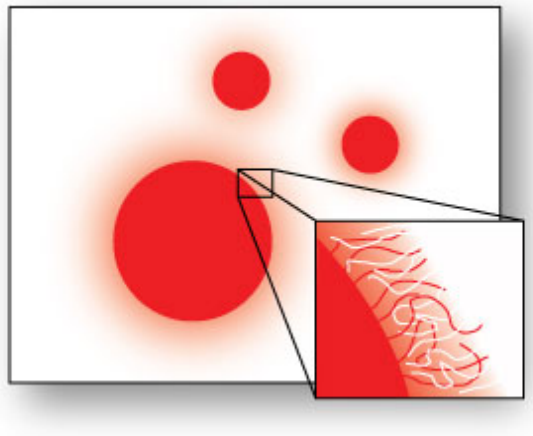

Figure 2. Polymer chains from both components penetrate into a relatively large interface region in partially miscible blends.

2.1.3 Immiscible Polymer Blends

The majority of polymer blends fall into a final category: fully immiscible blends with $\chi N > 2$ (known as "incompatible blends" in the works of Paul).[3] These blends feature two distinct phases bounded by a sharp interface. The interfaces have minimal interactions between the two phases, and as a result exhibit very poor cohesion. Hence, physical properties of immiscible blends are often worse than either of the neat components alone. When solidifying from a melt, the minor, dispersed phase thermodynamically favors specific geometries depending on blend composition. Below 25-30 wt%, spherical conformations develop to minimize the interfacial surface area, as seen in Figure 3.[28] Once solidified, additional thermal processing at higher temperatures yields unfavorable change in phase morphology. The spherical minor phase particles grow due to phase coalescence and Ostwald ripening.[29] Such poor stability to thermal

processing leads to further deficient mechanical properties due to large regions of interfaces with no cohesion, and thus has prevented the widespread use and exploration of immiscible polymer blends in both research and commercial applications.

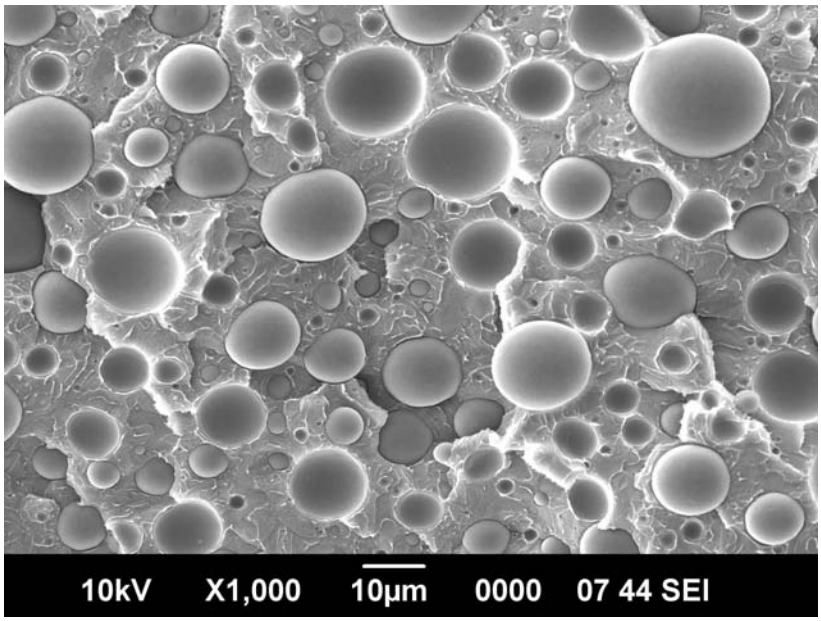

Figure 3. An immiscible, phase-separated polymer blend. Note the sharp interface transition.

2.1.4 Compatibilization of Immiscible Blends

Recently, methods have been developed to improve interactions across the interfacial region of immiscible blends. Termed "compatibilization," these interface modifications result in the stabilization of the dispersed morphology and minimization of the dispersed domain size.[28]

2.1.5 Definition and Determination of Compatibilization

One established definition of polymer blend compatibility is the average size of the dispersed phase. A successfully compatibilized blend of moderate composition (up to 30 wt% minority component) exhibits spherical dispersed phases with consistent diameters averaging on the micron and submicron scale.[29] Such consistent morphologies

can be achieved when the compatibilizing agent provides a steric hindrance to dispersed phase coalescence.[5, 30] Compatibilizers which provide steric hindrances operate as pictured in Figure 4. These chains act as anchors for minority phase droplets in the matrix, and also serve as repulsive "springs" when two droplets are in proximity.[29] Compatibilizing agents often provide additional morphology stabilization by acting as a surfactant and decreasing the interfacial surface tension.[31]

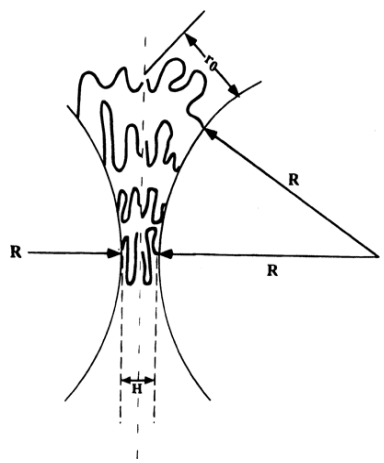

Figure 4. Steric compatibilizers act as both anchors for stability and repulsive springs to prevent coalescence [5]

A reduction in surface tension decreases the surface energy of the interface and allows smaller dispersed phase droplets to be thermodynamically favored when in the melt. When subjected to a shear force in the melt regime, such as when extruded or melt-mixed, a reduced surface tension encourages large dispersed droplets to triturate into smaller droplets, as predicted by the Taylor Limit theory:[32, 33]

$$D_0 = \frac{4\Gamma(\eta_r + 1)}{\dot{\gamma}\eta_m\left(\frac{19}{4}\eta_r + 4\right)} \qquad \eta_r < 2.5$$

Equation 6

This equation predicts the maximum drop size that would form and be stable in a particular shear flow regimen.The terms in Equation 6 include: $\dot{\gamma}$ as the melt shear rate, η_d as the dispersed phase viscosity, η_m as the matrix phase viscosity, η_r as the viscosity ratio of drop and matrix (η_d/η_m), Γ as the interfacial tension between phases, and D_0 as average dispersed drop diameter in shear flow.

Another metric for defining compatibility of immiscible polymer blends is the rate of phase morphology change at high temperatures in the melt state. Compatibility was determined by statically annealing a polymer blend for extended durations and measuring the rate at which the average dispersed phase size increases.[34] A successfully compatibilized blend will exhibit only a limited dispersed phase growth rate which is consistent throughout the blend bulk. This growth is due to Ostwald ripening and coalescence of the dispersed phase. Ostwald ripening is a thermodynamic process in which domains under a critical size will shrink as mass diffuses towards local, larger domains.[35] Coalescence is a kinetic process where mobile melt-phase dispersed domains collide and unify.[28] The combined effect of these two coarsening processes was modeled by Crist in:

$$D_n{}^3 = D_{0,n}{}^3 + Kt \qquad \textbf{Equation 7}$$

where D_n is the average dispersed domain diameter, $D_{0,n}$ is the initial average domain size, and *K* is the static growth constant (which is the sum of the coalescence and Ostwald ripening growth constants, K_C and K_{OR}).[36]

These two means of defining compatibilization, namely reduced average dispersed domain size and reduction of the static growth rate, were the primary

methodologies for determining compatibilization for the majority of this study. Extensions to these approaches are proposed that incorporate the size distribution of the dispersed domains into the definition of compatibilization. Traditionally, the industry seeks compatibilized blends to feature mechanical property enhancement.[17, 18] While mechanical improvements are not used to define compatibilization in this thesis, the relationship between the degree of compatibilization as defined by dispersed domain size and static growth rate and any changes in mechanical properties will be investigated in Chapter 6.

2.1.6 Functionalized Monomer and Discrete Species Compatibilization

Various studies have created or added compatibilizing agents to immiscible polymer blends to encourage phase interaction as previously discussed. Research into immiscible blend compatibilization initially focused on polymerizing the component species with low amounts (< 5 mol%) of functionalized monomers to promote secondary chemical interactions. The addition of carboxyl groups to chains of polystyrene increased miscibility in poly[n-butyl methacrylate-co-(4-vinylpyridine)].[37] Incorporation of vinyl amine groups into poly(vinyl alcohol) chains and acrylic acid groups into polyethylene chains significantly increased compatibilization, improving mechanical properties and transparency.[6] Polypropylene (PP) functionalized with maleic anhydride has been demonstrated to improve mechanical performance of several PP-based blends.[38, 39] This functionalized compatibilization method is limited to virgin specialty polymers synthesized from chemically modified monomers, which leads to higher component costs and prevention of widespread industry use.

Other compatibilization techniques involve the blending of a third component which is partially (or fully) miscible in the other blended polymers. Often these third species are relatively small organic molecules, such as phenoxy (bisphenol A).[28] Tertiary blends of chlorinated polyethylene and acrylic rubber were achieved by Wu with the addition of 3,9-bis(l, l-dimethyl-2 [beta-(3-tert-butyl-4-hydroxy-5-methylphenyl)propionyloxy] ethyl)-2,4,8, 10-tetraoxaspiro [5,5] –undecane.[40] These small molecule compatibilizers tend to leach from the bulk blend, leading to reduced compatibilization, retarded mechanical properties over time, and restricting use in food packaging or medical applications.

The addition of a third, discrete polymer species for compatibilization has also been reported. The third polymer must be partially miscible with the two other blend components, and can either act as a steric hindrance for a phase-separated blend or even promote full miscibility over a limited temperature and composition range. Poly(ε-caprolactone) added in minor amounts (several wt%) to an immiscible polycarbonate/styrene-acrylonitrile copolymer (PC/SAN) blend yields a miscible ternary mixture with a single T_g and depressed T_m.[41] The addition of PMMA to a PC/ABS blend created a ternary blend with a smaller ABS phase and suppressed coalescence.[42]

2.1.7 Block Copolymer Compatibilization

Much greater success has been reported by using block copolymers of the blend components as a long-chain surfactant species.[43-45] Block copolymers are thermodynamically favored to bridge the interface of immiscible polymer blends, as seen in Figure 5, and have been directly observed populating the interface of PS/LDPE blends.[46] Other forms of copolymers such as alternating, graft, or gradient copolymers

have been investigated,[24, 47] but are less common due to limited commercial availability and reports of pure diblock copolymers mechanically compatibilizing more effectively.[48] Block copolymers compatibilize through increasing steric hindrance of domain motion and decreasing interfacial surface tension.

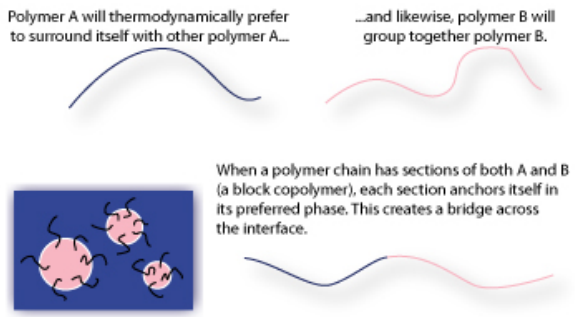

Figure 5. Use of block copolymers in stabilizing the interface

In order to provide proper steric hindrance, each block in a block copolymer must be larger than the molecular weight between entanglements for the neat polymer.[49] Molecule for molecule, a larger copolymer will provide greater compatibilization due to increased entanglement in both domains.[28] In general, 5% of the dispersed phase interface must be saturated with block copolymer to prevent dynamic coalescence, while 20% block polymer saturation would impart static stability.[5]

Block copolymers must be of sufficient chain size in order to provide the steric entanglements previously mentioned. In blends of PS and poly(2-vinylpyridine) (PVP) incorporating block copolymers with varying sizes of the PVP block, the percentage of delaminated dispersed domain interfaces dropped from 95-100% to ~0% when the length of the PVP block exceeded the molecular weight between chain entanglements, M_e, for PVP.[49] Copolymer chains underwent pullout from the PVP phase below this critical molecular weight, as confirmed through forward recoil spectrometry and scanning

electron microscopy.[50] These studies indicate that in order for a block copolymer to sterically stabilize an immiscible blend, each block must be at least M_e in length.

Initial studies into block copolymer compatibilization simply mixed the majority, minority, and copolymer species.[5, 51-53] Compatibilization was not successfully achieved via this method due to the block copolymer readily self-assembling into micelles within the matrix phase.[5] The formation of micelles prevented significant quantities of the block copolymer from diffusing to the interface. In PS/LDPE blends, block copolymers of hydrogenated poly(butadiene)-polyisoprene-polystyrene formed stable microdomains of HPB inside the LDPE domain instead of migrating to the PS/LDPE interface.[46] Additionally, these micelles acted as contaminant particles within the matrix phase, further decreasing blend performance.[5] When melt-mixing, longer block copolymers have significantly lower critical micelle concentrations (CMC), encouraging micelle creation and ultimately decreasing compatibilization.[28] Sandoval has studied the effects of relative chain lengths and copolymer composition on the CMC of styrene/(methyl methacylate) (S/MMA) copolymers in a PS/PMMA blend and found that doubling block copolymer length increases the CMC by a factor of ten.[54]

Almost all of the block copolymer compatibilization studies mentioned above were processed via melt mixing, but the method leads to necessary compromises between using larger, higher efficacy copolymers and transport/diffusion problems inherent to larger molecules. In situ copolymer reactions attempt to circumvent this issue by generating block copolymers within materials during processing at the blend interface. Reactive extrusion utilizes transesterification or condensation reactions to create copolymers as a blend transits a screw extruder.[28] While common in the industry, reactive

extrusion is tedious and difficult to control in a typical manufacturing facility without significant engineering support.[28] Often, these reactive extrusion processes require component polymers to be chemically altered with a reactive end group, such as maleic anhydride, increasing operating costs.[55-57] Hindrances of this processing method are a decreased processability of the blend as the reaction progresses in addition to being limited in product throughput by the slow reaction kinetics.[18]

2.2 Solid-State Polymer Processing

All of the previous blend compatibilization techniques introduced additional species or created block copolymers while the blend was in a melted or dissolved state. While having been successfully demonstrated in the academic setting, these processing methods have major limitations preventing commercial application. Solution-based compatibilization is restricted to small batch scales and requires the use of expensive and potentially hazardous organic solvents. Melt phase techniques require large amounts of heat to form and maintain the melt state, and can thermally degrade polymeric materials. Moreover, the heated state thermodynamically promotes the coalescence, not dispersal, of the minor phase component and leads to an "uncompatibilized" blend morphology. An alternative in situ reactive technique, mechanochemistry in the solid state, eliminates many of the problems found in the melt and solvated states.

2.2.1 Mechanochemistry of Solids

Chemical reactions can be initiated by mechanical forces. While not as exhaustively researched as thermo-, electro-, and photo-chemistry, mechanochemistry has founding origins going back to ca. 300 BC by Theophrastus of Ephesus in "De Lapidibus" (On Stones), which focused on reactions observed when using a mortar and

pestle.[7] Modern research into solid state chemistry began when Bridgman constructed his "Bridgman Anvil" to observe material responses to high stress and pressure.[58] Watson and Ceresa were the first to subject a polymer, natural rubber, to physical mastication, and reported an order of magnitude decrease in chain length and decreased viscosity.[59] It was hypothesized that the decrease in the rubber viscosity from physical manipulation was due to free radicals being formed upon the scission of polymer chains. Several groups have confirmed the creation of free radicals from chain scission using electron spin resonance.[60-63] Unlike rubber, uncrosslinked polyolefins (HDPE, LDPE, and LLDPE) independently subjected to certain mechanochemical shear exhibited a slight increase in viscosity, dependant on degree of initial chain branching, and no significant changes in number- and weight-averaged molecular weight.[64]

Should two polymers be mechanochemically processed together, several termination scenarios are possible for the created free radicals, as seen in Figure 6. Recombination between radicals on the same kind of chain re-forms a homopolymer, while disproportionation occurs when radicals on different chain types react, essentially creating a block copolymer between the two components.[59] Other termination routes can include hydrogen abstraction and chain transfer, both of which create branched species and can result in light crosslinking. The rate constants for recombination versus disproportionation during solution-based radical polymerization have been documented; radical termination through recombination was increasingly favored over disproportionation as polymerization temperature decreased.[65, 66] Similarly, mechanochemical disproportionation occurs at a lower rate than recombination.[67] Nevertheless, the level of block copolymer formation via disproportionation is sufficient

for stabilizing the interface between two polymers,[5, 34] and thus, mechanochemistry of polymers in the solid state is a simple and effective method of compatibilizing immiscible polymer blends.

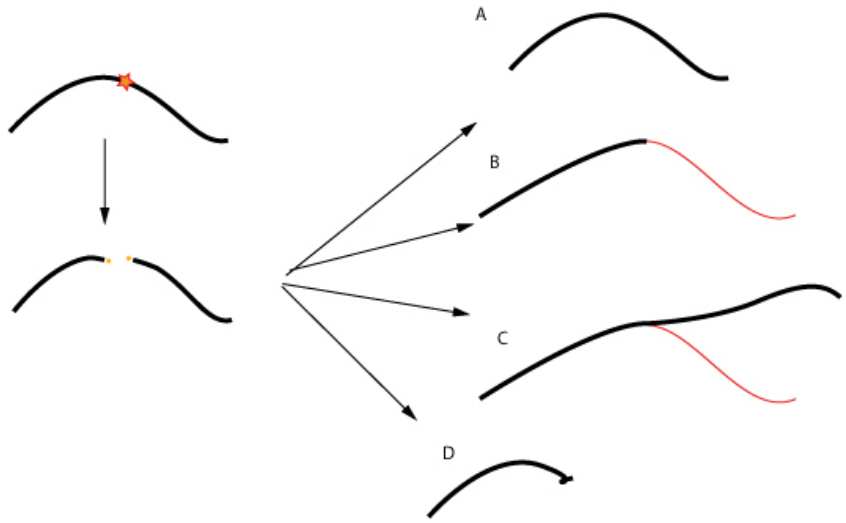

Figure 6. Free radical creation via chain scission and subsequent reaction pathways: A) Recombination B) Disproportionation (block copolymer formation) C) Grafting and crosslinking D) Ambient oxygen termination

2.2.2 Solid-State Batch Milling Methods

Various mechanical procedures have been explored to compatibilize immiscible polymer blends via free radical formation and in situ block copolymer formation. Pan milling followed by a twin-screw extrusion has been found to increase T_g and Izod impact strength in PP/PA6 blends.[68] Ball milling followed by powder pressing increased the tensile properties and Izod impact hardness for a low density polyethylene/polypropylene blend.[69] Both of these techniques are limited in their industrial application due to a batch basis and poor heat dissipation which necessitates long processing times to avoid melting and thermal oxidation. The milling rate can be

dramatically increased by actively cooling the milling chamber during processing using water,[68] dry ice,[69] or cryogenics such as liquid nitrogen.

Liquid nitrogen-cooled mechanical milling was first developed in 1985 by researchers at the Exxon Research and Engineering Company to produce high performance metallic alloys. While previous, non-cryogenic milling studies resulted in reduced grain size, they were limited in processing speed and throughput due to excessive heat buildup.[70, 71] Exxon researchers were able to achieve powder sizes less than 50 μm with grain sizes ranging from 0.05-0.6 μm.[72]

Similarly to the initial metallurgical research which prompted cryogenic milling, early studies in milling polymeric materials in the presence of liquid nitrogen focused on changes of morphology and crystallinity. Cryogenic milling of pure polymers was originally used to measure degradation of the structure of polystyrene during mechanical processing. Atactic and isotactic PS were cryogenically milled and exhibited asymmetric broadening of GPC peaks indicating preferential chain scission towards chain ends. Extended milling over 102 hours resulted in the re-formation of a narrow-distribution peak at a lower molecular weight (~10,000 g/mol).[73] This peak location is approximately the M_e of polystyrene, indicating that cryogenic milling will promote chain scission in only polymer chains larger than M_e. Pan and Shaw applied cryomilling technique to pure polyamide, finding that cryomilled material exhibits increased strength and toughness, while having minimum consolidation temperature of 100ºC, compared to a normal T_m of 285ºC.[74] Initial results also demonstrated that increased milling time resulted in improved mechanical properties, possibly due to a higher degree of crystallinity observed in cryomilled polyamide.[75] Cryomilling three grades of PMMA decreased the number-

averaged molecular weight, M_n, between 25-60% while the weight-averaged molecular weight, M_w, saw 49-76% reduction.[76]

The scope of cryogenic polymer milling research has recently shifted into milling two or more polymers into a blend, a process termed cryogenic mechanical alloying (CMA).[15] The critical goal of CMA is to create block copolymers between the blend components and stabilize the blend morphology, as previously discussed. Several immiscible blends have been compatibilized with varying success. Polystyrene/poly(ethylene terephthalate) (PS/PET) blends prepared via CMA were found to have a higher extent of compatibilization, as determined by the change in PET heat capacity, when compared to extruded blends.[77] This metric assumed that any change in heat capacity was due to entanglement of PET with PS and removal from the bulk amorphous material. Additionally, cryomilled PS/PET blends were found, via thermogravimetric analysis, to thermally degrade at a slower rate than the unprocessed component polymers or extruded blends. The interface was determined to contain 67% PET using energy dispersive x-ray spectroscopy.[77] A second study utilizing laser scanning florescent confocal microscopy probed the kinetics of PET recrystalization following CMA, finding the recrystallization rate decreased and amorphousness of PET phase increased with higher PET compositions.[78]

Poly(methyl methacrylate)/polyisoprene (PMMA/PI) and PMMA/poly(ethylene-*alt*-propylene) (PEP) blends have exhibited nano-scale dispersions following milling, and yielded significantly less molecular weight degradation and formation of species due to oxygen termination when milled at cryogenic temperatures as compared to ambient processing.[79] PMMA/PI (75/25 wt%) blends were determined to form a semicontinuous

PI network encapsulating the PMMA phase. The size of the PMMA domains were not dependant on press molding temperature but rather milling time, suggesting this morphology develops due to milling-induced crosslinking of the PI.[11, 13] Upon annealing at 150ºC, blends with lower milling times these blends formed domains averaging 200-500 µm.[80] The mechanical properties of the PMMA/PI (75/25 wt%) blends were improved upon the addition of a pre-made block copolymer into the CMA process. Blends with 2 wt% premade block copolymer had a smaller average dispersed domain size while blends of 10 wt% premade block copolymers created semi-continuous PI phase networks with dispersed PMMA domains as small as 20 nm in diameter. When cryomilled, the premade PMMA/PI copolymers were found to undergo chain scission and weight reduction in the PMMA blocks while the PI blocks experienced milling-induced crosslinking.[81] Smith et al. also associated the mechanical degradation seen in cyromilled PMMA to that of high-energy irradiation (electron or γ-radiation) with regards to increased crosslinking and reductions in molecular weight and crystallinity. Such a proposed relation allows for the use of widely-reported irradiation degradation data for guidance on the selection of polymers for solid-state processing.[76]

Stranz et al. have investigated the effects of cryogenic milling of polymers and blends with highly ordered repeat group structure. Isotactic polypropylene (iPP) that was cryomilled neat for 30 minutes was found to have irreversibly decreased its crystallinity 16% and raised the onset crystallization temperature (T_c) 7 ºC compared to non-cryomilled polymer.[82] Isotactic polypropylene (iPP) cryogenically alloyed with syndiotactic polystyrene (sPS) featured a similar decrease in crystallinity as measured by wide-angle x-ray diffraction and a 10ºC increase in onset crystallization temperature.[14]

Cryomilled poly(vinylideneflouride) (PVDF) exhibited an accelerated isothermal growth of crystals potentially (~40%) due to decreased molecular weight after 30 minutes of milling.[83] PMMA/PVDF blends offered significant strain-at-break improvement over neat PMMA, with a 50/50 wt% blend transitioning from brittle to ductile deformation behavior.[10]

Ultimately, cryogenic milling of polymer blends remains limited in commercial applications due to its batch nature, limited ability to scale due to poor heat dissipation, and high cost of cryogenics compared to other cooling media.

2.2.3 Solid-State Shear Pulverization

Another, novel solid-state polymer processing technique has been introduced by researchers at Northwestern University, called Solid-State Shear Pulverization (SSSP).[34, 84-89] This continuous and industrially-scalable process utilizes a modified twin-screw extruder to exert high shear forces and pressures onto a polymer blend while maintaining the solid state through continuous cooling. The apparatus is based on a Berstorff Maschinenbau PT-25 co-rotating twin-screw extruder with a variable barrel diameter of 23/25 mm and an L/D ratio of 26.5.[90] Cooling platens surround the barrel sections to maintain external temperatures from 0-10 ºC using a recirculating ethylene glycol/water solution.[85] The actual temperature of the screws and material within the barrels is not directly measured or controlled, but is maintained below the melt transition temperature of the material being pulverized. As seen in Figure 7, the screw design varies down the length of the barrel. A “Mixing Zone” of bi-lobed kneading elements performs initial fracturing and mixing of polymer pellets while the “Pulverization Zone” of tri-lobed

elements reduces the polymeric material to a fine powder. The barrel diameter decreases to 23 mm in the pulverization zone.

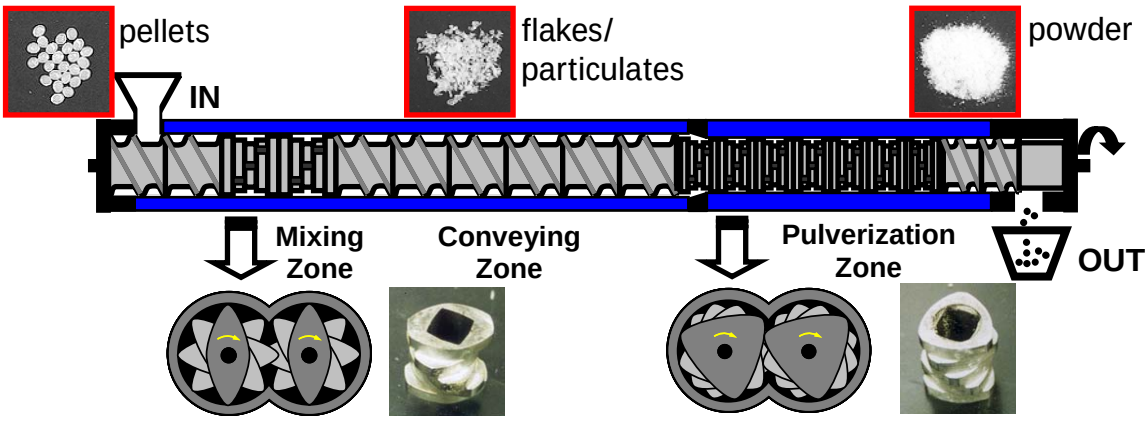

Figure 7. Regions of the Northwestern University Solid-State Shear Pulverizer screw design[89]

The relative sizes and conveying directions of these screw sections can be modified greatly due to a modular screw design. Adjusting the screw design was found to vary the severity of pulverization, and is considered one of the most influential SSSP operating parameters.[91]

Solid-state shear pulverization was originally developed as a novel means of pulverizing post-consumer recycled plastics and rubbers into a value-added product which could be easily and economically scaled to meet process demands.[84] Pulverization of unsorted, multi-colored recycled plastics resulted in a homogeneous powder with improved mechanical properties compared to a melt-mixed blend.[12] In the field of polymer composites and nanocomposites, SSSP has been shown to promote the exfoliation and dispersion of nanometer-scale fillers in a polymer matrix, including carbon nanotubes, modified and unmodified clays, starch, and graphite.[87, 89, 92-94]

When applied to immiscible polymer blends such as PS/HDPE or miscible blends with large viscosity ratios, blends processed via SSSP exhibited no delay in achieving morphology where the high-viscosity majority component formed the matrix phase, while conventionally processed blends required up to 35 minutes of melt mixing to achieve this phase inversion.[90] Work done by the Torkelson group at Northwestern University has expanded the investigation into achieving compatibilized immiscible polymer blends via SSSP. Lebovitz demonstrated that blends produced through SSSP exhibited greatly reduced dispersed domain sizes compared to traditionally melt-mixed blends (10-57% reductions) and predicted by the Taylor theory on immiscible domain size in a melt under shear.[95] Reduction in domain size was determined to be due to a stabilization of the dispersed domains and a reduction in the static growth rate.[34] In situ block copolymer generation during solid-state pulverization was confirmed using pyrene-labeled polymers and ultraviolet-active gel permeation chromatography.[9] Further decreases in dispersed domain size were achieved with the addition of pre-fabricated block and gradient copolymers to immiscible blends of PS/HDPE and PS/PMMA during pulverization, respectively.[47, 88]

3. Materials and Methods

3.1 Materials

Several polymeric materials were processed in this study. Polymers obtained from commercial venders are listed with their sources, grades, and reported properties relevant to this course of study. In the case of synthesized polymers, the reactants, reagents and catalysts, synthesis procedure, as well as purification and validation techniques are listed.

3.1.1 Polystyrene

Polystyrene (PS) utilized in this study was PS Crystal 158K KG2 (1300) by Ineos Nova, procured through Ashland. It does not include lubricants or additional processing aides. The following properties are reported: melt flow rate of 3 g/10 min at 200ºC and 5.0 kg, yield strength of 49 MPa, impact strength of 20 J/m, and a melt processing temperature of 360-530ºF.

3.1.2 High-Density Polyethylene

High-density polyethylene (HDPE) used was Petrothene LM6007 produced by Lyondell Basell and procured through Ashland. The supplier reports the following properties: melt flow rate of 0.8 g/10 min at 190ºC and 2.16 kg , yield strength of 31.7 MPa, impact strength of 64.1 J/cm, and brittleness temperature <-76ºC.

3.1.3 Pyrene-Labeled Poly(Methyl Methacrylate)

Poly(methyl methacrylate) containing pyrene-labeled side groups was specially synthesized for the cryogenic milling study in this thesis (Chapter 4), and will be referred to as pyPMMA. Pyrene, seen in Figure 8, is easily detectable by UV light fluorescence.[96] Polymer chains containing the label side groups can be selectively detected by a UV

detector upon elution from a GPC column.[9] The detection of in situ block copolymer formation can be confirmed through the transfer of low molecular weight labeled polymer segments to a higher-molecular weight component.

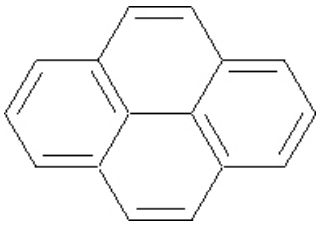

Figure 8. Chemical structure of pyrene (image from SigmaAldrich)

Synthesis of pyPMMA closely follows the procedure described in previous studies.[9] Synthesis of pyrene-labeled methyl methacrylate monomer (1-(1-pyrene)-methyl methacrylate, pyMA) is the first step. Table 1 lists the chemicals used during pyMA production, all procured from Sigma-Aldrich.

Table 1. Chemicals utilized during pyMA synthesis (all images from supplier)

Chemical Name	Structure	Sigma-Aldrich Catalog Number
1-pyrene methanol	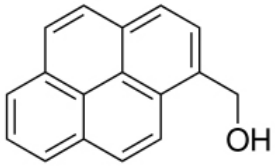	389439
methacryloyl chloride	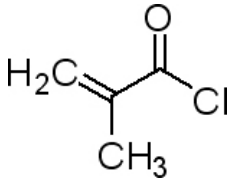	523216
triethylamine	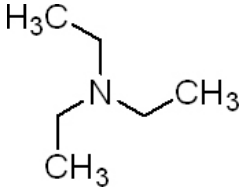	T0886
tetrahydrofuran (anhydrous, THF)	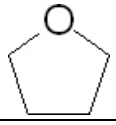	186562

pyMA is synthesized via the esterification of methacryloyl chloride to form 1-(1-pyrene)-methyl methacrylate, seen in Figure 9.[9, 97] The reaction is driven towards completion by including triethylamine in the reaction vessel, which forms triethylamine hydrochloride, a ternary ammonium salt with HCl.

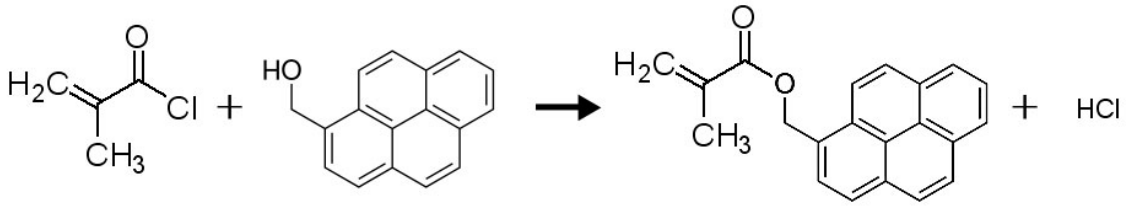

Figure 9. Esterification reaction to form pyMA

All glassware was heated in an oven at 150ºC and cooled under a nitrogen stream or flame-dried under continuous nitrogen flow. The reaction was carried out anhydrously to prevent the methacrylic chloride from reacting with ambient moisture. The primary reaction chamber, a 500 mL round-bottom flask, was filled with 5.0 g of 1-pyrene methanol prior to the assembly of the full reaction apparatus. The round-bottom was continuously stirred and placed into an ice bath. Anhydrous THF (200 mL) was transferred into the reactor through a cannula under nitrogen pressure. Triethylamine was opened under a directed nitrogen stream and 10 mL were syringed into the reactor flask. An addition funnel was charged with 20 mL of anhydrous THF and 6.8 mL of methacryloyl chloride. Both the funnel and reaction vessel were wrapped in foil to prevent a spontaneous photo-initialization. The contents of the addition funnel were added dropwise to the reaction vessel over an hour, under continuous nitrogen flow. After an additional hour of cooling and stirring, the reaction vessel was removed from the ice bath and stirred for 22 hours at room temperature. The impure products were washed

twice with a saturated sodium bicarbonate/water solution, and the resulting organic layer had solvent removed on a Buchi R-210 Rotovap with a water bath set to 40ºC. This yielded a viscous, clear fluid presumed to be methacrylic acid and a dark yellow solid precipitate. A 0ºC ethanol wash was used to remove the viscous fluid, while the yellow solid was recrystallized by dissolving in boiling ethanol and submersion in an ice bath. A second recrystallization was carried out to increase purity. The resulting pale yellow solid (4.8 g) had a melting point of 88-90ºC, similar to pyMA synthesized in previous reports.[98]

Successful synthesis of pyMA was further confirmed via nuclear magnetic resonance (NMR) spectroscopy. pyMA was dissolved in deuterated chloroform to minimize solvent detection. A Varian VNMRS-400 ^{1}H NMR (400 MHz) was used to generate Figure 10 by averaging eight repetitions. The structure of the solid was confirmed as pyMA through peak identification and integration. Peaks at $\delta = 7.9\text{-}8.3$ represent the aromatic hydrogens of the pyrene label, $\delta = 7.2$ is the chloroform solvent, peaks at $\delta = 6.1$ and 5.5 are chiral $CH_2{=}C$ hydrogens, the peak at $\delta = 5.9$ is $O\text{-}CH_2$, and $\delta = 1.9$ are methyl (CH_3) hydrogens. Peaks at $\delta < 1.8$ are impurities relating to the EtOH recrystallization and the calibration peak.

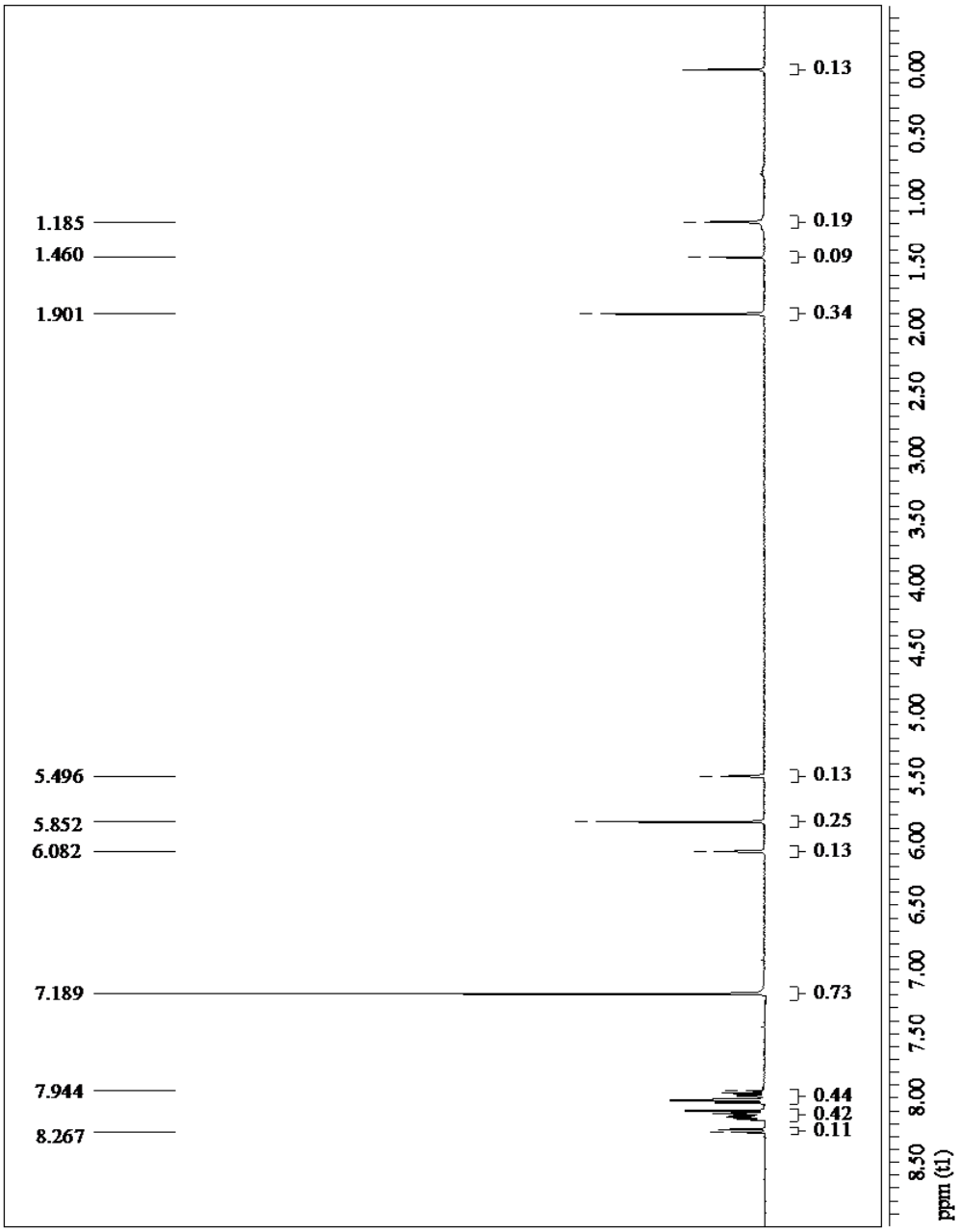

Figure 10. ^{1}H 400 MHz NMR spectrum of pyMA

The synthesized pyMA was polymerized with bulk methyl methacrylate to form the desired labeled polymer, pyPMMA. The goal of this polymerization was to produce a polymer with a molecular weight high enough to facilitate chain scission with minimal chain pullout, but low enough to have a GPC peak differentiable from the majority

polymer. The critical molecular weight at which a polymer will undergo chain scission rather than pullout, M_c, is estimated to be 2 or 3 times the molecular weight between entanglements, M_e.[99] The M_e for PMMA is reported as 7,000 g/mol, leading to an M_c of 14,000-21,000 g/mol.[100] To ensure chain scission over pullout, the target molecular weight for pyPMMA was set to be at least $2M_c$, or ~40,000 g/mol.

The bulk free radical polymerization of pyPMMA was conducted in a 500 mL round bottom flask. 10 mL of bulk methyl methacrylate from Sigma-Aldrich was added along with 0.066 M (0.197 g) pyMA and 0.064 M (0.105 g) 2,2′-azobis(2-methylpropionitrile) (AIBN). The flask was stopped and purged under nitrogen gas for ten minutes. The reaction was initiated by submersion of the reaction flask in a 70ºC water bath and terminated after 10 minutes by insertion into an ice bath. Dichloromethane (DCM) was used to solvate the reactor contents and pyPMMA was precipitated in methanol. The pyPMMA was washed three times to remove unreacted monomer while excess DCM and methanol was removed under vacuum overnight. The final yield was ~1.3 g of an off-white polymeric solid with an M_n of 64,000 g/mol and M_w of 119,000 g/mol.

Ultraviolet absorbance spectra of 1-methanol pyrene, pyMA, pyPMMA, and several pure polymers were generated using a SpectraMax M5 from Molecular Devices. Figure 11 shows that the neat polymers used throughout this thesis have minimal absorbance between 310-350 nm, while pyrene-containing compounds have strong absorbance peaks, as expected. The wavelengths of the absorbance peaks for these compounds, are listed in Table 2, and are comparable to previous reports.[98] The detection of pyPMMA used the third absorbance peak at 343 nm for a maximum response.

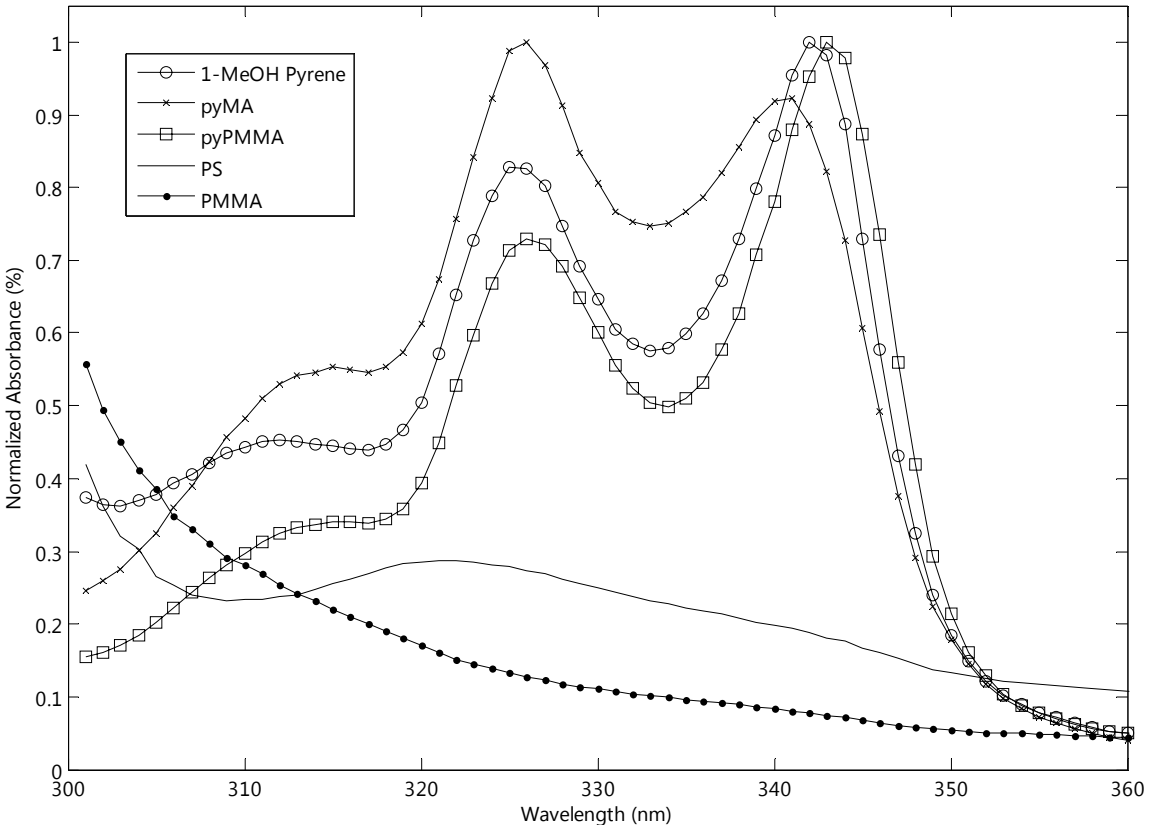

Figure 11. Ultraviolet spectra of 1-methanol pyrene, pyMA, pyPMMA, and several pure polymers over active absorbance range of pyrene

Table 2. Maximum peak absorbance wavelengths for pyrene-containing compounds

Compound	Maximum Absorbance Wavelength (nm) (*Strongest Response)		
	Peak 1	Peak 2	Peak 3
1-MeOH Pyrene	312	326	342*
pyMA	315	326*	341
pyPMMA	315	326	343*

3.2 Sample Preparation

3.2.1 Processing

There are several means of processing polymer blends to compatibilize the immiscible components. In this section, the two solid-state mechanochemical techniques under investigation are described in detail.

3.2.1.1 Cryogenic Milling

Cryogenic milling is a batch solid-state processing technique. Sample materials are placed within a vial and rapidly impacted by a milling medium. The degree of milling is often reported in terms of milling time, however the different cooling and mechanical configurations of mills lead to inconsistent accounts of the impact energy exerted. The milling energy has been delivered by either violently shaking the entire sample vial[15, 69, 74] or using electromagnetic energy to accelerate the milling media while keeping the sample vial fixed.[14] Systems with minimal mechanical parts, such as electromagnetic milling, provide the most consistent milling over the lifetime of the apparatus due to limited wear and fatigue. Continuous cooling required to maintain the solid state and prevent thermal degradation has been produced through refrigeration, pulverized dry ice, and liquid nitrogen. Liquid nitrogen (boiling point 77 K) offers the largest cooling gradient while its liquid state allows for intimate interaction with the milling chamber.[69] The application of liquid nitrogen varies widely from direct insertion into the milling vial,[101] fitting a jacket with liquid nitrogen circulation around the sample vial,[79] dripping onto the exterior of the milling vial,[102] or submerging the milling chamber in a liquid nitrogen bath.[11] The last configuration ensures consistent contact between the coolant and the milling chamber while mitigating sample contamination and containment issues.

A SPEX Sampleprep Freezer/Mill model 6870 (cryomill), seen in Figure 12, exhibits the desirable characteristics and was utilized for cryogenic milling. The cryomill features a ~80 L bath of liquid nitrogen to submerge a 50 mL polycarbonate sample vial isolated with two non-magnetic solid steel end caps. Milling action is induced in a stainless steel impact rod (147 g) via variable frequency electromagnets (Figure 13).

Figure 12. Cryomill and supporting equipment

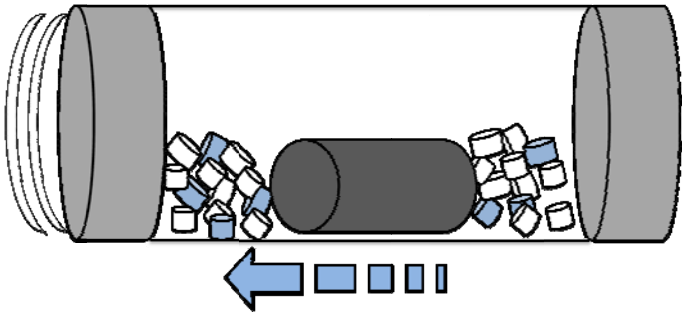

Figure 13. Diagram of cryomill vial design and magnetic driving

A maximum of 15 g of polymer were added to the vial along with the impactor with no additional modification or mixing. Samples were pre-cooled for fifteen minutes in the liquid nitrogen bath prior to processing to ensure that the bulk polymer was cooled

well below its ductile-brittle transition temperature. Each milling cycle consisted of operating the impactor for four minutes at a frequency of 10 Hz followed by a cool-off period of four minutes.[94] Degree of milling varied for each sample between five and fifteen cycles. Samples were removed from the vial immediately following milling and stored in sealed plastic bags.

3.2.1.2 Solid-State Shear Pulverization

Solid-state shear pulverization (SSSP) is a continuous and industrially-scalable solid-state processing method. The instrumentation comprises a twin-screw extruder which is cooled to sub-ambient conditions using recirculating coolant and specially-designed screws which impart high shear stresses to fracture polymers pellets to the point of pulverization, resulting in a fine powder exiting the process.[12, 34, 95, 98] This process has been shown to induce chain scission, resulting in molecular weight reduction and, when operating with two simultaneous polymer feeds, block copolymer creation.[9, 12, 91] Alternatively, the extruder barrel can be heated to typical polymer processing temperatures and, in conjunction with a "regular" screw design and die attachment, can operate as a twin-screw extruder (TSE).

Bucknell University's SSSP/TSE is a KrausMaffei Berstroff ZE-25A UTX: a co-rotational, intermeshing twin-screw extruder capable of continuous melt-state or solid-state processing (Figure 14). The nominal lengths of the screws element designs are 875/850 mm (SSSP/TSE) while the L/D is 35/34 (D = 25 mm). The length difference between SSSP and TSE modes comes from an additional element used to move powder from the apparatus during solid-state operation.

Figure 14. Bucknell University's Solid-State Shear Pulverizer/Twin Screw Extruder

Five of the six barrel zones are fully temperature controlled (in Figure 15, these are zones 2-6), with integrated solid-state electrical heaters, an integrated coolant recirculation system, and type J thermocouples. The feeding zone (Zone 1) has its temperature monitored, but is neither heated nor cooled. The fifth barrel section (Zone 5) is an open barrel with an attached degassing vent. When operating as a TSE, a heated, three-stranded die head is attached to the last barrel segment (left of Zone 6), while an additional screw-supporting bearing segment is attached when operating in the solid-state mode. In between each barrel segment is 12.5 mm of union space where an external clamp seals the segments together (see Figure 15). These union regions are not in direct contact with the cooling fluid nor electric heaters and are thusly not temperature controlled. The barrel sections are constructed of chromium steel, screw shafts of chrome-molybdenum steel, and screw elements of hardened chromium steel.

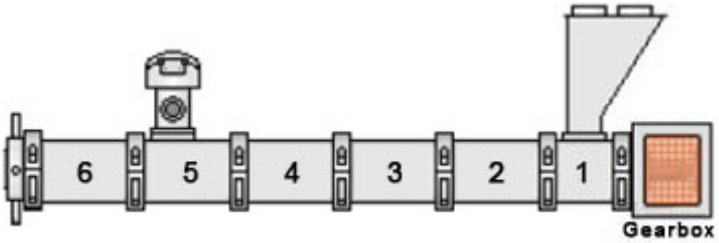

Figure 15. Schematic of the SSSP/TSE zone configuration with six barrel zones

Table 3 lists the screws currently available for the SSSP. Conveying elements are typical screw sections designed to transport material, while kneading blocks are composed of five bi-lobed blocks which break down pellets and impart the high shear forces desired during SSSP processing. Screw elements have designated driving directions, either forward or reverse along the barrel. Elements with a neutral driving direction impart no specific driving force and will retain their contents until displaced by additional material traveling down the barrel.

Table 3. List of available screw elements and descriptions

Identifier	Element Type	Length (mm)	Driving Direction	Image	Supplier Identification
Lc	Conveying	31.25	Forward	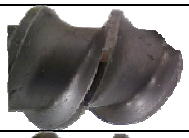	AZ-31.25/1/2
Mc	Conveying	25	Forward	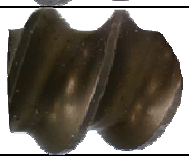	EAZ-25/1/2

(continued on next page)

Table 3. List of available screw elements and descriptions (continued)

Identifier	Element Type	Length (mm)	Driving Direction	Image	Supplier Identification
Sc	Conveying	18.75	Forward		EAZ-18.75/1/2
Lf	Kneading	31.25	Forward	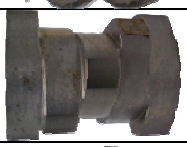	EAZ-KB31.25/5/45L
Sf	Kneading	18.75	Forward		EAZ-KB18.75/5/45L
Ln	Kneading	31.25	Neutral	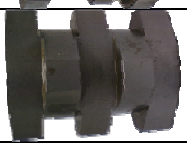	EAZ-KB31.25/5/90
Sn	Kneading	18.75	Neutral		EAZ-KB18.75/5/90
Lr	Kneading	31.25	Reverse	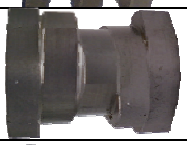	EAZ-KB31.25/5/45R
Sr	Kneading	18.75	Reverse		EAZ-KB18.75/5/45R
Mx	Transition Conveying	25	Forward	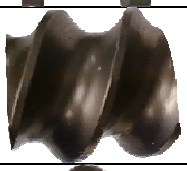	SEAZ-25/1/2
Xr	Conveying	10.5	Reverse		EAZ-25/0.5/2R
Sg	Mixing	18.75	Reverse		AZ-ZB18.75/3/10R

When operating in the SSSP mode, barrel zones 2-6 are chilled by recirculating coolant. Coolant is supplied by a Budzar Industries BWA-AC-10 water chiller with a cooling capacity of 10 tons of refrigeration (120,000 BTU/hr, 35.17 kW), set to -12ºC. The chiller unit is comprised of the following: a 10 HP working fluid compressor, an air-cooled condenser with twin $^{1}/_{2}$ HP fans capable of 6,000 CFM, a 1.5 HP coolant fluid pump capable of 24 GPM at 40 PSI, and a 30 gal coolant fluid reservoir. The coolant fluid is an ethylene glycol/water solution (50-60 vol% ethylene glycol), while the working fluid is HCFC-22 refrigerant.

Polymer pellets are added to the SSSP/TSE hopper by a Brabender DS28-10 Pellet Feeder (Figure 16). Pellet blends were pre-mixed and added to the feeder hopper capable of accurate dispensing at the rates of 20 - 10,000 g/hr. The DS28-10 features two interchangeable sets of tubes and augers. Feed rates were controlled by varying the frequency of electrical input to the feeder motor against calibrations for a variety of pellet types including glassy, malleable, and rubbery.

Figure 16. Brabender DS28-10 Pellet Feeder

3.2.2 Post-Processing

After solid-state processing, samples were melt-processed to mimic traditional post-processing encountered in industrial applications. Once in the melt, blends were formed into standard testing samples so that further characterizations could be performed.

3.2.2.1 Melt Mixing

Powdered blends were mixed in the melt state to simulate the shear and mixing forces exerted by commercial melt extrusion or injection molding. An Atlas Laboratory Mixing Molder (LMM, Figure 17) was used for batch melt mixing. The LMM is a small-scale rotor-in-cup style mixer with a heated cup (maximum capacity 4 cc, maximum temperature 400ºC) into which a rotating piston is inserted. Cup temperature is controlled via a digital controller while rotor speed is changed via an analog dial (0-173 RPM).[103]

Figure 17. Atlas Laboratory Mixing Molder

Samples were prepared in batches of approximately 3 g and mixed for a total of 5 minutes. Constant pressure was maintained on the piston lever to ensure close contact between the polymer and piston. The piston was raised halfway through the batch time and the sample was manually mixed with tweezers to disrupt any dead zones and ensure

complete mixing. Mixed samples were removed from the processing chambers using tweezers and allowed to slowly cool to room temperature on a watch glass.

3.2.2.2 Injection Molding

Mechanical testing of blends necessitated the molding of standardized samples which was accomplished through injection molding. Polymer powder or pellets were heated to a molten state and forced through an orifice into a mold by a piston. For polymers or blends with high working temperatures, the mold can also be heated prior to injection.

Tensile testing dogbones and smaller samples were processed using the injection molding capability of the Atlas LMM. Figure 18 shows the mold designs used in this research. To mold a sample, the LMM was operated as described in Section 3.2.2.1 Melt Mixing. Once the sample was molten and mixed in the mixing chamber, the injection orifice was opened and pressure was applied towards the mold. The mold was promptly removed once full and quenched in cool water.

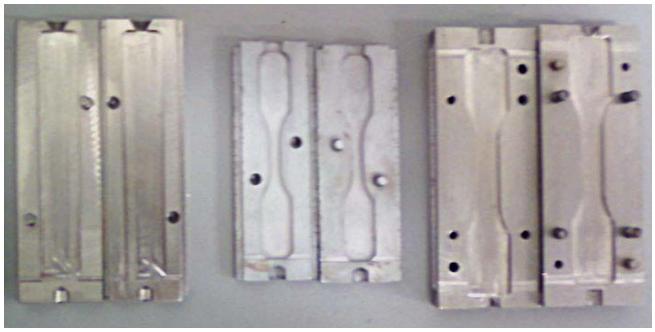

Figure 18. Molds for the Atlas LMM used in the course of study

3.2.2.3 Sheet Pressing

Following solid-state processing or melt mixing, samples are a powder or of inconsistent shape and thus were compression molded into consistent-thickness polymer

sheets for sampling. The top and bottom platens of the press are independently controlled and heated with electric resistance heaters. The sample was inserted with a guide between the platens, and a hydraulic pump raised and lowered the bottom platen to apply consistent pressure to molten polymer. Samples were left in the hot press for extended periods of time for isothermal heating.

Two Carver Laboratory Presses were used in this study, a green press and a grey press, seen in Figure 19. Both presses are capable of applying up to 5 metric tons of force. The platens on the green press are capable of achieving temperatures of 500ºF (top) and 475ºF (bottom), while the top and bottom grey press platens can reach 705ºF and 670ºF, respectively.

Figure 19. Carver presses used for pressing polymer sheets

3.3 Sample Analysis

Following post-processing, samples were analyzed for morphological, chemical, thermal, and mechanical characteristics using a variety of techniques.

3.3.1 Scanning Electron Microscopy

Scanning electron microscopes (SEM) use an electron beam focused by magnetic lenses to image fine details on sample surfaces placed within a vacuum chamber. Detectors within the chamber capture electrons which scatter off the sample from the incident electron beam (back-scatter electron imaging, BSE) or secondary electrons which are emitted from the sample surface after being excited by the incident electron beam (secondary electron imaging, SEI) . Non-conductive samples in SEMs can quickly develop a charge from the electron beam, resulting in poor image quality and ultimately heating and damaging the sample. These surfaces must therefore be coated with a conductive layer prior to SEM imaging.[104]

The most common method of coating is sputter coating, also known as sputter deposition. The sample is placed within a vacuum chamber and reduced to low pressures (<100 mbar). Argon gas is introduced to the chamber and an electrical field is induced at an anode to excite the argon into plasma and impact a gold foil cathode. The argon collisions fire gold atoms off the foil surface to deposit on the sample surface. Deposition layer thickness is controlled by varying the strength of the plasma-creating electric field and sputter time. Because the gold atoms are displaced due to the momentum of ionic argon, sputtering takes place at ambient temperatures.[105]

Pressed specimens were cryogenically fractured at a random location and adhered to the brass cube by conductive carbon tape with the fractured surface facing upwards.

SEM samples were prepared on acetone-washed brass discs with 1 cm^3 brass cubes, as shown in Figure 20. A distinctive pattern was drawn on top of the cube using a permanent marker to identify the sample orientation while in the SEM chamber. A Denton Vacuum Desk IV Coater/Etcher was used to sputter coat samples. Sample trays were sputter coated with a sputter strength of 50% and sputter time of 120 seconds.

SEM micrographs were digitally taken using a JOEL JSM-6390LV SEM in SEI mode. This SEM is practically capable of magnifying to 4,000x and resolving structures down to 0.2 µm. Micrographs were taken in SEI mode with an accelerating voltage of 10 kV, working distance ~7 mm, and spot size of 45-55. Analysis images were taken in high quality, 160 second refresh rate mode.

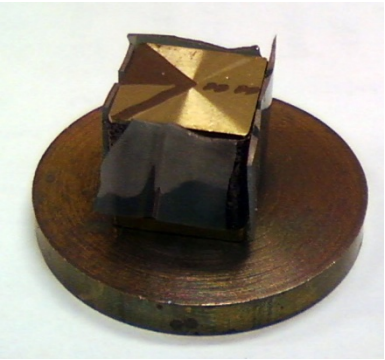

Figure 20. Example gold-coated SEM sample tray with orientation pattern

3.3.1.1 Polymer Blend Analyzer – Custom SEM Analysis Software

SEM micrographs were analyzed to measure the size of the dispersed phase domains, as seen in Figure 21. Automated digital detection of the dispersed domains was proven difficult due to the poor contrast differentiation between the two phases and non-ideal spherical morphology of the dispersed domains.

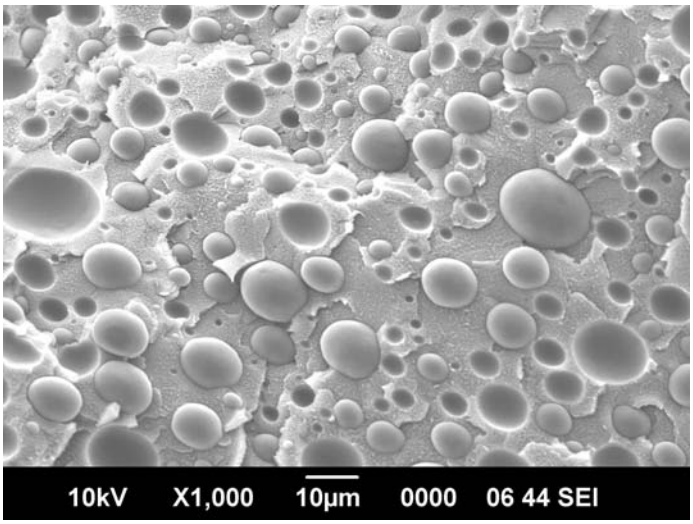

Figure 21. A typical SEM micrograph featuring a polymer blend with spherical dispersed domains and holes of varying size

In lieu of automated detection of the dispersed domains, masks of each micrograph were created in Adobe Photoshop using a Wacom Graphire tablet for precise drawing control. The resulting image differentiates the two phases, as seen in Figure 22.

Masks were loaded into a custom-written MATLAB program, Particle Size Analyzer, for particle size determination and analysis, as seen in Figure 23. The software detects and highlights the boundaries of each dispersed domain. Misshapen particles can be detected by two methods, Circular Area ID and Circular Ratio ID. Circular Area ID calculates the actual area of the particle mask and then compares it to a circle with a diameter with the average of the particle's two-dimensional height and width. Circular Ratio ID calculates the actual area of the particle mask, calculates an idealized particle diameter and compares it to an idealized particle diameter calculated by the particle circumference. Particles which are not misshapen (default is 80% tolerance from ideality) are accepted and have an idealized diameter calculated from their true area. All particle

diameter information was saved into separate Comma Separated Values (.csv) files for compounded average diameter and variance calculations.

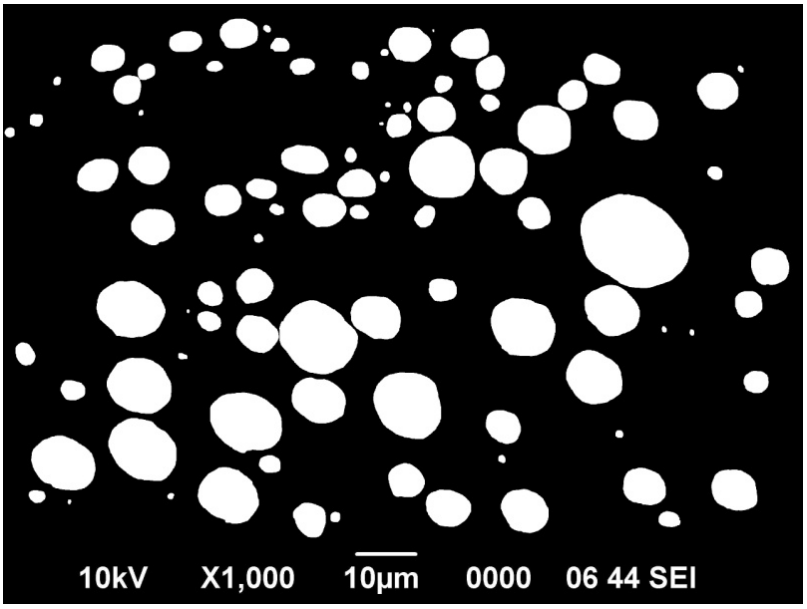

Figure 22. High-contrast mask of Figure 21

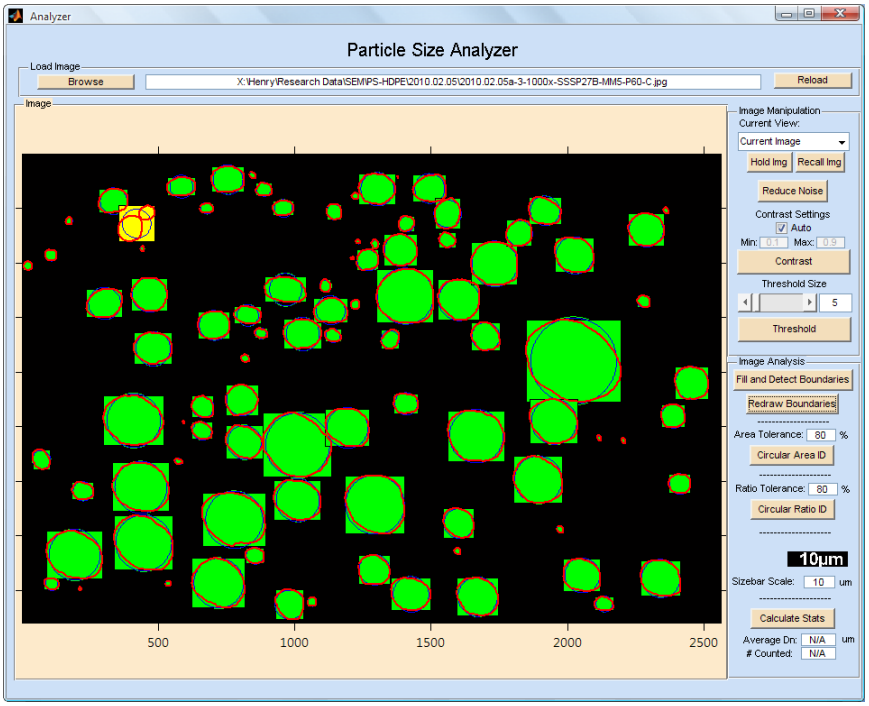

Figure 23. Mask from Figure 22 imported into Particle Size Analyzer software, after running boundary detection

3.3.2 Gel Permeation Chromatography

Gel permeation chromatography (GPC) uses packed columns of gel-based porous beads to size-exclude polymer chains based on their hydrodynamic radius and, by extension, molecular weight.[106] Molecules with higher hydrodynamic radii interact the least with the column packing pores and exit the column earlier than smaller molecules.

A Hewlett-Packard 1090 High Performance Liquid Chromatograph was utilized. The instrument was equipped with two 300 mm (I.D. 7.5 mm) PLgel 10µm MIXED-B organic GPC columns configured in series. Tetrahydrofuran (THF) was used as a mobile phase at 1 mL/min and ambient temperature. Eluate passed through a Linear UVIX-205 Ultraviolet Absorbance (UV) Detector, a Wyatt miniDAWN Treos Multi-Angle Light Scattering (LS) Detector, and a Hewlett-Packard 1037A Refractive Index (RI) Detector. Detector signals were collected using ASTRA 5.3.2.12 software from Wyatt. Varian Polystyrene Low EasiVials polystyrene standards (12 polystyrenes ranging from 0.1-38.6 kg/mol M_n) and narrow-distribution polystyrenes from Scientific Polymer Products (M_n of 196.7, 8.9, and 4.8 kg/mol) were used to calibrate the retention time of the columns.

Samples were prepared at 0.1-0.01 mg/mL concentration in THF and filtered through a 0.02 micron membrane to remove any undissolved solids. A 0.5 µL injection loop was used for inserting samples into the chromatography columns. Normal sample elution times ranged from 12-24 minutes.

3.3.2.1 GPC-SEC Analysis – Custom GPC Analysis Software

Raw RI, UV, and LS data were exported from the ASTRA collection program and analyzed using a custom MATLAB program, GPC-SEC Analysis, seen in Figure 24.

Molecular weights (n-, w-, and z- averaged) are calculated by defining the boundaries of peaks and comparing elution volumes to a standardized calibration curves.

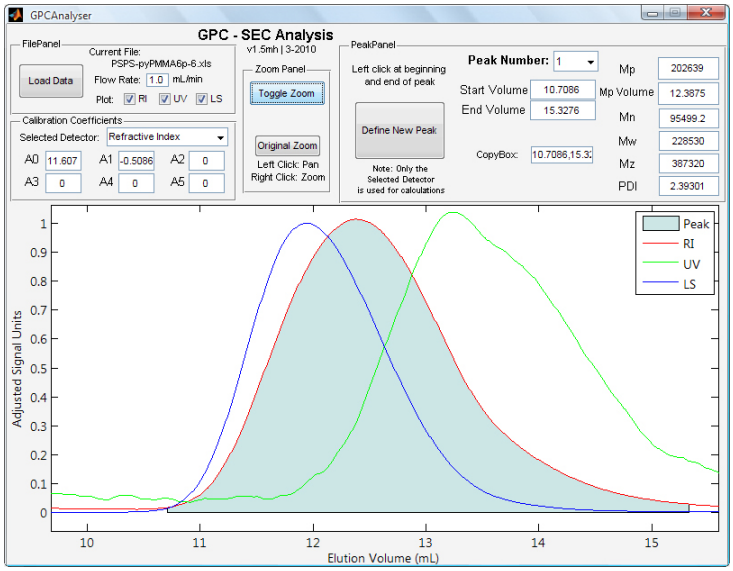

Figure 24. Interface of the GPC-SEC Analysis program with loaded GPC data featuring RI, UV, and LS traces

3.3.3 Differential Scanning Calorimetry

Differential scanning calorimetry (DSC) is used for precise characterization of latent heats and onset temperatures of thermal phase transitions. For polymeric samples, DSC can determine T_g, T_m, and the latent heat of these transitions. DSC heats a sample material within a sealed pan at a constant rate and measures the heat flux. By comparing this heat flux to that of a reference pan, the heat flow to the material under investigation is found. DSC is conducted in a nitrogen environment to minimize sample oxidation.[107]

A TA Instruments Q1000 was used for DSC. Samples of 5-10 mg were crimped in hermetic aluminum pans. An additional empty pan was used as a reference. Test runs consisted of 10ºC/min Cool/Heat/Cool/Heat cycles spanning -10ºC to 50ºC above the

highest T_g or T_m of the blend components. Data were analyzed using the TA Universal Analysis software package.

3.3.4 Thermogravimetric Analysis

In thermogravimetric analysis (TGA), a polymeric sample is continuously weighed while heated at a constant rate to the point of complete degradation. By plotting residual mass verses temperature, a thermal degradation profile of a material can be analyzed. TGA is thus capable of resolving the stability and lifetime of polymeric products in different thermal environments. In the case of polymer blends and composites, TGA is also capable of discerning compositions of the phases, presuming that the degradation temperatures are sufficiently different. TGA is conducted under a nitrogen environment to prevent oxidation of samples.[107]

A TA Instruments Q600 was used. Each run filled an alumina ceramic pan with 10-20 mg of sample material which was then placed, along with a reference pan, onto the balance arms in the Q600. Runs consisted of a 10 ºC/min ramp from 30-600 ºC. Data were analyzed using the TA Thermal Analysis software. Degradation temperature was calculated by two methods, onset point and 95% component mass. The onset point method found the intersection of the tangent lines of the mass curve at the initial plateau and during well-developed degradation. 95% component mass method defined the degradation temperature as the point where 5% of the total mass had been lost.

3.3.5 Tensile Testing

Mechanical testing of the samples was conducted in accordance to ASTM standards. Dogbone-shaped samples are pulled linearly at a constant extension rate until

failure. Analysis of the deformation profile provides yield strength, elastic (Young's) modulus, and breaking strength.

A Tinius Olsen H5K-S Universal Tester is equipped with a 1000 N load cell. Dogbone testing samples were melt pressed from powder, cut from pressed polymer sheets using a Dewes-Gumbs Manual Expulsion Press (ASTM D1708) or molded using the Atlas LMM (ASTM D638). Samples were tested at an extension rate of 0.5 in/min until failure and raw force vs. extension data were exported for further analysis.

3.3.5.1 Tensile Test Analyzer – Custom Destructive Tensile Analysis Software

Raw data from the Tinius Olsen Universal Tester were loaded into a custom-written MATLAB program, Tensile Test Analyzer (Figure 25). Force and extension is automatically converted to stress and strain by entering the sample dimensions.

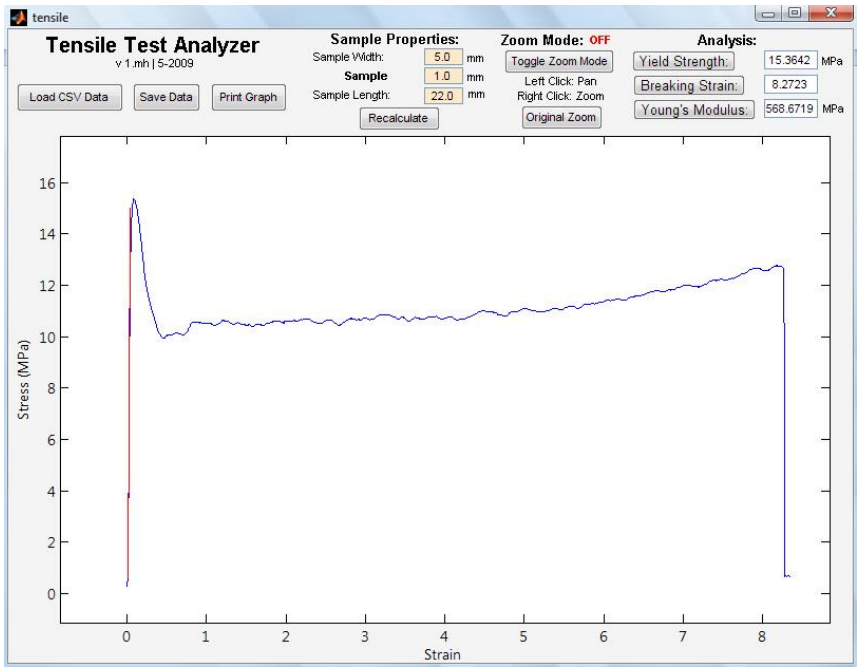

Figure 25. The Tensile Test Analyzer program with data from HDPE. Note red line on the left signifying initial slope to calculate Young's modulus.

Yield strength, as defined by the maximum strength prior to extended plastic deformation, and breaking strength are automatically calculated, while elastic modulus is calculated by selecting two points in the linear elastic regime which define the initial elastic deformation slope.

3.3.6 Dynamic Mechanical Analysis

Dynamic mechanical analysis (DMA) provides means of determining the mechanical response of materials over a wide range of temperatures or tension frequencies. Sinosoidal tensile strain is imposed on a sample slab and the stress response is separated into storage and loss components. Accordingly, storage and loss moduli are related by:

$$E^* = E' + iE'' \qquad \textbf{Equation 8}$$

where E^* is the complex modulus, E' is the storage elastic modulus, and E'' is the loss modulus. Alternatively the material damping coefficient, tan δ, can be calculated by:

$$\tan\delta = \frac{E''}{E'} \qquad \textbf{Equation 9}$$

DMA was conducted using a TA Instruments RSA3. Rectangular samples were cut from pressed sheets and subjected to dynamic temperature ramp tests over a temperature range from ambient to 150ºC with a heating rate of 5ºC/min at 0.01% strain.

4. Solid-State Polymer Blending via Cryogenic Milling

Cryogenic milling (cryomilling) is a batch-scale solid-state milling process in which the milling vial is maintained at very low temperatures by liquid nitrogen. In the case of polymers, repeated high energy impacts of a milling medium induces great amounts of shear, cold fracture, and welding in the polymer chains. While such non-equilibrium processing has been shown to affect the morphology of polymers, both neat and blended, the proposed mechanisms of these changes have not been directly demonstrated. In this chapter, two distinct studies of different polymer blend systems undergoing cryogenic milling are discussed. First, PS-PMMA blends containing labeled PMMA segments are used to chemically confirm the occurrence of mechanochemical in situ block copolymer formation during milling. Secondly, a model PS-HDPE system is subjected to varying levels of milling and post-milling processing for a fundamental understanding in processing-structure relationship.

4.1 Quantitative Detection of Block Copolymer Synthesis during Cryogenic Milling

While free radicals have been shown to be produced due to the mechanical processing and fracture of polymers,[60, 61] creation and behavior of these radicals have never been directly demonstrated for cryogenically milled polymer blends. The previous studies on cryomilled blends have only postulated or presumed the free-radical formation and in situ block copolymer formation.[28] The difficulty lies in isolation and detection of the block copolymers dispersed within the individual polymer species. Because the minimum block size created through chain scission is rather large (approximately the molecular weight of entanglement of the neat polymer), copolymers have similar solubility and insolubility in typical chemical solvents as the component polymers.

Additionally, due to the limited control of where along the backbone chains fracture during solid-state processing, the block copolymers form a large distribution of chain and block lengths, preventing effective size exclusion through chromatography.

Researchers at Northwestern University have developed a process for detecting the occurrence of block copolymer-forming reactions in another mechanochemical process, solid-state shear pulverization. A polymer was synthesized with a florescent label covalently attached to the chains, and pulverized with a different polymer species of higher molecular weight. The resulting blend was run through a GPC with an ultraviolet detector set to measure the elution concentration of only the labeled chains. Post-pulverization, 7% of all polymer chains containing the label were found to elute at molecular weights higher than the original labeled chain, indicating fragments of the labeled chain were transferred onto segments of the high molecular weight species. The scenario of high molecular weight labeled chains being formed through crosslinking was discounted when the blend readily dissolved in THF.[9]

This experiment applies the same principles and methods developed by Northwestern University to cryogenically milled blends to positively detect and quantify, for the first time, block copolymer species created via mechanochemical reactions. A blend of commercial grade polystyrene and synthesized, pyrene-labeled poly(methyl methacrylate) (pyPMMA) was chosen as the model system due to both components being readily solvated by THF and the increased affinity of PMMA radicals to terminate via disproportionation than other polymer species studied during free-radical polymerization.[65, 66, 100]

4.1.1 Experimental Procedure

Pyrene-labeled PMMA was synthesized as discussed in Chapter 3 (M_n=68,000 g/mol , M_w=115,000 g/mol) and polystyrene was procured from Polysar. The Polysar polystyrene offered a slightly higher molecular weight (M_n=114,000 g/mol M_w=326,000 g/mol) than the Ineos Nova polystyrene used throughout the remainder of this thesis and was used to encourage formation of high-MW copolymer species for detection. The two polymers were added to the cryomill vial at 80/20 wt% composition and cryomilled for 15 cycles consisting of 4 minutes of milling at 10 Hz followed by 4 minutes of cooling. The cryomilled powder was dissolved in THF and run through a GPC with a UV detector set to a wavelength of 343 nm, the maximum absorbance peak of the pyrene-labeled PMMA. For each sample, three GPC traces were taken to ensure reproducibility and minimize baseline noise.

4.1.2 Results and Discussion

Figure 26 shows the UV detection response (wavelength = 343 nm) of the pure PS and pyPMMA polymers when eluting from the GPC columns. As expected, the UV detector does not detect the PS while showing a strong response for the pyrene label of pyPMMA. These results confirm that the response of the UV detector at 343 nm is solely due to the presence of the pyrene label and can be used to quantitatively measure its distribution.

The results of cryogenically milling PS/pyPMMA can be seen in Figure 27, compared to the UV response of neat pyPMMA. Significant broadening of the response peak indicates that significant chain scission occurred, resulting in an M_n of 17,600 g/mol and M_w of 72,300 g/mol in the labeled components the milled blend. The shoulder seen at

~14 mL corresponds to molecular weights of ~33,000 g/mol, or approximately half the M_n of the original pyPMMA chains, suggesting chain scission occurred close to the center point of the chains.

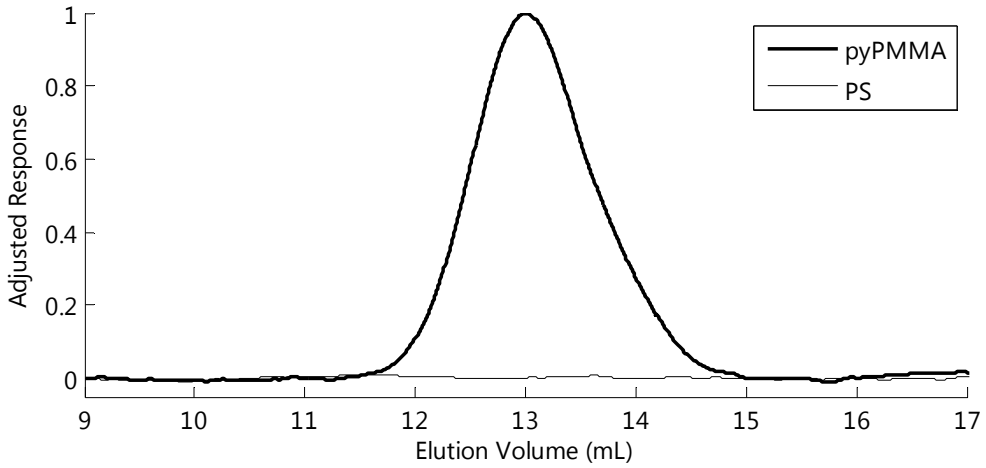

Figure 26. GPC-UV absorbance response of pure polystyrene and pyPMMA eluting from the GPC at a wavelength of 343 nm. The UV detector does not detect the unlabeled polystyrene while showing a strong response for pyPMMA

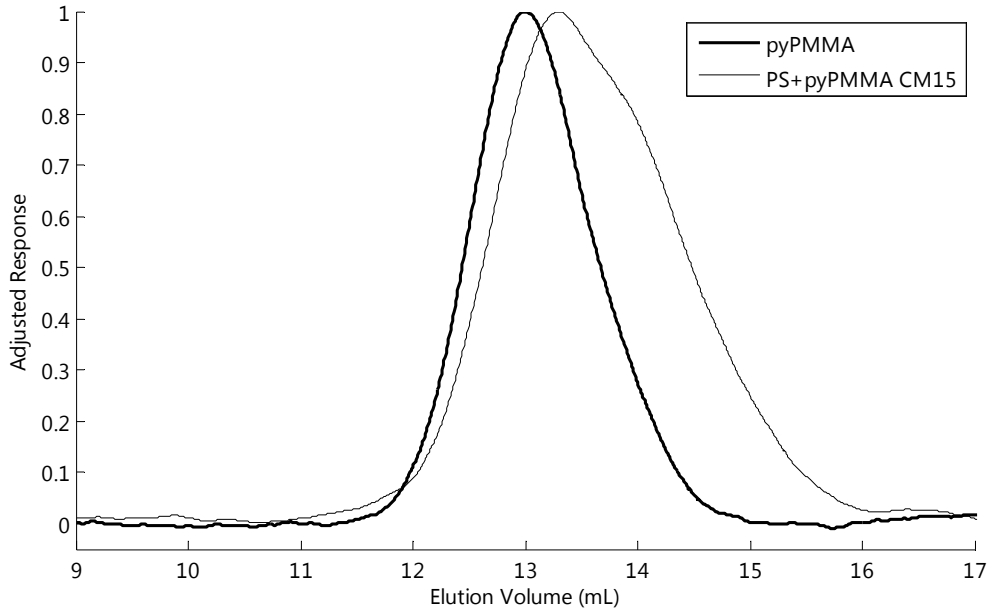

Figure 27. GPC-UV absorbance response of the PS/pyPMMA cryomilled blend compared to neat pyPMMA

The response between 10.5 mL and 12 mL elution volume shows that the cryomilled blend has an earlier peak onset. The signal peak begins at 10.75 mL for the cryomilled blend while the neat pyPMMA peak begins at 11.5 mL.This signal at earlier elution volumes indicates the cryomilled blend contains labeled polymer species of greater molecular weight than those contained within the neat pyPMMA. This response area is enlarged in Figure 28, and corresponds to molecular weights between 274,000 g/mol and 2,560,000 g/mol.

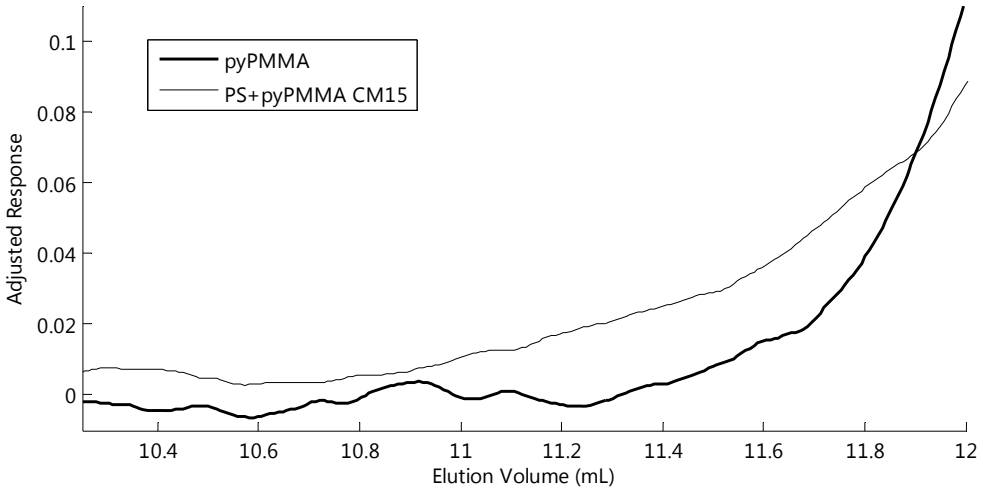

Figure 28. Enlarged response of blends from Figure 27 showing pyrene-labeled high-MW species in the PS+pyPMMA not originally present in the neat pyPMMA. Note the blend peak begins at 10.75 mL while the neat pyPMMA peak begins at 11.25 mL.

Integration of the cryomilled blend peak reveals that 1.5% of the pyrene label is contained within this early response. This indicates that at least 1.5% of the pyPMMA has undergone chemical modification and is now part of chains which are significantly higher molecular weight than those present in the initial polymer. These larger chains could be generated by either block copolymer-creating free radical disproportionation between the pyPMMA and high molecular weight PS or crosslinking between the labeled

species, as PMMA has been shown to undergo chemical crosslinking when cryogenically milled for extended periods.[76] If crosslinking is the cause of these high MW chains, milling pyPMMA alone would show a similar early peak onset. As seen in Figure 29, pyPMMA which was cryomilled alone for 15 cycles exhibited no UV absorbance signal before 11.5 mL elution volume, indicating no high-molecular weight species were present. This lack of an early peak onset or high-molecular weight polymer chains in the cryomilled pyPMMA indicates that the species formed in the cryomilled PS/pyPMMA blend are due to chain transfer between the two blend components.

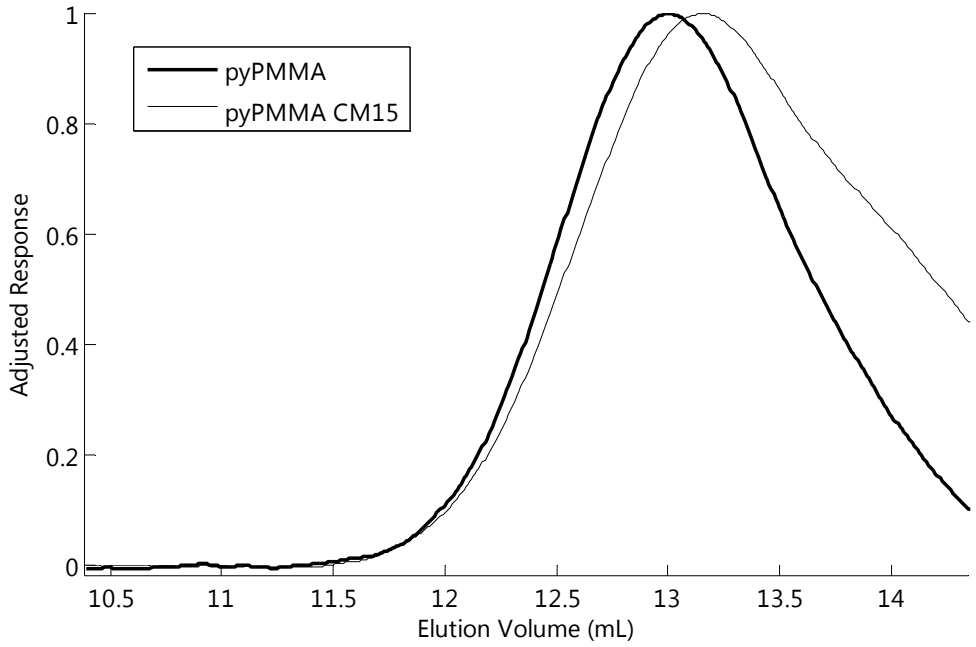

Figure 29. UV absorbance response of neat pyPMMA compared to pyPMMA which was cryogenically milled for fifteen cycles. Both peaks begin at ~11.25 mL.

While this study unquestionably confirms that at least 1.5% of the pyPMMA chains are forming copolymers with the higher molecular weight PS, it does not suggest that only this amount of chain transfer is occurring. Copolymers of a large distribution of

sizes are expected to be created as the point of scission on a polymer chain cannot be controlled during cryomilling. Copolymers of chain sizes equal to or smaller than the original pyPMMA material cannot be differentiated using GPC.

4.1.3 Summary

Although assumed to be occurring during cryogenic milling, the in situ production of block copolymers through mechanochemical reactions had not been observed until this study. Based on cryogenically milled labeled poly(methyl methacrylate) with higher molecular weight polystyrene, the creation of high-molecular weight species containing a florescent label was demonstrated. At least 1.5% of the labeled polymer chain was detected by a UV detector at the end of a GPC column at molecular weights higher than those in the neat labeled PMMA. It was shown that these high molecular weight species were not due to crosslinking of the labeled chains, but free radical disproportionation between the labeled polymer and the high molecular weight species with which it was blended. While at least 1.5% of the labeled PMMA was shown to react with polystyrene chains, this by no means is a full quantification of the amount of block copolymer created, as copolymers of sizes equal to or less than the original labeled PMMA chains could not be isolated.

4.2 Effect of Cryogenic Milling on the Static Growth of Dispersed Domains

There have been several studies into the development of cryogenically milled polymer blends when exposed to high temperatures, but only using samples press or injection molded directly from powder or cast from a solution. Powder of cryomilled PC/poly(aryl ether ether ketone) (50/50 wt%) was press molded and compared to injection molded samples created at different barrel temperatures using atomic force

microscopy, transmission electron microscopy, and scanning transmission x-ray microscopy. It was concluded that the fine microstructure of the pressed powder could not be retained when heating the blends above the glass transition temperature of the components.[16] Stranz reported a smaller, refined spherulitic morphology in a solution-cast thin film of a cryomilled blend of PMMA/polyvinylidene fluoride as compared to an unmilled blend.[83] An investigation by Smith pressed cryomilled PMMA/poly(ethylene-*alt*-propylene) powder and sustained a melt for up to one hour to qualitatively investigate static coarsening.[80]

In all previous studies, raw cryomilled powder was pressed or molded with limited mixing in the melt phase. However, in the real world, powdered materials are often subjected to more rigorous heat treatment, such as post-process modifications and product shaping. For example, many commercial polymers are pelletized prior to industrial applications due to containment, transportation, and safety concerns, and many final polymer products are produced through mixing-based extrusion processes. Given these operations, cryomilled blends must be able to retain their improved properties despite extended mixing while in the melt.

The system under study is a blend of polystyrene and high-density polyethylene (PS/HDPE) at 80/20 wt% composition. This system was chosen due to its complete immiscibility, inclusion of both amorphous and semi-crystalline components, and the widespread preexisting production and use of both components in the industry. The morphology of a cryogenically milled blend is analyzed following intimate mixing in the melt state and long-term exposure to elevated temperatures. Using a method developed by researchers at University of Minnesota,[29] Northwestern University,[34, 36] and

elsewhere,[5, 18, 28] monitoring the growth of the dispersed phase domains upon extended heat treatment will be used to determine the effectiveness of cryogenic milling in blend compatibilization and stabilization to melt-mixed processes.

4.2.1 Experimental Procedure

Blends of PS/HDPE (80/20 wt%) were fabricated through cryogenic milling with five and ten cycles, here on referred to as CM5 and CM10, respectively. Blends were melt-mixed using an Atlas Laboratory Mixer Molder for five minutes and then pressed and annealed in the presence of air into ~0.7 mm sheets using a Carver Laboratory Press at 204ºC. Annealing time (t_a) varied from 5, 30, 60, 120, to 240 minutes. Two control blends were similarly processed, one made from melt-mixing neat polymer pellets and the other from melt-mixing PS and HDPE powders cryomilled independently for 10 cycles, referred to as the pMM (pellet melt-mixed) and mMM (milled melt-mixed) blends, respectively. Melt-mixing in these samples was conducted in the Atlas LMM for five minutes. After annealing, samples were cryogenically fractured and analyzed using an SEM to measure the size of the dispersed HDPE domains. For each processing condition and anneal time, 200-1,200 domains were measured to ensure a reliable particle size measurement using a custom image analysis software, as described in Chapter 3. The average dispersed domain diameter, D_n, and the second moment of the domain distribution, μ_2, were calculated from these measurements.

4.2.2 Results and Discussion

SEM micrographs were taken between 300x-4000x magnification to maximize number of dispersed domains captured while still being able to resolve the smallest domains. As previously mentioned, blends which were compatibilized to a greater degree

would exhibit smaller domains due to stabilization of the interface by block copolymers created by milling-induced mechanochemical reactions.[28, 34] Figure 30 shows the typical micrograph of a processed blend. Two dimensional projections of the dispersed domains appear well-defined and slightly elliptical with a gradual shading gradient from the edges to center. Occluded domains are dispersed domains which are partially obstructed. Fully-exposed dispersed domains can be distinguished from occluded domains from the well lit edges created by the reflection of secondary electrons from the PS surface. Holes, or the impressions left in the continuous PS phase by dislodged HDPE domains, also have highlighted edges, but can be distinguished by a much sharper shading gradient to a dark center.

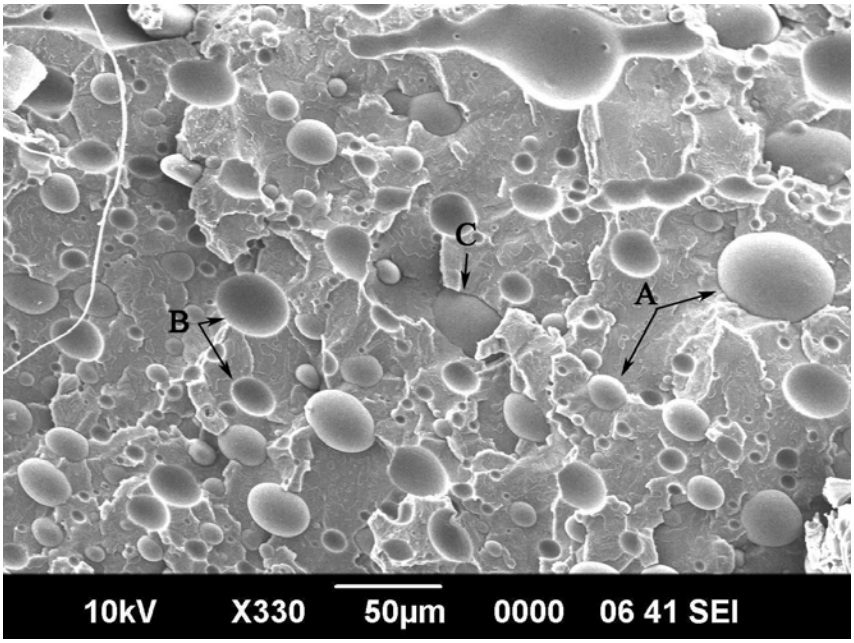

Figure 30. A typical SEM micrograph of a cryomilled PS/HDPE following post-processing. A: Well-defined projections of HDPE domains, B: Holes left by dislodged HDPE domains, C: An occluded HDPE domain

In this study fully visible, non-occluded dispersed phases were measured while holes and occluded domains were disregarded. Previous studies using SEM micrographs

to determine D_n have included holes in determination of an average domain size.[34, 95] As seen in Figure 31, holes can only reflect dispersed domain size accurately when the fracture occurs on the center line of a domain. Also possible is that the immediate environment around the dispersed domain promotes fractures favoring a particular side of the sphere, resulting in the domain being preserved in one side of the new surface and the creation of a hole which is non-representative of the size of the domain which was dislodged. As these ideal and non-ideal holes cannot be distinguished, including holes in average diameter calculations biases the results towards smaller sizes.

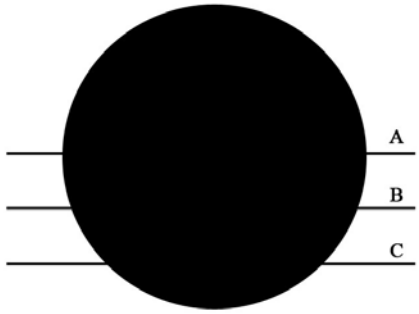

Figure 31. Diagram showing how hole size cannot be an accurate approximation to dispersed phase diameter. A: Ideal fracture site gives a true measure of the domain diameter, B&C: Fractures at non-ideal sites induced by the local environment and defects will produce holes with greatly reduced diameters on one side of the fracture and occluded domains on the other.

A graph of the average dispersed phase diameter (D_n) growth in cryomilled blends subjected to melt mixing and static annealing can be seen in Figure 32. Initially, the mMM, CM5, and CM10 blends have a smaller D_n than found in the pMM blend. This grouping indicates that simply milling results in a reduction of initial D_n, however, upon annealing the D_n for mMM rapidly grows to values surpassing the pMM control while CM5 and CM10 remain on average 0.97 μm and 1.8 μm smaller than the pMM blend, respectively. These widely divergent growth patterns indicate that while the mMM blend

is capable of forming reduced domain sizes in the shear flow of melt-mixing, it is not compatibilized against further heat treatment like the alloyed blends. The initial reduction in D_n of the milled blends following shear flow could be due to a reduction in viscosity from decreased molecular weights, as seen in polymers of the pyrene-labeled study (Section 4.1.2) and reinforced by the viscosity-dependence of the Taylor Equation in Chapter 2 (Equation 6). This concept is explored further below with analysis of the molecular weights of the current blends. Meanwhile, the stabilization of the initial domain reduction is exclusive to the cryogenically alloyed blends, suggesting that the block copolymers previously showed to be created during blend milling are successfully compatibilizing the blends, regardless of any molecular weight decreases. CM10 maintains a D_n smaller than CM5 throughout all anneal times, indicating that the increased number of milling cycles created additional block copolymers. The overall compatibilization effect between the CM5 and CM10 blends is less than that seen between the pMM and CM5 blends. This suggests that there is a diminishing return with increased milling cycles. The additional five cryomilling cycles between the CM5 and CM10 blend did not produce as much compatibilization as seen between the pMM and CM5 blends.

An explanation for the decreasing compatibilization efficiency, along with the low initial D_n for the mMM blend followed by rapid growth during annealing, can be described by the molecular weight reduction associated with the milling process. Table 4 shows molecular weight data from the GPC analysis of the PS phase of cryomilled PS/HDPE blends and cryomilled neat PS.

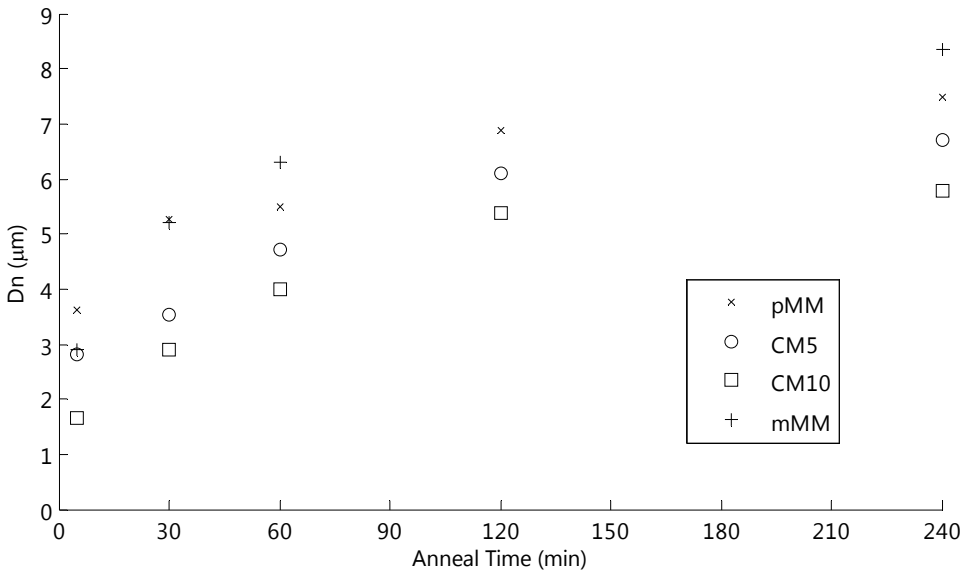

Figure 32. Growth of the average dispersed phase diameter following melt mixing and sustained static anneal at 204ºC

Selective dissolution of the PS from the PS/HDPE blend was conducted using THF at room temperature with five minutes of agitation. Solids were filtered from the solution using a 0.02 µm filter. The filtered PS solution did not contain any PS-HDPE block copolymers created during milling, which was confirmed via lack of an HDPE melting point observed on DSC trials. Additional confirmation that block copolymers were not solvated in THF was found by dissolving the cryomilled blends in THF, casting a thin film from the filtered solution and performing Fourier Transform Infrared Spectroscopy (FTIR). Films were cast on coated aluminum in a fume hood until solid and dried in a vacuum oven at 100°C for 24 hr to remove excess solvent. FTIR analysis was conducted using a Nicolet 380 FT-IR from the Thermo Electron Corporation. The thin films were confirmed to lack the characteristic wide PE absorbance peak between 2,700-3,100 cm^{-1}.

It can be seen that number average PS molecular weight of the blends is significantly reduced with increasing milling time (16.9-32.5% reduction). Weight

averaged molecular weight initially rose 7% in CM5 and then fell 8% (compared to neat PS) in CM10. These values for M_n and M_w indicate that there are a greater number of shorter chains present in the cryomilled blends than the initial PS, which is reasonable considering that chain scission is promoted during cryomilling.

Table 4. GPC data for cryomilled PS and the PS phase of PS/HDPE blends

Sample	M_n (g/mol)	ΔM_n (%)	M_w (g/mol)	ΔM_w (%)	PDI
Neat PS	97,700	-	251,000	-	2.6
Cryomilled PS/HDPE 5 Cycle	81,200	-17	268,000	7	3.3
Cryomilled PS/HDPE 10 Cycle	65,900	-33	231,000	-8	3.5
Cryomilled PS 10 Cycle	69,400	-29	247,000	-2	3.7
Cryomilled PS 15 Cycle	55,900	-43	272,000	8	4.9

The PDIs showed a large increase from neat PS to CM5 while the increase between CM5 and CM10 was much smaller. This broadening of the chain size distribution concurs with previous reports of initial peak broadening during cryogenic milling of polystyrene.[73] Similar trends were seen when polystyrene alone was cryomilled, indicating that the presence of the HDPE component in the alloyed blends neither inhibited nor promoted chain scission.

The large reduction in PS M_n indicates an increase in the number of smaller-length chains in the cryomilled blends. Smaller polymer chains, as predicted in the Flory-Huggins theory,[19, 20] will result in increased chain mobility at elevated temperatures and in the melt. In an immiscible blend, the lower melt viscosity of the matrix would

ultimately increase the general mobility and diffusion rate of the dispersed phase. In terms of quantities measured, a higher diffusion rate would promote quicker growth of D_n or a larger D_n for any given anneal time. Such phenomena would account for the differences in D_n between the two control blends at longer anneal times and could also be a contributing factor to the gradually diminishing compatibilization efficiency of successive cryomilling cycles. While additional block copolymer is being created, its stabilizing effect is countered by the overall reduction in M_n. Such a mechanism would result in overall compatibilization being a balance between the degree of molecular weight reduction and block copolymer formation.

An application of Crist's polymer blend growth model (Equation 7) to the cryomill blends results in the trends seen in Figure 33. Individual figures with the linear regression equations and R^2 values can be found in Appendix A.

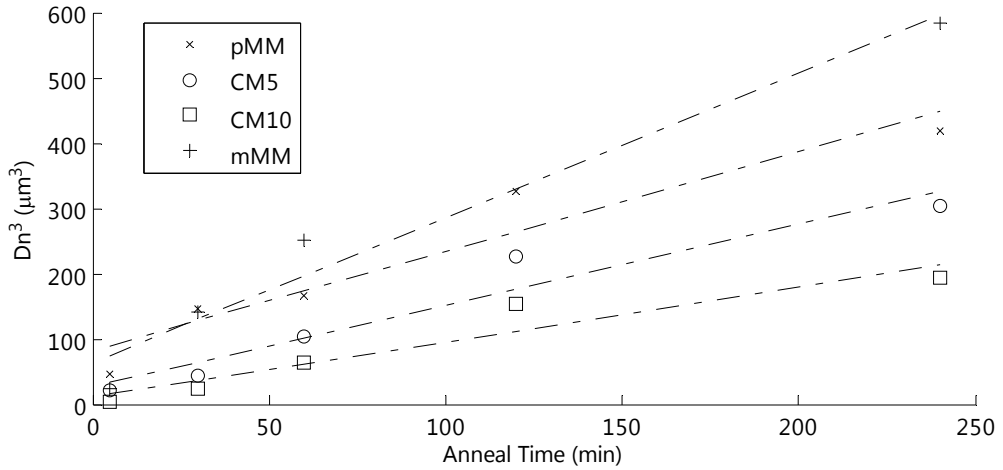

Figure 33. Application of the Crist growth model to the cryomilled PS/HDPE blends

Although all R^2 values are reasonable (>0.9), data points at 120 minute anneals consistently fall above the predicted trend while 240 minute anneals are consistently beneath the trend, indicating a poor model fit. Previous studies have demonstrated that

highly immiscible blends exhibit very rapid initial growth due to vigorous coalescence before transitioning into the typical Ostwald ripening and moderate coalescence regimes described by Crist. Such growth rate evolutions have been documented in polyethylene/hydrogenated polybutadiene and polyisoprene/polybutadiene (PI/PB) blends.[108, 109] In the PI/PB blends at 82°C, a rapid growth rate of on the order of 1 μm^3/min was observed for the first thirty minutes, followed by a 40 minute transition growth of approximately 0.01 μm^3/min, and finally the blend exhibited a final consistent growth rate of 10^{-4} μm^3/min.[108] A similar phenomenon may be occurring in the current PS/HDPE blend. Table 5 lists the "initial" growth constants observed for data points between 5 and 120 minutes and the "second stage" growth rate between the 120 and 240 minute data points. The 120 minute data point for mMM was extrapolated from the initial regression. Individual plots of the regression for each blend can be found in Appendix A. The initial growth rates are comparable to the rapid growth previously reported in the PI/PB blends, while the second stage growth for each blend is of similar magnitude as the reported transition region. The R^2 values for the initial growth rates were in all in excess of 0.98. These growth rates indicate that the cryomilled and control PS/HDPE blends are exhibiting a more complex growth mechanism than the Crist model predicts, but has been documented to other blend systems.[108, 109]

Table 5. The initial growth constant of PS/HDPE blends (omitting the 240 minute annealing data point), and the growth between the 120 and 240 minute data points.

Sample	Initial K $\left(\frac{\mu m^3}{min}\right)$	120min→240min K $\left(\frac{\mu m^3}{min}\right)$
pMM	2.29	0.77
CM5	1.84	0.63
CM10	1.34	0.32
mMM	4.11	0.68

Comparing the values in Table 5 shows the mMM blend exhibits the greatest initial growth rate, while that of the pMM blend is the second largest. This indicates that the 30% reduction of M_n in the milled control blend increased chain mobility and therefore promoted the initial growth rate to rise by 44%. While the CM5 and CM10 blends also had significant reductions in M_n (17% and 33%, respectively), they were compatibilized by the mechanochemically-synthesized block copolymers and featured initial K decreases of 20% and 42% compared to blending pellets. The second stage growth data above 120 minutes indicate that the pMM, mMM, and CM5 blends exhibit similar rates. CM10 continues to have a reduced growth rate of approximately half of the other rates.

All analysis thus far has utilized previously-reported techniques of imaging the idealized two dimensional projections of the three dimensional dispersed domains to characterize the compatibilization of cryomilled PS/HDPE blends. This technique relies upon a simple arithmetic mean of the dispersed domain diameter without statistical characterization regarding the distribution. This may be sufficient when measuring and minimizing dispersed phase size is the primary goal or comparing results between research groups, but when material compatibilization is the metric of study, this value may be overly simplistic. For example, while both sets of figurative particles in Figure 34 have approximately similar average particle sizes, the left set is monodisperse while the right has a large variance. A sample with monodisperse domains has all interfaces saturated with compatibilizing block copolymers and growing at a low, constant rate. A sample with large variance, on the other hand, has poor dispersion of block copolymers

or insufficient copolymers for critical interface saturation, resulting in some domains growing faster than others. Mechanically, the properties of large-variance samples are unfavorably inconsistent due to larger defects.

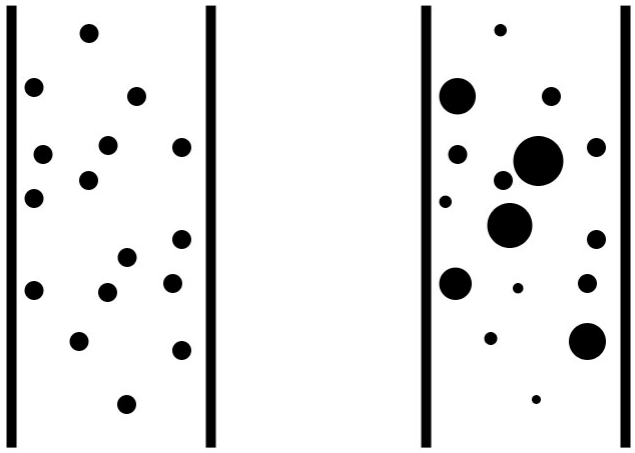

Figure 34. Example of the importance of characterizing the dispersed phase distribution with regards to compatibilization

For these reasons, it is proposed that the definition of compatibility incorporates a second factor that takes into account the distribution of dispersed domain sizes, in addition to the established D_n values. The simplest means of conveying this information is through histograms of D_n values, such as in Figure 35. Histograms allow for rapid conveyance of how the domain size distribution grows with increasing annealing time. Histograms for each blend can be found in Appendix A. Limitations arise when attempting to compare two similar distributions (see the 120 and 240 minute histograms in Figure 35), or when quantitative descriptions of the distributions are desired. The simplest and most statistically sound method of describing the domain distribution is to calculate the variance of the sample domains.

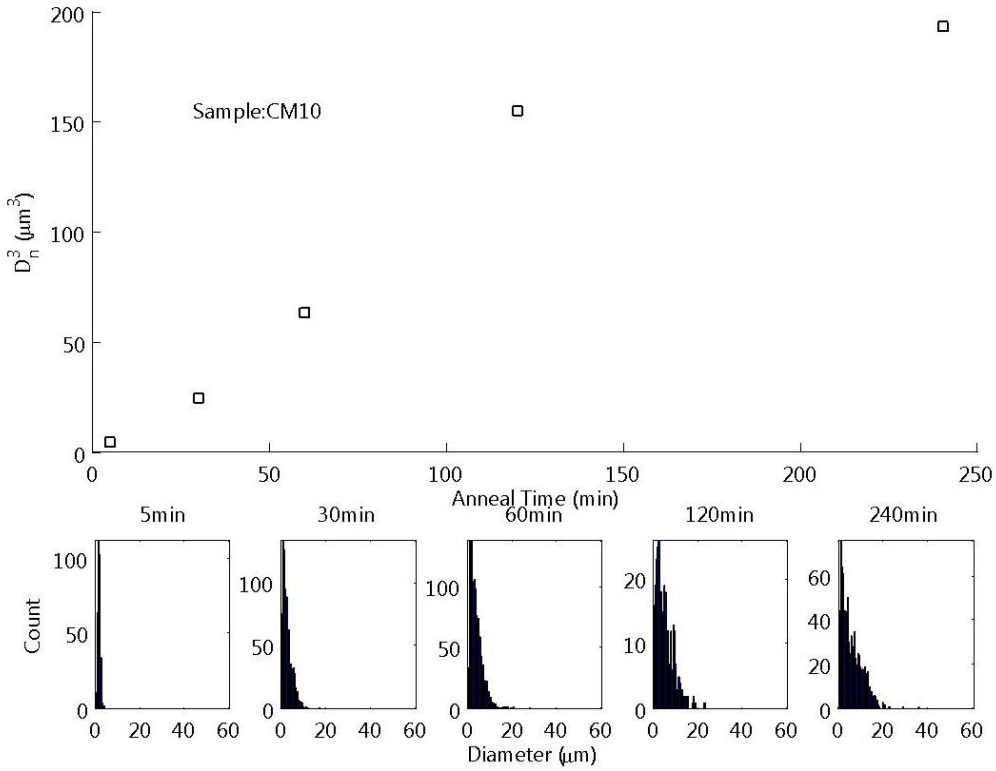

Figure 35. Inclusion of histograms allow for rapid identification of domain size distribution and growth during annealing

Variance, also known as second moment of the distribution (μ_2), is calculated by:

$$\boldsymbol{\mu_2 = \frac{1}{N}\sum_{i=1}^{N}(D_i - D_n)^2}$$

Equation 10

where N is the number of domain diameters, D, in a distribution and D_n is the average domain diameter. Third, forth, and higher moments describe skewness (sidedness) and kurtosis (peakness) relative to a normal distribution.[110] As all distributions in this investigation are essentially single-sided and present well-resolved peaks, these higher order values were not considered. Physically, the significance of the domain variance in a sample is dependent on the relative magnitude of the average domain size. A sample with

a D_n of 1 would have a much more significant variance of 3 than a sample with a D_n of 20 and variance of 3. To account for this sensitivity, a "variance ratio" is defined as seen in:

$$\mu_2' = \frac{\mu_2}{D_n}$$

Equation 11

This term tends to zero as a distribution becomes monodisperse and is unbounded as variance increases.

Table 6 compiles the variance calculations for the cryomilled and control blends. Note that the variance and variance ratios generally start low and grow with increasing anneal time.

Table 6. Variance analysis of PS/HDPE (80/20 wt%) cryomilled blends when annealed at 204°C

Sample	Anneal Time (min)	D_n (μm)	μ_2 (μm)	μ_2'
pMM	5	3.62	6.26	1.73
	30	5.27	18.8	3.58
	60	5.50	40.0	7.27
	120	6.88	33.3	4.83
	240	7.48	45.5	6.09
CM5	5	2.82	2.46	0.87
	30	3.53	8.66	2.45
	60	4.71	13.3	2.82
	120	6.10	30.4	4.98
	240	6.72	29.2	4.35
CM10	5	1.67	0.29	0.18
	30	2.91	4.64	1.59
	60	3.98	8.76	2.20
	120	5.37	15.9	2.96
	240	5.78	20.7	3.58
mMM	5	2.90	5.14	1.77
	30	5.19	21.8	4.20
	60	6.31	20.1	3.19
	240	8.35	26.7	3.19

CM5 and CM10 exhibit much smaller initial variance ratios than pMM and mMM, demonstrating that the block copolymer formed during the cryomill process not only

reduces the initial domain size, but also reduces the variance of the domain sizes. Blend mMM also exhibits low variance ratios compared to the other control, indicating that the reduced M_n caused by cryomilling might be a contributing factor to the consistency of the domain diameter variance during annealing.

4.2.3 Summary

The growth of PS/HDPE (80/20 wt%) polymer blends fabricated via cryogenic milling subjected to static annealing at 204ºC following melt-phase mixing has been studied. Cryogenically milled blends exhibited decreased average dispersed domain sizes throughout all anneal times compared to two control samples made by melt mixing as-received polymer pellets and melt mixing independently cryomilled polymers. Blends cryomilled for ten cycles showed smaller domain sizes than those cryomilled for five cycles, however, the suppression of the dispersed domain growth between the ten and five cycle blends was less than that seen between the five cycle and control blends. The initial domain size of the CM10 was smaller than the CM5 or mMM blends, and much smaller than the pMM blend. This indicates the alloying process decreased the interfacial surface tension experienced by the blends during the shear flow of the melt-mixing process, allowing for greater drop shear and smaller particle creation. Analysis of the molecular weight of the PS component in the cryomilled blends indicates that increasing numbers of milling cycles leads to a decrease in number-averaged molecular weight. This decrease could account for the diminishing effectiveness of milling cycles, as lower molecular weight PS would allow for easier and faster growth of the HDPE dispersed domains.

Rather than directly applying the single rate constant model for immiscible polymer blend domain growth by Crist, the data were separated into an initial, rapid growth period from 5-120 minutes and a second growth region between 120 and 240 minutes. Determining growth constants in these stages led to comparable values to published blend growth data which exhibits rapid growth followed by a slower growth regime that conforms to the Crist model at long anneal times. The M_n decrease due to milling encourages chain mobility, lower melt viscosity, and by extension, greater growth rates. The mMM blend has the largest initial growth rate followed by the pMM blend. The CM5 blend featured a reduced initial K compared to the pMM control, while the K of CM10 was even smaller, indicating that additional cryomilling cycles decrease the initial dispersed domain growth rate. The second stage growth showed CM10 continued to have a reduced K while the other three blends had similar values.

It was also proposed that more information is needed in addition to the average dispersed phase diameter when reporting the change in domain sizes of immiscible blends. In quantitatively describing compatibilization, the variance of the domain sizes could be as important as the average itself. The new methods of reporting this variance were the inclusion of a histogram to demonstrate the spread and means, and the calculation of a variance ratio which describes the variance of the domain size distribution relative the average particle size. Blends subjected to increasing anneal times featured increasing variance ratios, with the mechanically alloyed blends showing smaller ratios throughout all heating times.

4.3 Conclusions

This chapter covered two independent experiments which fabricated polymer blends via the cryogenic mill, a batch scale solid-state processing unit. The blends were cooled to liquid nitrogen temperatures and repeatedly impacted with a stainless steel impactor rod. Morphology analysis was performed using SEM micrographs while molecular weights were characterized using GPC.

Combining the results of both experiments, the successful compatibilization of the cryogenically alloyed blends can be contributed to the block copolymer species mechanochemically synthesized during cryogenic milling, as seen in the labeled polymer study. Additional copolymers are created with additional milling cycles, allowing the ten cycle blend to exhibit the greatest compatibilization. However, the improvements seen between the ten and five cycle alloyed blends was less than seen between the five cycle blend and controls. This indicates that despite additional block copolymer production, successive milling cycles impart less compatibilization. Such an effect could be explained due to the greater reduction of M_n with additional milling cycles, which increases polymer mobility through viscosity reductions to encourage larger domain sizes and variance. Thus, successful cryomill compatibilization becomes an optimization between block copolymer creation and molecular weight reductions.

5. Optimizing Solid-State Shear Pulverization: Effects of Screw Design and Operating Conditions

The newly installed Bucknell University Solid-State Shear Pulverizer (BU SSSP) is an industrially-scalable, continuous instrument for immiscible polymer blend compatibilization. It is more customizable than the cryogenic mill or the SSSP at Northwestern University previously used for blend compatibilization, but the complexity of the system results in the need to elucidate fundamental processing-structure-property relationship, which can be applied to produce the most compatibilized blends. The Northwestern SSSP studies have described the different levels of compatibilization through arbitrary means such as 'harshness' of screw designs. These designations are based largely on tacit experience of operators, and may not fully describe the process. The BU SSSP features an updated design with modified screw configurations not possible on the original SSSP. The goal of this study is to identify and quantify the most significant factors and interactions of factors which contribute to polymer blend compatibilization on the BU SSSP through detailed experimental design and a rigorous application of statistics.

5.1 Full-Factorial Analysis of the Solid-State Shear Pulverizer Operation

The SSSP is a significantly more robust solid-state process than the cryogenic mill. Whereas batch size, milling time, and impact frequency can adequately describe the processing of the cryomill, the SSSP requires many more parameters to fully characterize its operation. Four of these parameters were selected to be investigated in a full 2^4 factorial experiment: number and type of kneading blocks, distribution of kneading blocks, rotation speed of the screws, and material feed rate. Each key factor is described

in additional detail below. Other factors that can be considered in SSSP operations include chiller set point, zone temperature profiles, retention time, feed material shape and size, and final particle size. Many of these additional factors were considered to be directly or indirectly related to the four chosen primary factors. Such secondary factors were deemed to not be overtly influential of the final blend morphology and thus not considered in the full-experimental analysis.

Factor A: Kneading Block Type and Number

Kneading blocks are the primary means of generating the high shear and compression forces which are critical in SSSP. With forward-driving, neutral, and reverse-driving directions available, these kneading elements have a large effect on the retention time, and thus the degree of pulverization action the materials are subjected to while advancing down the barrel. In general, excessive material retention and energy build-up are principal causes of overheating and undesired and irreversible transition from solid state operation to melt state operation. Studying the effect of the different number and types of kneading blocks on final blend compatibilization and SSSP operation will allow screws to be designed for a tailored degree of pulverization and product throughput. In this one factor under consideration, the effects of kneading element number and types are coupled due to processing constraints to maintain the solid state. Analysis of zone operating temperature was later used to differentiate between the contributions of changing kneading block number and changing kneading block type.

Factor B: Distribution of Kneading Blocks

Researchers at Northwestern University were limited in where kneading blocks could be placed in screw designs. The primary pulverization zone was restricted to the

final seven elements, resulting in large heat build-up at the end of the process stream. With the BU SSSP, there is no such concern and the 'pulverization zone' can be distributed along the entire 35 L/D barrel length. This allows materials to cool more efficiently when conveying elements are strategically allocated between the pulverizing kneading blocks. Since such separation is an entirely new configuration, it is important to determine whether this distribution benefits or hinders compatibilization of polymer blends.

Factor C: Screw Rotation Speed

The BU SSSP is capable of achieving higher screw rotation speeds than the first SSSP at Northwestern University. The original SSSP studies limited the screw rotations between 100-400 RPM, while the BU SSSP is capable of up to 600 RPM. Screw speed affects both the retention time of material within as well as the rate of shear applied by each kneading block. Such a combined effect likely has a large impact on the degree of compatibilization.

Factor D: Polymer Pellet Feed Rate

The final factor under consideration is pellet feed rate. Experiments at Northwestern University have indicated that increasing the rate of polymer pellet feeder elevates processing temperatures which could result in the undesirable loss of the solid state. Industrial applications often require very high product output, and therefore determining the maximum feed rate for a given case of polymer blend compatibilization is very pertinent.

5.2 Experiment Design

A full two-factorial experiment was designed with the four selected operating factors in either a 'high' or 'low' setting, as described in Table 7. These high and low settings were set in reference to the typical operating conditions of the NU SSSP: 13 kneading blocks, which are not distributed, rotating at 300 RPM.[98] The feed rate set points were determined by operating the SSSP with the four factors set in a configuration suspected to be the harshest (most heat-generating), defined as the "+ - - +" configuration in the discussion below, and increasing the feed rate until the solid state was lost within the barrel. The high feed rate was set to just below this value while the low feed rate was set at 70% of the maximum.

Table 7. High and low settings for the four experimental factors

	High (+) Setting	**Low (-) Setting**
Kneading Blocks (Factor A)	17 Kneading Blocks Total 11 Forward 4 Neutral 2 Reverse	10 Kneading Blocks Total 7 Forward 3 Neutral
Distribution (Factor B)	Kneading blocks are individually separated by conveying elements	Kneading blocks are grouped into three or four element zones separated by conveying element zones
RPM (Factor C)	450 RPM	250 RPM
Feed Rate (Factor D)	~250 g/hr	~175 g/hr

The experiment consisted of 16 (2^4) sample runs of the SSSP, as described by Table 8. For each experimental factor, high and low settings were utilized, symbolically represented as '+' and '-', respectively. The polymer blends themselves will be referred to using the +/- run abbreviation throughout this study, while the individual factors

(kneading blocks, distribution, RPM, and feed rate) and their effects on measured quantities will be notated by their factor letter (A, B, C, or D).

Table 8. List of all sample run settings for full factorial experiment. + indicates 'high factor' while – indicates 'low factor'

Run Abbreviation	Kneading Blocks (Factor A)	Distribution (Factor B)	RPM (Factor C)	Feed Rate (Factor D)
- - - -	-	-	-	-
- - - +	-	-	-	+
- - + -	-	-	+	-
- - + +	-	-	+	+
- + - -	-	+	-	-
- + - +	-	+	-	+
- + + -	-	+	+	-
- + + +	-	+	+	+
+ - - -	+	-	-	-
+ - - +	+	-	-	+
+ - + -	+	-	+	-
+ - + +	+	-	+	+
+ + - -	+	+	-	-
+ + - +	+	+	-	+
+ + + -	+	+	+	-
+ + + +	+	+	+	+

Two of the experimental factors are based on the screw element configuration, necessitating 4 different screw designs for the factorial analysis, as shown in Figure 36. Certain criteria were maintained while designing these four screw sets. First, the larger 31.25 mm screw elements were exclusively used in Zones 1 and 2 to convey and initially fracture the large polymer pellets. Second, a special transition element followed these larger elements to seamlessly change from their large-flight to the smaller flight of the 25 mm elements. Third, kneading blocks were placed towards the center of each cooling zone, whenever possible. Each zone has 12.5 mm of union space on each end which is

not directly contacted by the recirculating coolant, and thus kneading blocks were not placed within these sections to prevent excessive heat accumulation.

A model blend system of 80 wt% polystyrene (PS) and 20 wt% high-density polyethylene (HDPE) was used during this experiment, allowing the BU SSSP results to be compared to those of the cryogenically milled blends (Chapter 4) and Northwestern University's SSSP.[98] Compatibilization was first defined as minimization of the dispersed HDPE domain size over the course of static annealing (t_a= 5, 60, or 240 min) following melt-based mixing and was quantified by measuring the averaged dispersed domain diameter (D_n), the domain variance (μ_2), and the variance ratio $\left(\frac{\mu_2}{D_n}\right)$ via SEM micrographs and the Polymer Blend Analyzer software. Morphological results were then compared with molecular weight analysis of the SSSP blends.

5.3 Statistical Analysis

All data generated in this study were evaluated through full-factorial analysis to calculate the main effects of each experimental factor in addition to interaction effects. The statistical analysis is based on a model described by Daniel.[111, 112] Equation 12 shows the calculation for a main effect of factor "X", which is simply the difference between the data averages of when X is high (+) and low (-). Note that Equation 12 does not only use the two experimental runs in which X is the sole high factor and the base case, but rather determines the effect of factor X using all experimental runs where X is high compared to all experimental runs where X is low.

$$\mathbf{ME}_X = \frac{1}{n_+}\sum^{n_+} X_+ - \frac{1}{n_-}\sum^{n_-} X_- \qquad \textbf{Equation 12}$$

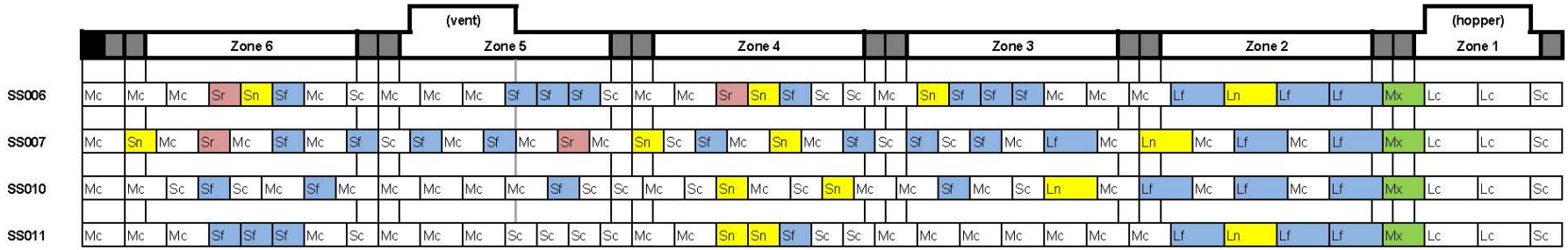

Figure 36. The SSSP screws designed for the full 2^4 factorial experiment. SS006 is High Kneading Block (A+) and Low Distribution (B-). SS007 is A+ and B+. SS010 is A- and B+. SS011 is A- and B-. The first letter in each block is the element length (S – 18.75 mm, M – 25 mm, L – 31.25 mm) while the second letter designates the type of block (c – conveying, x – transition conveying, f – forward driving kneading, n – neutral kneading, r – reverse driving kneading).

The second-order interaction term of factors X and Y is calculated through Equation 13. Similar to how the main effect was calculated, each term in Equation 13 utilizes all runs in which factors X and Y are in the desired high/low configuration.

$$\mathbf{IE}_{\boldsymbol{XY}} = \frac{1}{2}\left(\frac{1}{n_{X+Y+}}\sum^{n_{X+Y+}} X_+Y_+ - \frac{1}{n_{X-Y+}}\sum^{n_{X-Y+}} X_-Y_+\right) - \frac{1}{2}\left(\frac{1}{n_{X+Y-}}\sum^{n_{X+Y-}} X_+Y_- - \frac{1}{n_{X-Y-}}\sum^{n_{X-Y-}} X_-Y_-\right) \quad \textbf{Equation 13}$$

Equation 13 can be rewritten in terms of main effects, compounding the four terms into two as seen in Equation 14. By extending this concept, higher order interaction effects are easily defined in terms of lesser ordered effects. For this study, third and fourth order interaction terms were found (Equation 15 and Equation 16). Three and four-way interactions are often assumed to be insignificant in industrial applications of experimental design to reduce the total number of trial runs required for calculations. As the BU SSSP is a highly complex system which had never been characterized, minimizing assumptions while fully describing all interactions was deemed to be worth the additional processing and analysis.

$$\mathbf{IE}_{\boldsymbol{XY}} = \frac{1}{2}\left(\mathbf{ME}_{X|Y+}\right) - \frac{1}{2}\left(\mathbf{ME}_{X|Y-}\right) \quad \textbf{Equation 14}$$

$$\mathbf{IE}_{\boldsymbol{XYZ}} = \frac{1}{2}\left(\mathbf{IE}_{XY|Z+}\right) - \frac{1}{2}\left(\mathbf{IE}_{XY|Z-}\right) \quad \textbf{Equation 15}$$

$$\mathbf{IE}_{\boldsymbol{XYZV}} = \frac{1}{2}\left(\mathbf{IE}_{XYZ|V+}\right) - \frac{1}{2}\left(\mathbf{IE}_{XYZ|V-}\right) \quad \textbf{Equation 16}$$

By repeating similar trial runs in this experimental study, a normal Gaussian distribution of error should be introduced into the data. This error will carry through the

main and interacting effects calculations (Equation 12 through Equation 16). In order to differentiate between results from experimental error and actual parameter effects, the statistical significance of each effect was evaluated. To easily determine and evaluate significance, the distribution of effects was compared to a Gaussian normal distribution by standard normal and half-normal quantile plots. Quantile plots compare any two sets of data to determine whether they have similar distributions. If both sets of data points are similarly distributed, they will form a linear trend of positive slope. On normal quantile plots, the set of data are compared to a normal distribution by assigning each value a rank, *i*, and plotting against the quantiles of a normal distribution. Quantiles are points which are spaced with equal probability along a cumulative distribution function. For example, Figure 37 demonstrates the location of the 4-quantiles of a normal distribution and that the probability between each quantile is equal.

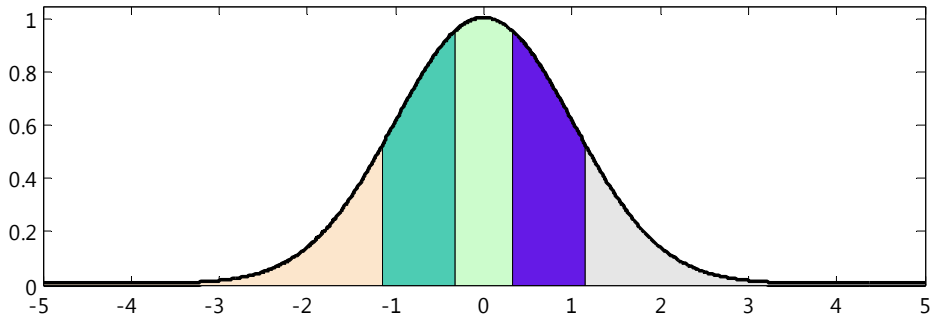

Figure 37. A segmented Gaussian probability distribution (mean=0, variance=1) with four quantiles represented as vertical black lines. The five probabilities (areas) between the four quantiles are equal.

On a normal quantile plot, the data are sorted in ascending values and assigned a rank *i*. The lowest value is assigned a rank of 1 while *i* iterates to a maximum of the total number of data points (*I*). This maximum is assigned to the datum with highest value.

The ranked values are plotted against the normal quantiles as calculated by Equation 17, where Φ^{-1} is the inverse normal cumulative distribution function.

$$\mathrm{q}(i) = \Phi^{-1}\left(\frac{i - 0.5}{\mathrm{I}}\right) \qquad \textbf{Equation 17}$$

If the data have a normal distribution, they form a linear trend on a normal quantile plot, as seen in Figure 38. Outliers from the linear trend indicate deviance from a normal distribution. In Figure 38, the first and last data points deviate greatly and would be considered significant, however, it is difficult to visually discern which is more significant on this plot.

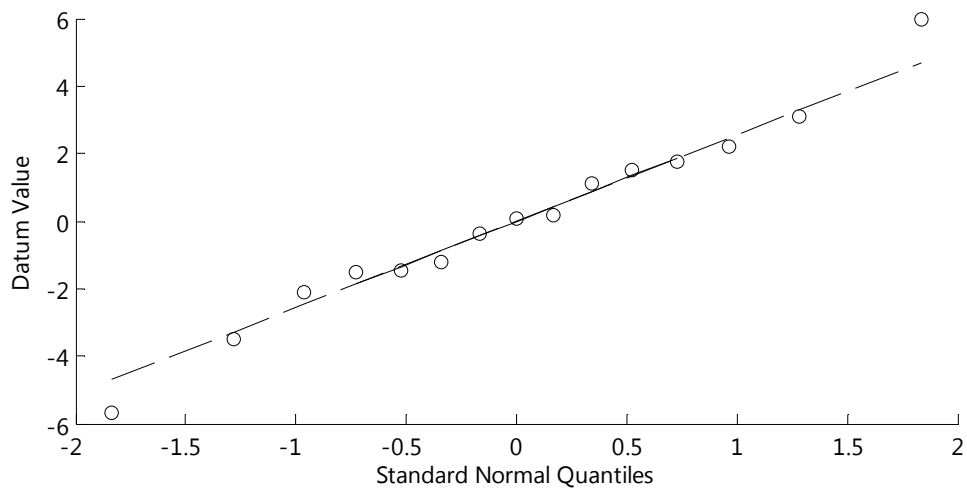

Figure 38. A random set of data on a standard normal quantile plot. The data are shown to be a normal distribution due to the linear trend. The linear regression is added for a visual aid, and is calculated from the median 50% of data points (shown as a solid line).

Half-normal quantile plots allow the relative significance of data to be easily determined by comparing the absolute values to the positive portion of the normal distribution. The absolute value of the data are sorted in ascending value, given ranks, and plotted against the half-normal quantiles, as defined by Equation 18.

$$q_{1/2}(i) = \Phi^{-1}\left(0.5 + 0.5 \times \left(\frac{i - 0.5}{\mathrm{I}}\right)\right) \qquad \textbf{Equation 18}$$

Applying the data from Figure 38 to a half-normal quantile plot results in Figure 39. The most significant data points will be in the upper right corner of the graph. With the given data set, Figure 39 shows that the last, positive value from Figure 38 is more significant than the first, negative value.

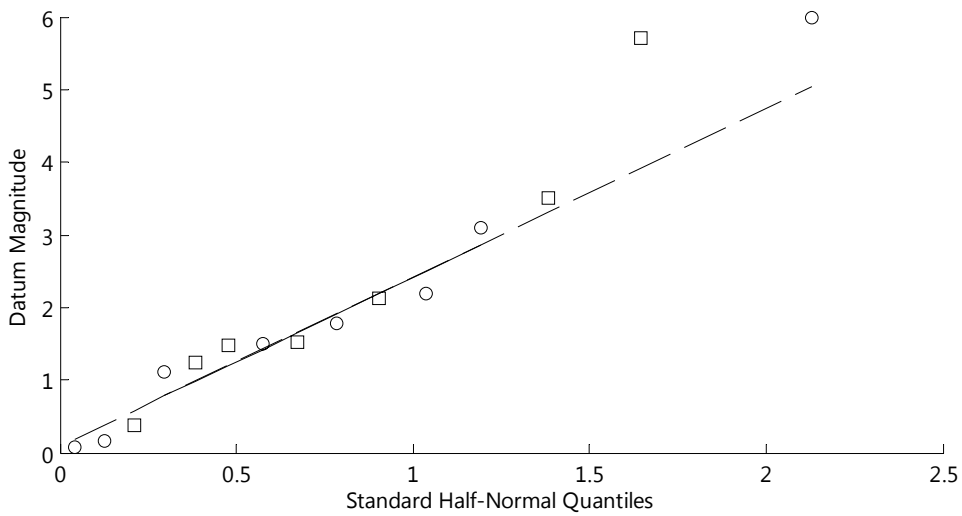

Figure 39. A standard half-normal quantile plot of the data from Figure 38. Negative data points are shown as squares for identification.

Normal and half-normal quantile plots pertaining to this SSSP factorial analysis have each point labeled with the effect for which is represents. For example, a datum labeled "ABD" is the three-way interaction of Factors A, B, and D while datum "C" is the main effect of Factor C. Recall that factorial effects are not representations of single experimental runs, but rather all runs which incorporate a certain high/low pattern compared to all runs which do not. Thus the two-way effect datum labeled "BD" is not to be confused with the "- + - +" blend.

5.4 SSSP Operation Considerations

Initial commissioning of the SSSP showed that for each run, the apparatus reached a thermal equilibrium within 15 minutes, as seen in Figure 40. Samples were collected from the SSSP only after this thermal steady state was achieved.

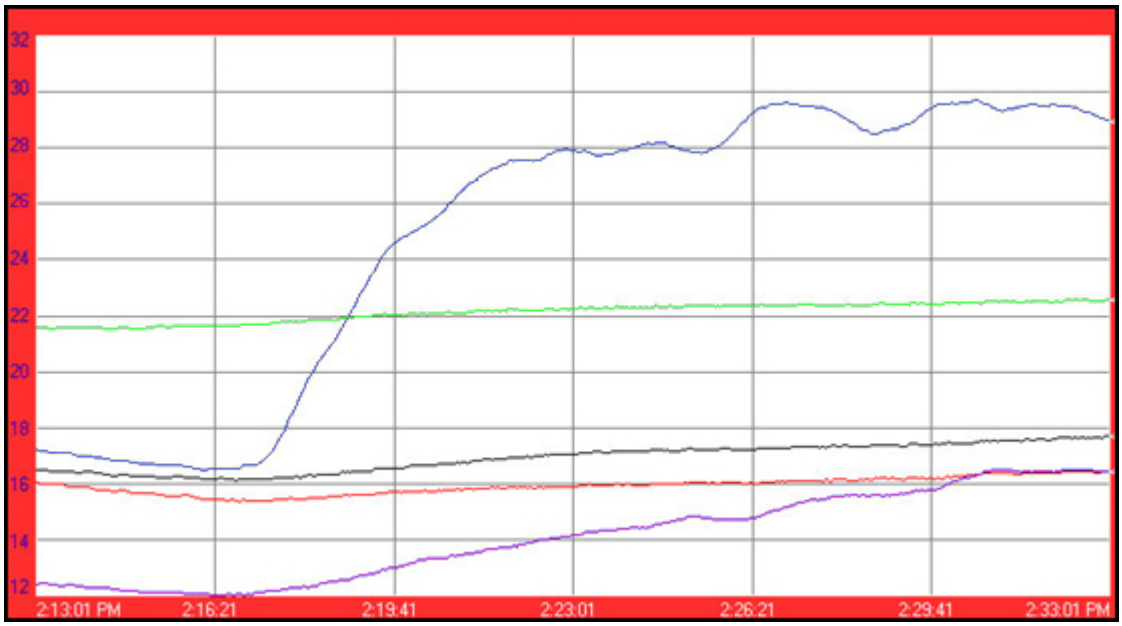

Figure 40. Temperature profiles (in °F) of the five temperature-controlled SSSP barrel zones following the introduction of pellets at 2:17. Thermal steady-state was achieved within 15 minutes (2:32).

The topmost trace in Figure 40 is the temperature of Zone 2; where pellets first encounter kneading blocks for pulverization. The large variance in the temperature of this zone can be explained by the choppy delivery of the pellet feeder at low feed rates. When operating at conditions close to causing melt formation, this variance is large enough to cause an irreversible, cascading melt to progress through the entire barrel, prompting catastrophic heat generation and requiring run abortion. Two large deliveries of pellets in succession are sufficient to destabilize the thermal steady state and as such the pellet feeder must be monitored closely.

The operation and maximum feed rate of the SSSP is limited due to poor heat transfer from the screws to the barrel walls. This reduced heat conduction allowed regions of the screws to maintain elevated temperatures at steady state much higher than the reported zone temperature. Positioning high heat-generating screw elements, such as kneading blocks, in contact with the union space between cooling zones also resulted in exceptionally poor heat conduction to the barrel, resulting in large screw temperature increases. Additionally, cooling zones two and six exhibited consistently higher temperatures than the three other zones. Conduction of heat from the uncooled feed zone and ball bearing attachment (as seen in Figure 15) accounts for these elevated temperatures.

5.5 Results and Discussion

5.5.1 D_n and Variance Analysis

The growth of the average dispersed domain diameter, D_n, for the blends created under the conditions listed in Table 8 can be seen in Figure 41. At first glance, it can be seen that slight changes in the screw design and operating conditions of the SSSP can produce blends with highly varying compatibilization. While the initial D_n for all blends are closely grouped between ~2-5 μm, the range grows to ~2-13 μm after a 240 minute anneal at 204ºC. Note that the previously published results from Northwestern University using this blend system and composition had a smallest dispersed domain size (with zero growth with annealing) of 3.8 μm.[31] Two blends ('+ + + +' and '+ – + +') created in this study exhibited minimal growth and domains smaller than 3.8 μm over the range of annealing, indicating the BU SSSP is capable of compatibilizing blends in excess of what was seen at Northwestern University. In terms of the magnitude of D_n, the order of blends

is not preserved between 5, 60, and 240 minute anneals, indicating that the initial D_n is not a sufficient estimation of compatibilization or D_n following annealing. This sentiment was shared in Chapter 4 where the cryomilled blend samples showed variation between the initial D_n and D_n growth rate.

Factorial analysis of D_n at different annealing times was performed and summarized in Figure 42. For the discussions henceforth, the factors assignments are reminded from Table 7: Factor A is kneading block type and number, Factor B is distribution of the kneading blocks, Factor C is screw rotation speed, and Factor D is feed rate. At a 5 minute anneal, all of the effects form a mostly linear trend, indicating that no factor or interaction of factors significantly affect the initial dispersed domain size, $D_{0,n}$. Interaction effect AB does deviate slightly below the linear trend, but is not physically significant. At 240 minutes, the growth of D_n is most pronounced in the blends. The half-normal plot of the effect of the experimental factors on D_n after a 240 min anneal can be seen at the bottom of Figure 42. The main effect of Factor A and the ACD interaction effect are shown to have very significant negative effects on D_n, indicating positives effects on compatibilization. The CD interaction and D main effects are also slightly significant in increasing and decreasing the 240 min D_n, respectively. Thus, the factors under consideration only become significant to D_n at long anneal times, where the number/type of kneading block and the interaction of kneading blocks, high screw speed, and high feed rate dramatically reduce average domain diameter. At t_a=240, high feed rates and the interaction between high screw speeds and high feed rates increase D_n slightly.

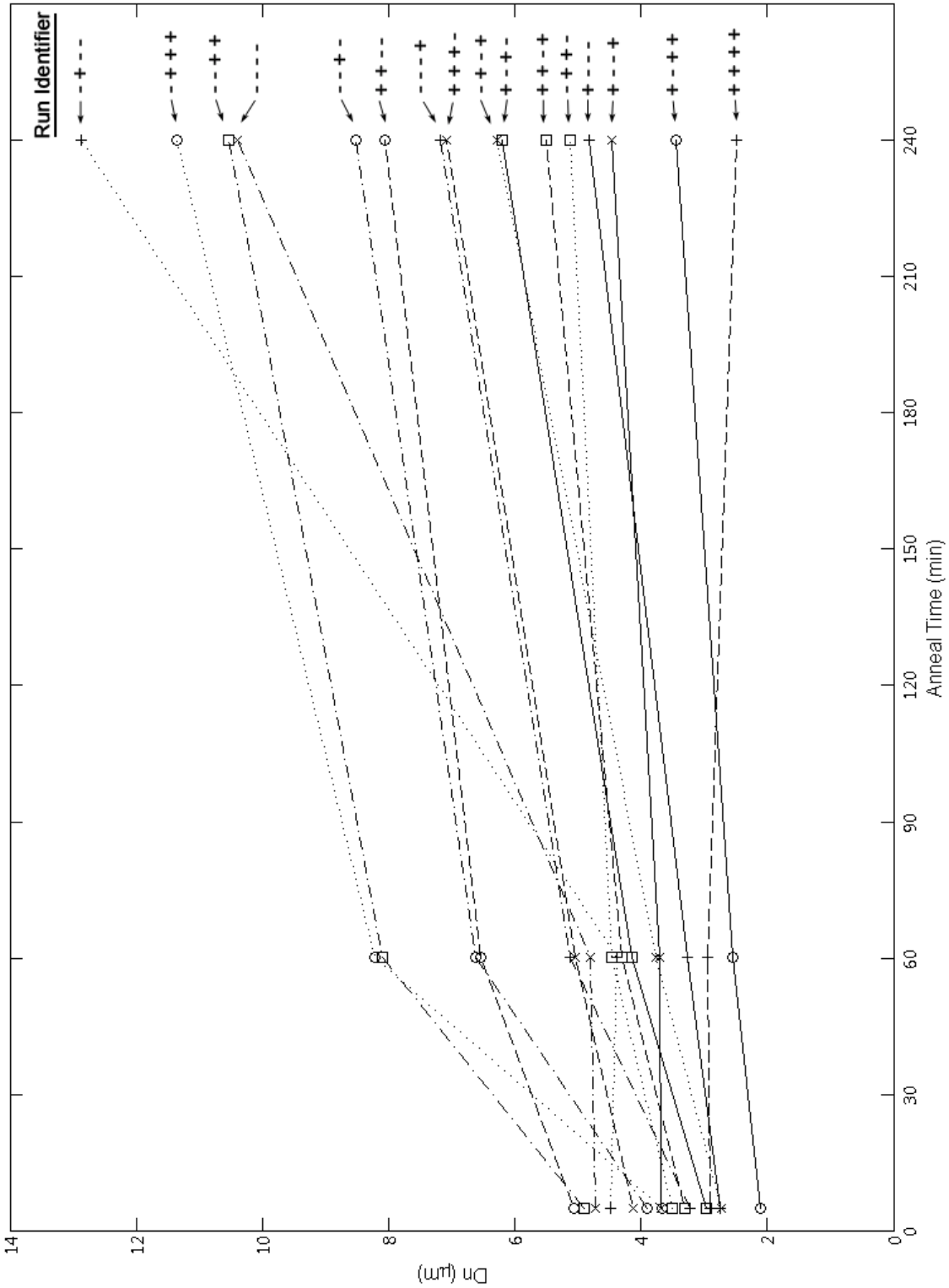

Figure 41. Growth of D_n for PS/HDPE blends fabricated via SSSP after anneal at 204ºC. Runs are identified beside the final data point. Lines are added as a guide.

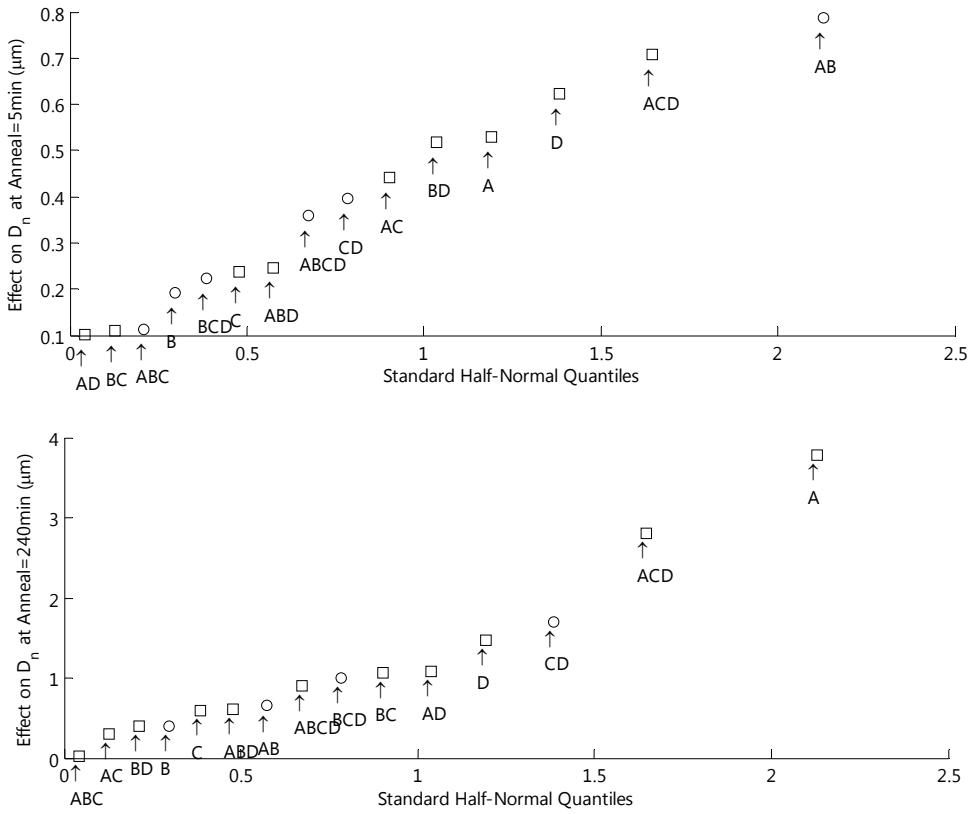

Figure 42. Half-normal plots of the effect of the experimental factors on D_n in a PS/HDPE (80/20 wt%) blend fabricated via SSSP after 5 minute (top) and 240 minute (bottom) anneals at 204°C. Note that negative values are represented as squares.

Variance analysis of the SSSP domain sizes was conducted in a similar manner as the cryogenically milled blends, as reported in Section 4.2.2. Table 9 lists the variance analysis of the average domains seen in Figure 41. At the initial data point, most blends featured small variance ratios (< 3) which grew with additional anneal time. Blends which exhibited the lowest D_n growth in Figure 41 also featured small variance ratios over all anneal times. Blends which followed a complex growth mechanism similar to the cryogenically milled and control blends from Chapter 4 started with large initial variance ratios (> 3) which continued to grow with annealing to very large values (> 6). The variance ratios of blends featuring a moderate amount of growth in Figure 41

demonstrated inconsistent changes with annealing, ranging from consistently large (e.g. blends "- - + -" or "- + + -") to initially small but large increases with annealing (e.g. "- + + +" or "+ - + -"). Consistent variance ratios in both medium- and low-growth blends indicate that block copolymers created during SSSP are effectively dispersed within the blend, similarly to the ability of SSSP to effectively disperse nanocomposite fillers throughout a polymer matrix.[94, 113, 114]

In terms of consistent, minimal variance over the range of annealing times, blends "+ - + +" and "+ - - +" are the most compatibilized, with "+ - - -" and "+ + + +" demonstrating slightly less compatibilization.

Table 9. Variance analysis of blends fabricated via SSSP following anneal at 204ºC

Sample	Anneal Time (min)	D_n	μ_2	$\frac{\mu_2}{D_n}$
- - - -	5	4.72	10.6	2.26
	60	4.81	21.3	4.43
	240	10.4	27.4	2.64
- - - +	5	3.23	4.06	1.26
	60	5.13	14.7	2.86
	240	7.18	25.8	3.59
- - + -	5	3.91	12.9	3.30
	60	6.62	20.8	3.14
	240	8.53	34.9	4.09
- - + +	5	4.90	4.14	0.84
	60	8.10	18.5	2.28
	240	10.5	26.1	2.47
- + - -	5	4.48	11.4	2.55
	60	4.39	12.9	2.94
	240	12.9	89.1	6.69
- + - +	5	2.72	5.77	2.12
	60	3.77	6.63	1.77
	240	6.28	29.8	4.74
- + + -	5	3.50	13.9	3.99
	60	4.46	14.1	3.16
	240	5.13	11.9	2.33
- + + +	5	3.67	3.97	1.08
	60	8.22	28.3	3.45
	240	11.4	81.5	7.18

Table 9. Variance analysis of blends fabricated via SSSP following anneal at 204ºC (continued)

Sample	Anneal Time (min)	D_n	μ_2	$\frac{\mu_2}{D_n}$
+ - - -	5	2.75	3.68	1.34
	60	3.26	3.96	1.21
	240	4.82	10.2	2.12
+ - - +	5	3.68	4.46	1.21
	60	3.71	6.34	1.71
	240	4.47	6.28	1.41
+ - + -	5	2.96	3.55	1.20
	60	4.15	3.58	3.58
	240	6.20	31.2	5.03
+ - + +	5	2.10	1.21	0.58
	60	2.55	1.60	0.63
	240	3.44	5.80	1.69
+ + - -	5	5.07	20.1	3.96
	60	6.55	27.3	4.17
	240	8.06	52.1	6.47
+ + - +	5	3.31	8.62	2.60
	60	4.30	14.9	3.46
	240	5.50	25.7	4.68
+ + + -	5	4.12	11.9	2.89
	60	5.03	12.9	2.57
	240	7.09	28.5	4.03
+ + + +	5	2.91	3.61	1.24
	60	2.95	5.74	1.94
	240	2.49	5.28	2.11

Factorial analysis of the variance ratios previously listed can be seen in Figure 43. Interestingly, the effects which encouraged decreased D_n do not significantly impact variance ratios. At t_a=5 min, Factors B and D significantly affect domain size variance. Distributing the kneading screw elements (B) increases variance ratios by nearly 1 while operating at a high feed rate (D) decreases the variance ratio by ~1.3. By t_a=240 min, Factor B continues to have a slight positive effect, meaning that dispersal of the kneading elements lead to more inconsistent domain sizes, while Factor D is no longer significant. The physical explanation of these significant effects is not overt, as these factors are insignificant in all other means of testing. Distributing the kneading blocks could limit

the dispersal of the block copolymers in the blend or indicate that groups of kneading elements produce viable block copolymers more efficiently than those which are separated by conveying elements.

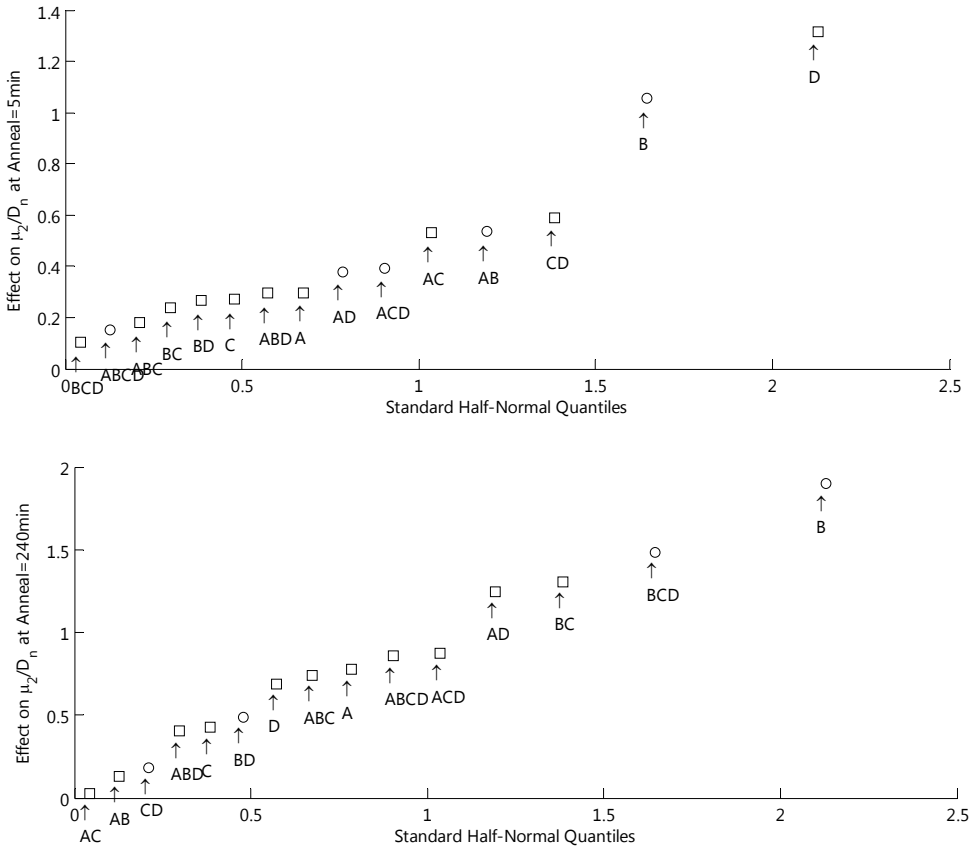

Figure 43. Half-normal quantile plots of the effects of the experimental factors on the variance factor of PS/HDPE (80/20 wt%) blends fabricated via SSSP after 5 minute (top) and 240 minute (bottom) anneals at 240ºC. Negative values are represented with squares.

Applying the Crist growth model to the SSSP blends yields much better fits than those of the cryogenically milled samples in Chapter 4, as seen in Figure 44 and Table 10. Additional graphs for each blend can be found in Appendix A. In most SSSP blends, sufficient compatibilization was achieved to prevent the rapid initial coalescence seen in the cryogenically milled blends which necessitated the two-stage model. The growth constants calculated for the BU SSSP blends are very comparable to the growth constants

reported for 80/20 PS/HDPE blends fabricated on the NU SSSP.[98] The larger-K blends are slightly higher than the largest values documented at Northwestern, but this discrepancy is likely the result of the difference in anneal temperatures (204ºC v. 190ºC). Comparing the K values in Table 10 to the initial growth rate of the pMM blend (melt-mixed pellets) from Chapter 4 (2.3 μm^3/min) shows that SSSP can result in blends with a K of essentially zero or much larger than that seen in simple melt-mixed blends of pellets. As such, optimizing the process is critical to successful mechanical annealing of polymers.

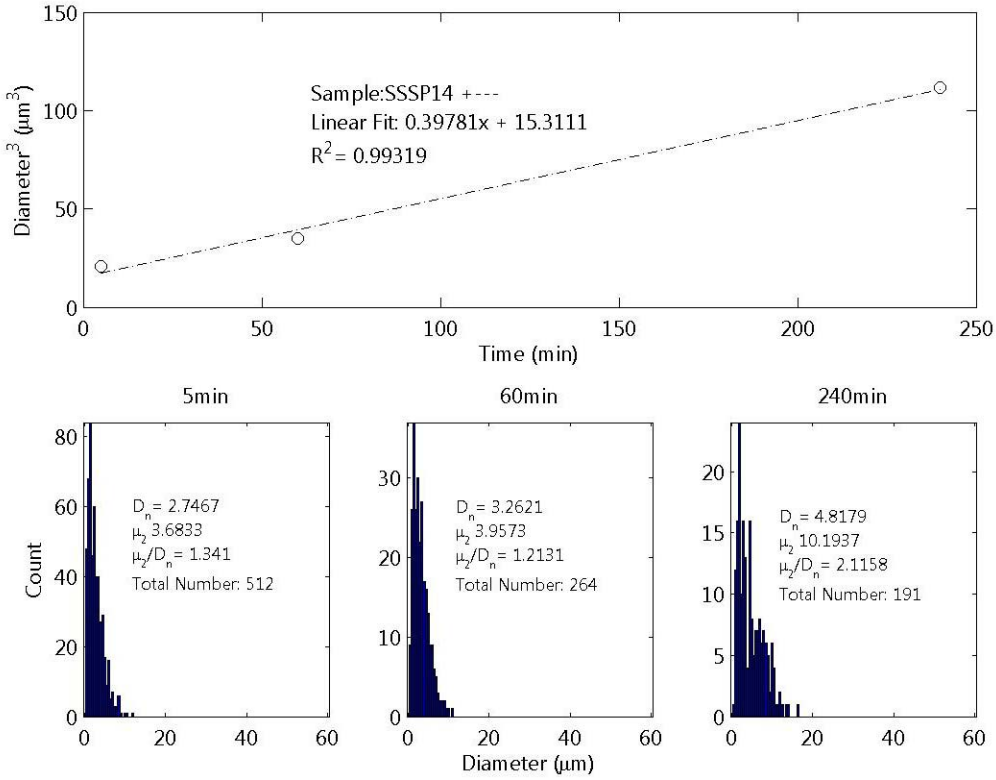

Figure 44. Application of the Crist growth model to the "+ - - -" blend with histogram data for each anneal point

Table 10. Values generated from applying the Crist growth model to the SSSP blends

Sample	K (μm^3/min)	$D_{0,n}$(μm)	R^2
+ + + +	-0.0431	2.97	0.89
+ - - +	0.117	3.56	0.96
+ - + +	0.134	2.05	1.00
- + + -	0.358	3.74	0.91
+ - - -	0.398	2.48	0.99
+ + - +	0.527	3.41	0.99
+ - + -	0.912	2.69	1.00
- + - +	0.997	1.81	0.99
+ + + -	1.23	3.91	1.00
- - - +	1.40	3.34	0.99
+ + - -	1.59	5.31	0.97
- - + -	2.25	4.55	0.96
- - + +	4.25	5.58	0.97
- - - -	4.64	-2.97	0.95
- + + +	5.77	4.69	0.98
- + - -	9.37	-5.68	0.95

The static growth constants reported in Table 10 are shown to be a normal distribution in Figure 45 with three significant outliers. Main effect A and the interaction of Factors A, C, and D both greatly reduced the value of K while the interaction of Factors C and D increased the growth constant significantly. Note that the three most significant factors seen in Figure 45 are the same previously seen when determining influence on D_n in Figure 42, namely kneading block type and quantity. This demonstrates that minimizing the growth constant K, rather than initial domain size, is the most important criteria for compatibilization when attempting to stabilize blends to static anneal.

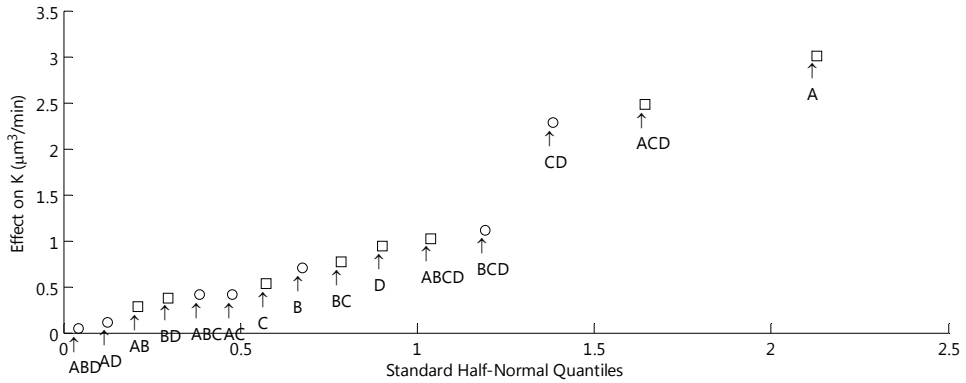

Figure 45. Half-normal plot of the effect of the experimental factors on the static growth constant, K. Negative values are represented by squares.

5.5.2 Molecular Weight Analysis

The polystyrene phase was selectively dissolved in THF and had molecular weight analysis performed via GPC, as seen in Table 11. SSSP processing results in significant reductions in both M_n and M_w, but does not drastically alter PDI.

Table 11. GPC molecular weight characterization of the PS phase of the SSSP blends

Blend	M_n (g/mol)	ΔM_n (%)	M_w (g/mol)	ΔM_w (%)	PDI
As Received PS	106,000	0.0	256,000	0.0	2.4
- - - -	64,900	-39	161,000	-37	2.5
- - - +	73,400	-31	176,000	-31	2.4
- - + -	63,800	-40	178,000	-31	2.8
- - + +	78,200	-26	171,000	-33	2.2
- + - -	67,400	-36	202,000	-21	3.0
- + - +	70,200	-34	185,000	-28	2.6
- + + -	84,600	-20	183,000	-29	2.2
- + + +	76,500	-28	192,000	-25	2.5
+ - - -	64,500	-39	139,000	-46	2.2
+ - - +	57,200	-46	170,000	-34	3.0
+ - + -	91,700	-14	205,000	-20	2.2
+ - + +	77,900	-27	188,000	-27	2.4
+ + - -	59,000	-44	115,000	-55	1.9
+ + - +	60,900	-43	122,000	-52	2.0
+ + + -	65,300	-38	178,000	-31	2.7
+ + + +	57,500	-46	127,000	-50	2.2

Factorial effect analysis of M_n and M_w produces Figure 46 and Figure 47. The main effect of Factor C (increasing screw rotation speed) resulted in significantly less reduction in M_n. Such a reduction is reasonable as higher screw rotation speeds decrease the retention time of material in the pulverizing elements. Other interactions (ABD, AC, ABCD) appear to offer much smaller decreases in M_n reduction. No factors impart significantly larger reductions in M_n. The effects of C and AC continue to promote less reduction with regards to M_w as well, reinforcing the hypothesis that decreased retention time in the kneading elements decreases molecular weight reduction. The interaction effect AB and main effect A result in much greater reductions in M_w. The main effect of adding more and reverse-driving was expected, as greater numbers of harsher elements were added specifically to encourage chain scission. However, the interaction of a large number of kneading blocks and their distribution contributing to significant M_w reduction was unforeseen. This effect could be the result of the placement of the distributed kneading blocks within certain regions of the SSSP barrel with heat removal limitations. This explanation is expanded upon in the next section.

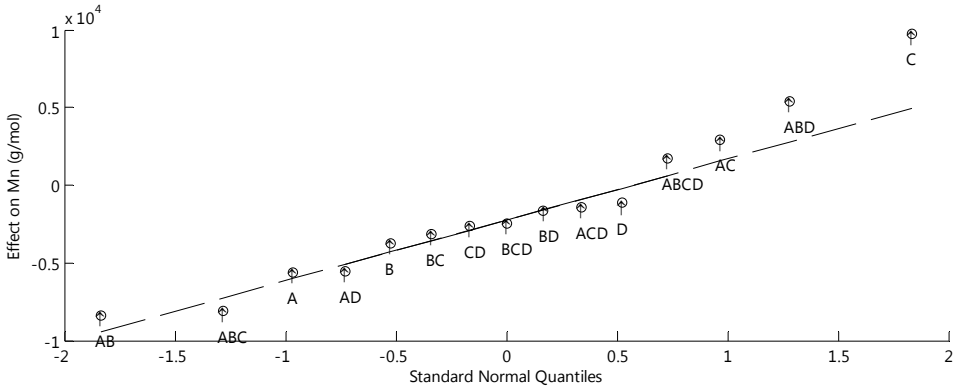

Figure 46. Normal quantile plot of the effect of the experimental factors on the number averaged molecular weight of blends fabricated via SSSP

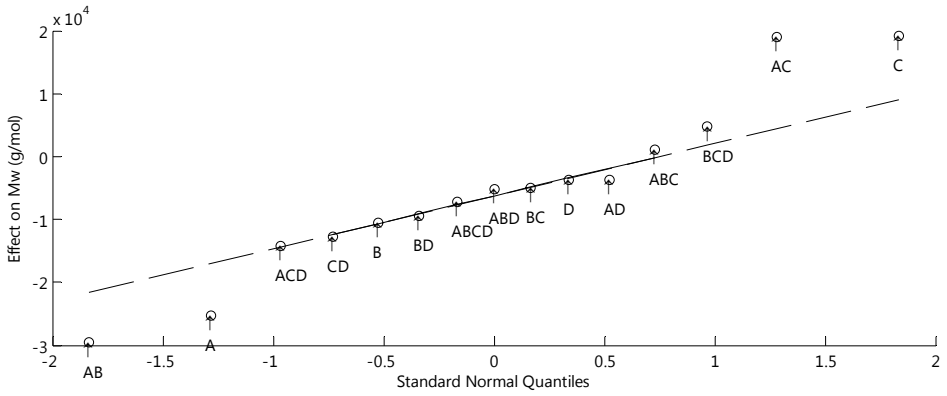

Figure 47. Normal quantile plot of the effect of the experimental factors on the weight averaged molecular weight of blends fabricated via SSSP

5.5.3 Uncoupling Contributions to Factor A and Zone Temperature Analysis

Due to processing constraints, Factor A combines the effects of both the variety and number of kneading blocks. Factor A was the most significant effect on the static growth constant and one of the largest reducers of Mw. As such, uncoupling the kneading block variety contributions from the kneading block number contributions in Factor A is vital to using the results of this study in future SSSP operations. Table 12 attempts to differentiate these combined effects using the steady state processing temperature of SSSP Zone 4. High shear rates which cause polymer chain scission during SSSP also result in increased heat generation. Screw designs with higher operating temperatures should indicate higher shear and greater contribution to Factor A.

At first glance, Table 12 indicates that screw design D3 has the highest operating temperature and that the number of kneading blocks is the most significant contributor to factor A. The first and last kneading elements in D3 are positioned within the union areas between Zones 3 and 4 and Zones 4 and 5, respectively. As previously mentioned these areas are not in contact with the recirculating coolant and result in unfavorably large

buildups of heat in the polymer and screws — likely the cause of the elevated temperatures seen in design D3.

Table 12. Temperature analysis of SSSP Zone 4 with regards to screw design and operating conditions. C+/- indicates high/low screw RPM while D+/- indicates high/low feed rates

Identifier	Zone Design	Operation	Temperature (ºF)
D1	Mc Mc Sr Sn Sf Sc Sc	C-D-	23
		C-D+	28
		C+D-	19
		C+D+	22
D2	Mc Mc Sn Sn Sf Sc Sc	C-D-	18
		C-D+	22
		C+D-	18
		C+D+	20
D3	Sn Sc Sf Mc Sn Mc Sf	C-D-	25
		C-D+	30
		C+D-	20
		C+D+	29
D4	Mc Sc Sn Mc Sc Sn Mc	C-D-	17
		C-D+	20
		C+D-	17
		C+D+	19

This heat generation due to kneading blocks overlapping union areas could also be the explanation of the unexpected contribution of the AB interaction to M_w reduction. Screw design SS007 (see Figure 36), which had a high kneading block and distributed design, featured five kneading blocks overlapping unions, while other designs had one or zero. As material traversed these elements with significantly raised temperatures, it may have become pliable enough to incur significant chain damage when subjected to high shear forces.

Considering this effect of kneading block positioned over union spaces, a more accurate comparison with regards to the effect of number of kneading blocks is the temperature difference between D2 and D4. The addition of a forward-driving kneading

block results in a temperature increase of 1-2ºC across various operating conditions. A rise of 1-6ºC can be seen when a neutral kneading element is replaced with a reverse kneading element between D2 and D1. This greater temperature change indicates that the addition of reverse driving elements has a greater effect on the operating temperature of Zone 4 than changes in the number of forward or neutral kneading elements, and by extension is the primary contributor to the effects previously seen attributed to Factor A. Table 12 also shows the trend of operating temperature with regards to changes in screw rotation speed and feed rate (factors C and D). Across all screw designs, increases in pellet feed rate resulted in an increase in operating temperature. As heat transfer from the screw and polymer to the barrel walls is the limiting cooling step, increasing the amount of polymer undergoing shear was expected to increase operating temperature. Conversely, increases in the screw rotation speed resulted in decreases in operating temperature, a rather counterintuitive finding. An increase in operating temperature with screw speed was expected due to increased shear rate of faster-spinning kneading blocks, but the reduced residence time of polymers due to higher rotation speeds nullified or even overcame this hypothesized effect and prevents barrel heating.

5.5.4 Combined Results

Unifying the results of the analyses reveals that while no factors have a direct effect on the initial D_n, the main effect of reverse-driving kneading elements and interaction effect of reverse elements, high RPM, and high feed rates on the static growth constant are confirmed via analysis of D_n at t_a=240 min. The inclusion of reverse kneading blocks also contributed large decreases in M_w, suggesting that harsher solid-state screw designs can create greater quantities of block copolymers through chain

scission. Significant reductions in M_w cannot be directly used to describe compatibilization, as the interaction of distributing large numbers and types of kneading blocks greatly reduced M_w while not contributing to any D_n measurements.

None of the significant effects of the D_n, K, or molecular weight analysis were found to significantly alter dispersed domain variance. Initial domain variance ratios were reduced when running high feed rates and increased when the kneading blocks were distributed. After a 240 minute anneal, the kneading block distribution continued, to a smaller degree, promote narrower variance ratios.

5.6 Summary

This study investigated the importance of several key SSSP parameters, namely kneading block type and quantity, kneading block distribution, screw rotation rate, and pellet feed rate, on a model PS/HDPE (80/20 wt%) blend through a full factorial experiment. It was determined that initial domain size was not an accurate measure of blend compatibilization or predictor of final domain size following static annealing. The main effect of having reverse-driving kneading blocks and the interaction effect between the reverse kneading blocks, high screw rotation speed, and high feed rate both greatly reduced the final dispersed domain size after a 240 minute static anneal at 204ºC. By fitting the Crist growth model to the experimental data, it was determined that this domain size reduction was due to suppression of the static growth constant, which describes both Ostwald ripening and coalescence coarsening regimes. An interaction between a high screw rotation rate and high pellet feed rate was determined to significantly increase the static growth constant.

Molecular weight characterization showed that the number and weight averaged molecular weights of the polystyrene phase of the blends decreased between 10-50% compared to virgin material. The reduction in both M_n and M_w was minimized by increasing the rate at which the pulverizer screws rotate. Incorporating reverse-driving kneading blocks into screw design resulted in the largest factors with regards to decreasing M_w, with additional decreases observed when reverse kneading elements were distributing along the full length of the pulverizer barrel instead of being grouped into separate pulverization zones. The latter is potentially the result of excessive heat buildup on kneading blocks positioned within union zones combined with the high shear forces. It was observed that while adding reverse kneading blocks significantly improved compatibilization, the interaction between the reverse kneading block and distribution did not impart significant improvements of compatibilization. This indicates that molecular weight reduction is not directly related to a degree of compatibilization.

Analysis of cooling zone temperatures with varying screw designs and operating conditions showed that increasing pellet feed rate will increase operating temperature, while in most cases increasing the screw rotation speed will also decrease operating temperature.

6. Correlation of Domain Size Compatibilization to Physical Properties

Throughout this thesis, compatibilization of immiscible polymer blends was defined as minimization of the growth rate of the dispersed phase domain size upon static, extended heat treatment. While this definition has been used by many research groups interested in achieving compatibilized blends of immiscible polymers, the current method for determining blend compatibilization, namely identification of the dispersed domain size through scanning electron microscopy, is laborious and highly time-intensive and prone to various experimental errors as described in Chapter 4. In addition, the industry is less concerned with the microstructure of the blend and more interested in additive or synergistic property enhancement.[2, 18]

Block copolymers have been shown to improve the cohesion between immiscible blend interfaces and increase mechanical performance, but are required to be at least equivalent in size as the molecular weight between entanglements, M_e.[49, 50] Previous studies have determined that polymer chains less than approximately $2M_e$ will not undergo chain scission during solid-state processing due to energy dissipation through chain pullout and slip.[73, 99] Hence, block copolymer species formed in situ during solid-state milling are expected to be of sufficient length to provide improved mechanical force transfer across the interface.

This chapter focuses on testing two blends fabricated by SSSP for improved mechanical properties. The quantification of blend compatibilization could be streamlined greatly if the results of common material property analysis differentiated between degrees of compatibilization in a similar manner as domain-size analysis. The

physical property measurements of interest are differential scanning calorimetry, thermogravimetric analysis, and static and dynamic tensile testing.

6.1 Experimental Procedure

Two polystyrene/high-density polyethylene (PS/HDPE) blend samples from the SSSP optimization study in Chapter 5, namely "+ + + +" and "+ – + –", were used. These blends were chosen as they exhibited the greatest reduction in K, the static growth constant, (blend "+ + + +") and a modest reduction in K ("+ – + –") when compared to a melt-mixed blend of neat pellets (pMM). In this study, these blends will be referred to as the low-K blend (LK), the mid-K blend (MK), and the high-K blend (HK), respectively. According to the currently accepted definition, the LK blend is the most compatibilized system of the three, while the HK sample is considered incompatible. If the reduced dispersed growth rate in the chosen blend system correlates with enhanced physical properties, the LK blend would show the greatest improvement followed by the MK blend.

Samples were prepared by melt-mixing in the Atlas LMM for five minutes at 180°C and press molded into sheets or standardized testing specimens at 180°C. A lower temperature than previous studies (Chapters 4 and 5) to ensure samples were not thermally degraded. Once pressed, samples were quenched between two room-temperature metal plates. Differential scanning calorimetry (DSC) was used for glass transition and melting/crystallization behavior measurement. Thermal gravimetric analysis (TGA) was used for content verification and degradation temperature probing. Static and dynamic tensile testing measured the stiffness and elasticity of the blends. Operation of each piece of equipment followed the procedures detailed in Chapter 3.

6.2 Blend Analysis and Discussion

6.2.1 Previous Results

Initial characterization of the HK, MK, and LK blends was conducted in Chapters 4 and 5, and is compiled in Table 13. As indicated by the naming convention, the blends feature largely different static growth constants. Additionally, the molecular weights of the PS component in each blend vary between 54-100% of the neat PS.

Table 13. Compilation of all previous analysis results on the blends selected for further analysis using common techniques. Molecular weight characterization for the HK blend is from pure PS pellets.

Sample	K (μm^3/min)	M_n (g/mol) (of PS matrix)	M_w (g/mol) (of PS matrix)	PDI	D_n(5 min) (µm)	D_n(60 min) (µm)
LK	0.0	57,500	127,000	2.2	2.91	2.95
MK	0.9	91,700	205,000	2.2	2.96	4.15
HK	2.3	97,000	251,000	2.6	3.62	5.27

6.2.2 Thermogravimetric Analysis

The addition of compatibilizing agents to polymer blends has been shown to thermally stabilize the blend and increase the onset temperature of thermal degradation. Previous studies involving PS/PMMA blends have shown that an addition of 3 wt% block copolymer has significantly decreased the thermal degradation rate,[115] while four different types of compatibilizers were found to dramatically increase the half-life of LDPE/poly(dimethyl siloxane) rubber blends.[116] Thus, the block copolymers created in situ during pulverization may provide stabilization to degradation onset or reduce the degradation rate.

Table 14 lists the results of TGA tests. All blends exhibit similar degradation onset temperatures as polystyrene in both 95% mass and slope intercept methods,

indicating that neither block copolymers created in situ nor molecular weight changes incurred from solid-state shear pulverization affected blend thermal stability. TGA does, however, quantify the exact composition of the blends due to differences in degradation temperatures. It is surprising to see the nominal (20 wt%) composition was not achieved in the blends, despite careful attempts to meter and mix the two components in proper proportions. This variance could be the result of the pre-mixed pellets being fed from a single feeder, low pellet feed rate, or non-homogeneous mixing in the melt-mixer.

Table 14. Results of thermogravimetric analysis of blends (10°C/min heating rate)

Sample	Degradation Onset Temperature (ºC)		Composition (wt% HDPE)
	95% Mass Method	Slope Intercept Method	
PS	378	392	0
HDPE	453	463	100
LK	384	395	15
MK	385	395	23
HK	387	394	17

6.2.3 Differential Scanning Calorimetry

DSC has been used to define compatibilization between cryogenically milled blends by way of shifts in transition temperatures from those of the neat polymers. It was proposed in a blend of PS/PET that alloyed blends showed compatibilization due to shifts of the lower PET T_g and higher PS T_g towards each other by approximately 25%.[77] Although the HDPE phase of the current blend does not clearly exhibit a T_g over the measurable range of temperatures, any changes in the T_m or onset recrystallization temperature of the HDPE and the T_g of the PS component would be easily detected.

Figure 48 and Table 15 document the thermal transitions observed during DSC analysis. Blends were analyzed from melt-mixed samples before and after they were

annealed for 120 minutes at 204°C to determine whether annealing had an effect on crystallinity. As seen in Figure 48, the peak melting temperature for all blends were reduced ~6°C from neat HDPE. All other transition temperatures, including HDPE component onset T_m and recrystallization temperature and the PS component T_g, in the PS/HDPE blends are consistent with the neat polymers, indicating transition temperature shift is not related to any of the properties described in Table 13.

Table 15. Relevant thermal phase transition values determined during DSC analysis. Marked samples were isothermally annealed at 204°C for 120 minutes before measurement.

Sample	Onset T_m (ºC)	ΔH_{melt} of HDPE Component (J/g)	Onset Crystallization Temperature (ºC)	PS Phase T_g (ºC)
PS	N/A	N/A	N/A	106.8
HDPE	126	253	124	N/A
LK	127	193	122	105.5
LK (anneal)	128	191	121	105.6
MK	128	278	123	106.4
MK (anneal)	127	271	122	107.6
HK	127	185	124	108.9
HK (anneal)	127	198	123	109.4

The enthalpy of melting of the HDPE component did exhibit large differences between blends. This value is the energy required to melt the crystalline regions of the HDPE phase, and is directly proportional to the degree of crystallinity. The HK blend showed that blending PS with HDPE resulted in a decreased ΔH_{melt} of the HDPE component by 27%, indicating a suppression of overall crystallinity. Similar results have been reported in the literature.[117] Annealing HK for two hours increased the crystallinity of the blend. This improvement is likely the result of HDPE domain coalescence which created larger bulk HDPE regions capable of crystallization without PS interference.

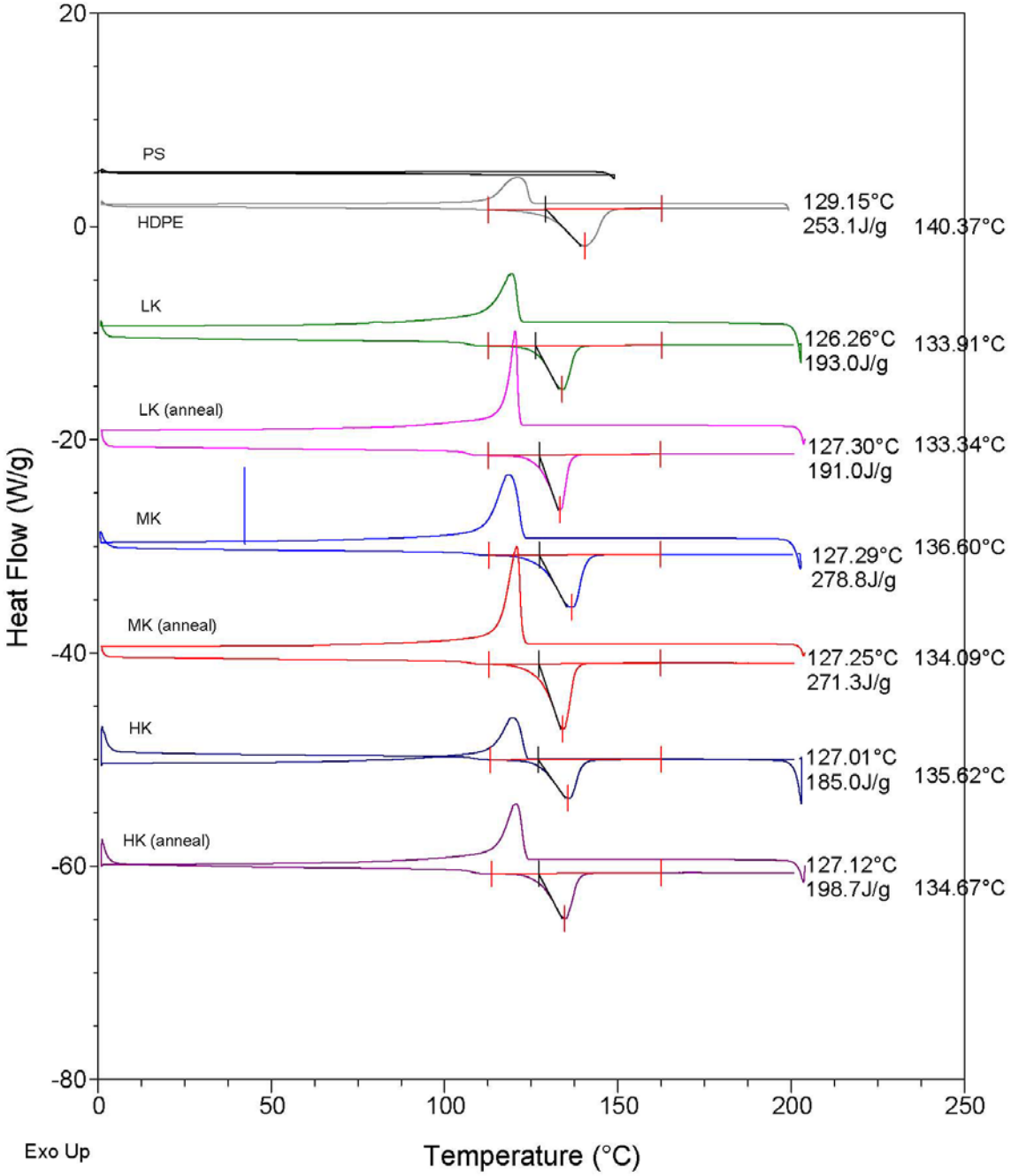

Figure 48. DSC traces for each blend with and without anneal. Each trace is labeled with onset melting temperature, ΔH_{melt} of the HDPE component, and peak melting temperature. Traces are shifted in 10 W/g increments.

The MK blend showed an enhancement in crystallinity beyond that seen the neat HDPE, while the LK blend demonstrated a similar drop as HK. The harsh pulverization incurred by LK (as evidenced by the large molecular weight reduction) obstructed the formation of crystalline structures possibly because of excess scission of HDPE chains, reducing their crystallizability. On the other hand, the relatively moderate pulverization of MK promoted crystallinity. This synergistic change is very peculiar. It is possible that PS chains that were intimately mixed with HDPE chains are taking part in co-crystallization. Of note is that both pulverized blends had consistent results pre- and post-anneal, indicating that these thermal properties are not sensitive to extended heat treatment.

6.2.4 Tensile Mechanical Testing

While tensile testing of PS/HDPE blends with the addition of premade PS/HDPE block copolymer have not been reported, similar blends have been analyzed with the addition of polystyrene/hydrogenated poly(butadiene) (PS/HPB) copolymers.[48] At 20 wt% HDPE, blends exhibited a 25% decrease in yield strength and no change in breaking strain compared to neat PS. Addition of 10% copolymer improved both values slightly, but did not result in large additive nor synergistic effects. As seen in Table 16, similar results were found in the SSSP blends under investigation. Young's modulus of the HK blend was most similar to PS, while MK and LK blends featured lower values. All blend breaking strains were between 20-40% less than neat PS, while the yield strength of the pulverized blends were less than both PS or HDPE and HK showed a slight additive improvement. Of note is that the results of both MK and LK blends were identical considering experimental variance, indicating that simple tensile testing is unable to differentiate between pulverized blends of varying growth rate compatibilization.

Table 16. Results from tensile testing sample materials using rubber clamps at 0.2 inches/min extension rate

Sample	Young's Modulus (MPa)	Breaking Strain	Yield Strength (MPa)
PS	792 ± 77	0.101 ± 0.005	51.1 ± 4.2
HDPE	591 ± 107	4.315 ± 0.936	29.1 ± 1.6
LK	665 ± 57	0.057 ± 0.009	23.4 ± 6.0
MK	683 ± 60	0.066 ± 0.013	23.7 ± 5.0
HK	768 ± 69	0.079 ± 0.010	36.4 ± 3.3

6.2.5 Dynamic Mechanical Analysis

Figure 49 compares the E′ value, storage tensile modulus, of the three blends to those of the neat component polymers. All three blends expectedly followed a similar trend as pure PS, the majority component. This nearly identical behavior, with slight variation in the modulus values as seen in static tensile modulus in Table 16, persisted over the temperature range of 30-105°C. At 105°C, however, the blends diverged and exhibited strengths of up to an order of magnitude larger than the neat polystyrene. This unexpected synergistic effect persists up to 140°C, the maximum measured temperature. The MK blend showed the largest increase, followed by HK and then LK. This blend order is the same as HDPE composition seen in Table 14, indicating that the synergistic strength enhancement at high temperatures is dependent on HDPE content rather than block copolymer content or compatibilization. Nevertheless, this is a very interesting observation, considering how the storage modulus of pure HDPE is much lower (essentially a melt) above 100°C.

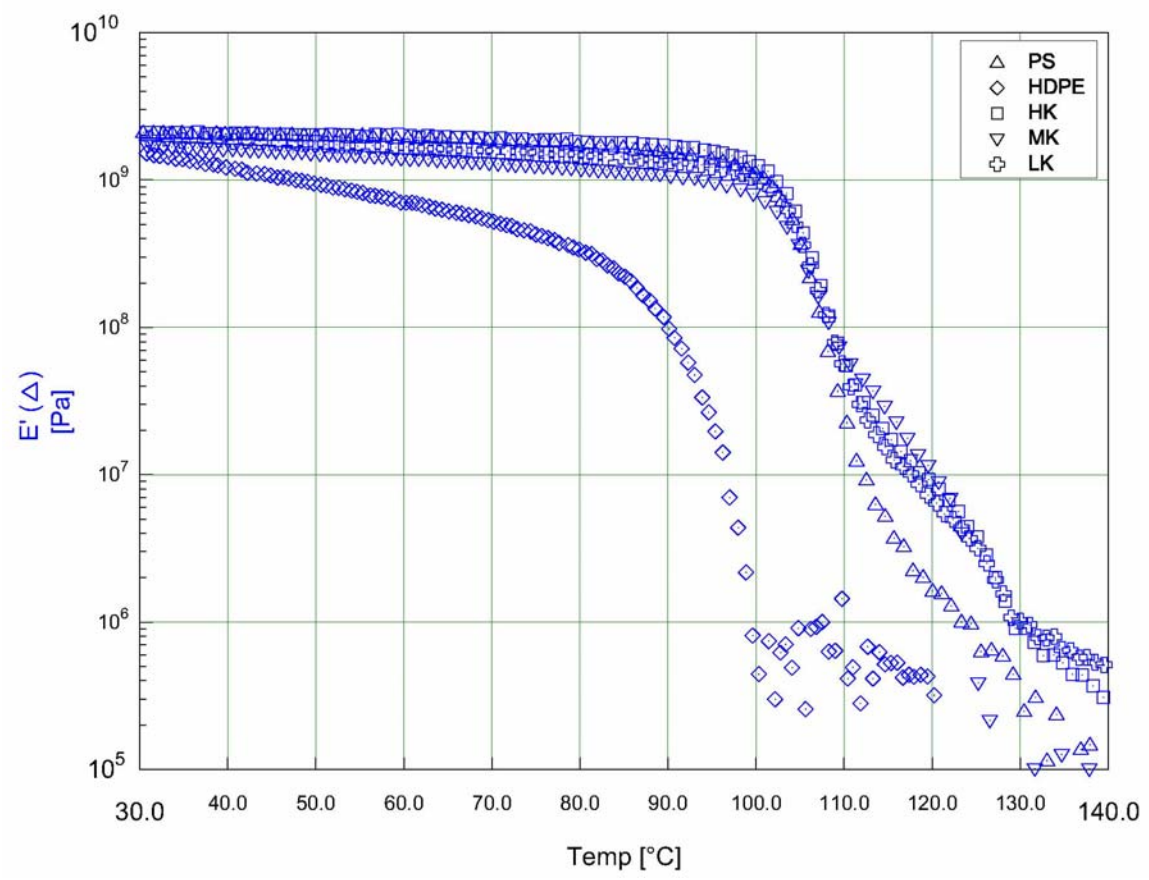

Figure 49. Measurement of blend strength via dynamic mechanical analysis with a temperature ramp of 5°C/min

6.3 Summary

This chapter subjected three previously characterized PS/HDPE blends to additional post processing and analysis through several common material characterization techniques. Results of these physical tests were compared to the results from the microstructure and morphological characterization, namely the static growth constant, molecular weight, and initial average dispersed domain size, to seek any correlations that can enhance the current blend compatibilization analysis method.

Thermogravimetric analysis successfully determined exact blend compositions, but did not indicate changes in thermal stability between the blends and neat PS.

Differential scanning calorimetry determined that blending nor pulverization affected the important thermal transition temperatures of blend components. Blending PS and HDPE resulted in decreased HDPE crystallinity which mirrored previous reports,[117] but this crystallinity could be improved by annealing at 204°C and allowing phase coalescence to increase the amount of bulk HDPE free to recrystallize without disruption by the PS phase. A moderate degree of pulverization resulted in a higher degree of HDPE crystallinity than the melt-blended sample or even the neat HDPE, while harsh pulverization greatly hindered crystal formation. This peculiar but non-monotonic change in HDPE crystallizability were unaffected by long-term heat treatment. Tensile testing proved ineffective in differentiating between the degrees of compatibilization in the blends. Dynamic mechanical analysis indicated that the stiffness of the blends closely followed that of the majority PS component up to 105°C. From this elevated temperature to 140°C (the end of the testing range), all blends demonstrated a substantial synergistic improvement in strength which is likely dependant on HDPE composition.

Despite several interesting relations observed during the previous analysis, no testing regimen successfully differentiated between the high, medium, and low static domain growth rate determined via SEM analysis. This suggests that for the current system, the measured mechanical properties were not related to the degree of compatibilization as defined by dispersed domain size and growth minimization, and cannot be utilized as an alternative to microscopy-based particle measurement. Nonetheless, this study was key in demonstrating that morphological compatibilization of polymer blends are far different from mechanical or thermal compatibilization that industry may be seeking in real-world polymer blends.

7. Conclusions and Recommendations

This thesis focused on processing incompatible polymer blends by two solid-state processes, cryogenic milling and solid-state shear pulverization. This section summarizes the important findings from each study, and provides recommendations for future experimentation on the current blend system and how future solid-state blending operations can be improved.

7.1 Major Conclusions

An 80/20 wt% blend of polystyrene (PS) and pyrene-labeled poly(methyl methacrylate) (PMMA) was cryogenically milled for quantitative detection of the formation of block copolymer species using ultraviolet-absorbance gel permeation chromatography. At least 1.5% of the labeled polymer chains were incorporated into higher molecular weight PS, demonstrating that PMMA and PS successfully formed block copolymer species.

The compatibilization of polystyrene/high-density polyethylene (PS/HDPE) blends (80/20 wt%) following five or ten cycles of cryogenic milling, intimate melt-phase mixing, and long-term annealing was determined through dispersed HDPE domain diameter measurement via scanning electron microscopy. Cryogenic milling of the blends followed by melt mixing demonstrated reduced initial domain diameters than either blends of melt-mixed pellets or components milled independently. This reduction was due to the in situ synthesized block copolymer species, which reduced the interfacial surface tension of the blend and allowed smaller domain formation during the shear flow of melt-mixing. Upon static annealing, it was found that blends alloyed by additional

cryomilling cycles exhibited both initial domain sizes and initial static growth constants smaller than the mixed pellet blend and significantly reduced compared to the independently milled blend. The reduction of domain size between the five and ten cycle cryomilled blends was less than that between the melt-mixed pellet and five cycle cryomilled blends, suggesting additional milling cycles become less effective in terms of overall compatibilization. The rate at which the dispersed domain grow upon static annealing occurs in two stages, where the "second stage" growth of the ten-cycle cryomilled blend continued to be approximately half of the other blends. It was proposed that in addition to arithmetic mean dispersed phase diameter, the definition of compatibilization should incorporate the variance of the dispersed domain sizes. A new quantity, termed the variance ratio, was defined and applied to further characterization. The variance ratios of the blends cryomilled together or independently were much smaller than that of the mixed-pellet blend, potentially due to changes in molecular weight incurred during milling. The number averaged molecular weight of the PS phase in the blends decreased with additional milling cycles and was not affected by the presence of HDPE in the alloyed blends.

The new Bucknell University Solid-State Shear Pulverizer was commissioned and optimized with regards to compatibilizing PS/HDPE (80/20 wt%) blends. A full factorial blending experiment was conducted by varying kneading element type, quantity, and distribution, in addition to screw rotation rate and pellet feed rate. Blends were classified and compared through analysis of molecular weight reduction and the average dispersed domain size, variance, and growth rate. While no effects reduced the initial average domain size significantly, the final dispersed domain size after annealing was greatly

reduced by both the main effect of reverse-driving kneading blocks and the interaction effect between the reverse kneading blocks, high screw rotation speed, and high feed rate. It was determined that this domain size reduction was due to suppression of the static growth constant. An interaction between a high screw rotation rate and high pellet feed rate was determined to significantly increase the static growth constant. Molecular weight characterization revealed that reverse-driving kneading blocks significantly reduces both number- and weight-averaged molecular weight. Distributing these elements showed greater molecular weight reduction while not increasing blend compatibilization, indicating that placement of kneading elements within the union regions between barrel segments encourages chain degradation without promoting block copolymer creation. Distributing the kneading elements along the SSSP barrel was also found to increase dispersed domain diameter variance.

Three PS/HDPE blends of varying compatibilization were subjected to common thermal and mechanical property measurements to seek correlation with the results from the morphological characterization. Mechanical or thermal improvements which mirrored the degree of compatibilization as defined by dispersed domain size and growth minimization were not found, however several intriguing blend properties were uncovered. Differential scanning calorimetry indicated that melt-mixing PS with HDPE dramatically reduced the crystallinity of the HDPE regions, but could be improved through annealing. Moderate degrees of pulverization significantly increased the degree of crystallinity of the HDPE component, while excessive pulverization and chain scission dramatically decreased crystallinity. Dynamic mechanical analysis revealed PS/HDPE

blends exhibit synergistic stiffness improvements at high temperatures (< 105°C) which may be dependent on blend composition.

7.2 Recommendations for Future Work

Despite reaching the conclusions previously mentioned, several questions regarding solid-state processing of polymer blends remain for future research efforts. In all cases when conducting blend processing trials, a masterbatch should be created through twin-screw extrusion to improve composition consistency. Alternatively, a second pellet feeder could be used to independently meter the minority component. In order to contrast the energy efficiency and operation economics of SSSP versus cryogenic milling, a metric quantifying the energy incorporated into the product material versus the energy lost through heat generation should be created.

With regards to the cryogenic mill, the labeled polymer study should be repeated with a higher molecular weight, monodisperse polystyrene. The increased PS block size will improve isolation of the block copolymer species from the bulk homopolymers via GPC and ease their detection. Increasing the quantity of pyMA used in the synthesis of pyPMMA could aide in the detection of the copolymer species as well. Analysis of the dispersed domain sizes at static annealing times in excess of 240 minutes should be conducted to confirm the dual-stage growth of the cryogenically alloyed blends. In order to elucidate the trend of compatibilization effectiveness of successive milling cycles, blends should be milled in excess of 10 cycles to find an optimal compatibilization which is a balance between block copolymer generation and molecular weight reduction. Finally, to determine transferability of the cryomilling conclusions reached in this thesis, a different blend system should be similarly processed and analyzed.

As for additional blends research on the SSSP, several experimental routes warrant further study. A tracer study on material transport within the SSSP for varying screw designs should be undertaken to determine material mixing efficiency and retention times. The operation optimization results determined in this thesis should be extended to a blend system which had previously demonstrated improved mechanical performance with the addition of block copolymers or through reactive extrusion, such as PP-PA6,[118] PA6-Ultra high molecular weight PE,[119], HDPE-ethylene vinyl alcohol,[120] or forms of rubber toughening.[6]

Research with the PS/HDPE system should continue to investigate the synergistic crystallinity seen via DSC under moderate pulverization. Additionally, the improved stiffness of the PS/HDPE blend seen in the DMA study should be investigated in detail to find an optimal HDPE composition and determine whether annealing blends of varying degrees of compatibilization (as defined by growth constant reduction) affects high-temperature performance.

8. References

(1) Shultz, A. R.; Beach, B. M. *Macromolecules* **1974**, *7*, 902-909.

(2) Robeson, L. M., Ed. *Polymer Blends : a Comprehensive Review;* Hanser: Munich ; Cincinnati, 2007.

(3) Paul, D. R., Bucknall, C. B., Eds. *Polymer Blends;* Wiley: New York, 1999.

(4) Francis, P. S., Wambach, A. D., Eds. *Engineered Materials Handbook, Vol. 2: Engineering Plastics;* ASM International: Metals Park, OH, 1988.

(5) Macosko, C. W.; Guegan, P.; Khandpur, A. K.; Nakayama, A.; Marechal, P.; Inoue, T. *Macromolecules* **1996**, *29*, 5590-5598.

(6) Robeson, L. M.; Kuphal, J. A.; Vratsanos, M. S. *J. Appl. Polym. Sci.* **1996**, *61*, 1561-1569.

(7) Beyer, M. K.; Clausen-Schaumann, H. *Chem. Rev.* **2005**, *105*, 2921-2948.

(8) Boldyrev, V. V.; Tkacova, K. *J. Mater. Synth. Process.* **2000**, *8*, 121-132.

(9) Lebovitz, A. H.; Khait, K.; Torkelson, J. M. *Macromolecules* **2002**, *35*, 9716-9722.

(10) Stranz, M.; Koster, U.; Katzenberg, F. *J. Metastab. Nanocryst.* **2005**, *24-25*, 609-614.

(11) Smith, A. P.; Spontak, R. J.; Ade, H.; Smith, S. D.; Koch, C. C. *Adv. Mater.* **1999**, *11*, 1277-1281.

(12) Khait, K.; Torkelson, J. M. *Polym. Plast. Technol. Eng.* **1999**, *38*, 445-457.

(13) Smith, A. P.; Ade, H.; Balik, C. M.; Koch, C. C.; Smith, S. D.; Spontak, R. J. *Macromolecules* **2000**, *33*, 2595-2604.

(14) Stranz, M.; Koster, U. *J. Mater. Sci.* **2004**, *39*, 5275-5277.

(15) Farrell, M. P.; Kander, R. G.; Aning, A. O. *J. Mater. Synth. Process.* **1996**, *4*, 151-161.

(16) Martin, J. P.; Mccartney, S. R.; Kander, R. G. *J. Mater. Sci.* **2003**, *38*, 195-200.

(17) Koning, C.; Van Duin, M.; Pagnoulle, C.; Jerome, R. *Prog. Polym. Sci.* **1998**, *23*, 707-757.

(18) Paul, D. R.; Barlow, J. W. *J. Macromol. Sci.-Rev. M.* **1980**, *C18*, 109-168.

(19) Flory, P. I. *J. Chem. Phys.* **1942**, *10*, 51-61.

(20) Huggins, M. L. *J. Chem. Phys.* **1941**, *9*, 440-440.

(21) Lohse, D. J.; Fetters, L. J.; Doyle, M. J.; Wang, H. *Macromolecules* **1993**, *26*, 3444.

(22) Coleman, M. M.; Painter, P. C. *Prog. in Polym. Sci.* **1995**, *20*, 1-59.

(23) Weeks, N. E.; Karasz, F. E.; MacKnight, W. J. *J. App. Phys.* **1977**, *48*, 4068-4071.

(24) Datta, S., Lohse, D., Eds. *Polymeric Compatilibilizers: Uses and Benefits in Polymer Blends;* Hanser Publishers: Cincinnati, Ohio, 1996.

(25) Benni, P.; Cernia, E.; Demma, G.; D'Ilario, L.; Martinelli, A.; Martuscelli, E. *J. Mater. Sci. Lett.* **1989**, *8*, 358-360.

(26) Kim, W. N.; Burns, C. M. *J. Appl. Polym. Sci.* **1990**, *41*, 1575-1593.

(27) Yokouchi, M.; Seto, S.; Kobayashi, Y. *J. Appl. Polym. Sci.* **1983**, *28*, 2209-2216.

(28) Utracki, L. A. *Can. J. Chem. Eng.* **2002**, *80*, 1008-1016.

(29) Sundararaj, U.; Macosko, C. W. *Macromolecules* **1995**, *28*, 2647-2657.

(30) Hlavata, D.; Horak, Z.; Hromadkova, J.; Lednicky, F.; Pleska, A. *J. Polym. Sci. Part B* **1999**, *37*, 1647-1656.

(31) Fayt, R.; Hadjiandreou, P.; Teyssie, P. *J. Polym. Sci.: Polym. Chem.* **1985**, *23*, 337-342.

(32) Taylor, G. I. *Proc. Royal Soc. of London A* **1932**, *138*, 41-48.

(33) Taylor, G. I. *Proc. Royal Soc. of London A* **1934**, *146*, 0501-0523.

(34) Lebovitz, A. H.; Khait, K.; Torkelson, J. M. *Macromolecules* **2002**, *35*, 8672-8675.

(35) Rhee, J.; Crist, B. *Macromolecules* **1991**, *24*, 5663.

(36) Crist, B.; Nesarikar, A. R. *Macromolecules* **1995**, *28*, 890-896.

(37) Zhu, L.; Jiang, M.; Liu, L.; Zhou, H.; Fan, L.; Zhang, Y. *J. Macromol. Sci. - Phys.* **1998**, *B37*, 827-839.

(38) Marco, C.; Ellis, G.; Gomez, M. A.; Fatou, J. G.; Arribas, J. M.; Campoy, I.; Fontecha, A. *J. Appl. Polym. Sci.* **1997**, *65*, 2665-2677.

(39) Papadopoulou, C. P.; Kalfoglou, N. K. *Polymer* **2000**, *41*, 2543-2555.

(40) Wu, C. F. *J. Appl. Polym. Sci.* **2001**, *80*, 2468-2473.

(41) Shah, V. S.; Keitz, J. D.; Paul, D. R.; Barlow, J. W. *J. Appl. Polym. Sci.* **1986**, *32*, 3863-3879.

(42) Yang, K. M.; Lee, S. H.; Oh, J. M. *Polym. Eng. Sci.* **1999**, *39*, 1667-1677.

(43) Helfand, E.; Sapse, A. M. *J. Chem. Phys.* **1975**, *62*, 1327-1331.

(44) Helfand, E.; Tagami, Y. *J. Polym. Sci. Part B-Polym. Let.* **1971**, *9*, 741-&.

(45) Lindsey, C. R.; Paul, D. R.; Barlow, J. W. *J. Appl. Polym. Sci.* **1981**, *26*, 1-8.

(46) Fayt, R.; Jerome, R.; Teyssie, P. *J. Polym. Sci. Part C: Polym. Let.* **1986**, *24*, 25-28.

(47) Tao, Y.; Kim, J.; Torkelson, J. M. *Polymer* **2006**, *47*, 6773-6781.

(48) Fayt, R.; Jérôme, R.; Teyssié, P. *J. Polym. Sci. Part B: Polym. Phys.* **1989**, *27*, 775-793.

(49) Creton, C.; Kramer, E. J.; Hadziioannou, G. *Macromolecules* **1991**, *24*, 1846-1853.

(50) Creton, C.; Kramer, E. J.; Hui, C. Y.; Brown, H. R. *Macromolecules* **1992**, *25*, 3075-3088.

(51) Thomas, S.; Prudhomme, R. E. *Polymer* **1992**, *33*, 4260-4268.

(52) Holstimiettinen, R.; Seppala, J.; Ikkala, O. T. *Polym. Eng. Sci.* **1992**, *32*, 868-877.

(53) Cigana, P.; Favis, B. D.; Jerome, R. *J. Polym. Sci. Part B-Polym. Phys.* **1996**, *34*, 1691-1700.

(54) Sandoval, R. W.; Williams, D. E.; Kim, J.; Roth, C. B.; Torkelson, J. M. *J. Polym. Sci. Part B* **2008**, *46*, 2672-2682.

(55) Ide, F.; Hasegawa, A. *J. Appl. Polym. Sci.* **1974**, *18*, 963-974.

(56) Nisho, T.; Suzuki, Y.; Kojima, K.; Kakugo, M. *J. Polym. Engr.* **1991**, *10*, 124.

(57) Roeder, J.; Oliveira, R. V. B.; Gonçalves, M. C.; Soldi, V.; Pires, A. T. N. *Polym. Test.* **2002**, *21*, 815-821.

(58) Bridgman, P. W. *J. Appl. Phys.* **1953**, *24*, 560-570.

(59) Ceresa, R. J.; Watson, W. F. *J. Appl. Polym. Sci.* **1959**, *1*, 101-106.

(60) Backman, D. K.; Devries, K. L. *J. Polym. Sci. - Polym.Chem.* **1969**, *7*, 2125-34.

(61) Bresler, S. E.; Zhurkov, S. N.; Kazbekov, E. N.; Saminskii, E. M.; Tomashevskii, E. E. *ZH. Tekh. Fiz+.* **1959**, *29*, 358-364.

(62) Campbell, D.; Peterlin, A. *J. Polym. Sci. - Polym. Let. Part B* **1968**, *6*, 481-485.

(63) Kolbert, A. C.; Didier, J. G.; Xu, L. *Macromolecules* **1996**, *29*, 8591-8598.

(64) Ganglani, M.; Torkelson, J. M.; Carr, S. H.; Khait, K. *J. Appl. Polym. Sci.* **2001**, *80*, 671-679.

(65) Gleixner, G.; Olaj, O. F.; Breitenbach, J. W. *Makromol. Chem.* **1979**, *180*, 2581-2590.

(66) Schreck, V. A.; Serelis, A. K.; Solomon, D. H. *Aust. J. Chem.* **1989**, *42*, 375-393.

(67) Moad, G.; Moad, C. L. *Macromolecules* **1996**, *29*, 7727-7733.

(68) Chen, Z.; Wang, Q. *Polym. Int.* **2001**, *50*, 96-972.

(69) Cavalieri, F.; Padella, F.; Bourbonneux, S. *Polymer* **2002**, *43*, 1155-1161.

(70) Curwick, L. R., International Nickel Co Inc. *Oxide Dispersion Strengthened High Volume Fraction Gamma Prime Ni-Cr-Al Alloys Made by Mechanical Alloying.* Defense Technical Information Center: Ft. Belvoir, 1976.

(71) Suryanarayana, C. *Prog. Mat. Sci.* **2001**, *46*, 1-184.

(72) Petkovic-Luton, R.; Vallone, J. *Composite Dispersion Strengthened Composite Metal Powders.* Oct 28. 1968. US Pat Num: 4,619,699.

(73) Vivatpanachart, S.; Nomura, H.; Miyahara, Y. *J. Appl. Polym. Sci.* **1981**, *26*, 1485-1491.

(74) Pan, J.; Shaw, W. J. D. *J. Appl. Polym. Sci.* **1994**, *52*, 507-514.

(75) Pan, J.; Shaw, W. J. D. *J. Appl. Polym. Sci.* **1995**, *56*, 557-566.

(76) Smith, A. P.; Spontak, R. J.; Ade, H. *Polym. Degrad. Stab.* **2001**, *72*, 519-524.

(77) Schexnaydre, R. J.; Mitchell, B. S. *Polym. Eng. Sci.* **2008**, *48*, 649-655.

(78) Schexnaydre, R. J.; Mitchell, B. S. *J. Polym. Sci. Part B* **2008**, *46*, 1348-1359.

(79) Smith, A. P.; Shay, J. S.; Spontak, R. J.; Balik, C. M.; Ade, H.; Smith, S. D.; Koch, C. C. *Polymer* **2000**, *41*, 6271-6283.

(80) Smith, A. P.; Spontak, R. J.; Koch, C. C.; Smith, S. D.; Ade, H. *Macromol. Mater. Eng.* **2000**, *274*, 1-12.

(81) Smith, A. P.; Harald, A.; Koch, C. C.; Smith, S. D.; Spontak, R. J. *Macromolecules* **2000**, *33*, 1163-1172.

(82) Stranz, M.; Koster, U. *Colloid Polym. Sci.* **2004**, *282*, 381-386.

(83) Stranz, M.; Koster, U. *J. Alloy Compd.* **2007**, *434-435*, 447-450.

(84) Khait, K., Carr, S. H., and Mack, M. H., Eds. *Solid-state shear pulverization : a new polymer processing and powder technology;* Technomic Pub. Co.: Lancaster, 2001.

(85) Furgiuele, N.; Lebovitz, A. H.; Khait, K.; Torkelson, J. M. *Macromolecules* **2000**, *33*, 225-228.

(86) Nesarikar, A. R.; Carr, S. H.; Khait, K.; Mirabella, F. M. *J. Appl. Polym. Sci.* **1997**, *63*, 1179-1187.

(87) Kasimatis, K. G.; Nowell, J. A.; Dykes, L. M.; Burghardt, W. R.; Ramanathan, T.; Brinson, L. C.; Torkelson, J. M. Society of Plastics Engineers Annual Technical Conference 2005, ANTEC 2005; Vol. 5, pp 291-295.

(88) Tao, Y.; Lebovitz, A. H.; Torkelson, J. M. *Polymer* **2005**, *46*, 4753-4761.

(89) Wakabayashi, K.; Pierre, C.; Dikin, D. A.; Ruoff, R. S.; Ramanathan, T.; Brinson, L. C.; Torkelson, J. M. *Macromolecules* **2008**, *41*, 1905.

(90) Furgiuele, N.; Lebovitz, A. H.; Khait, K.; Torkelson, J. M. *Polym. Eng. Sci.* **2000**, *40*, 1447-1457.

(91) Wakabayashi, K.; Tao, Y.; Lebovitz, A. H.; Torkelson, J. M. Society of Plastics Engineers Annual Technical Conference: Plastics Encounter at ANTEC 2007; Vol. 3, pp 1520-1524.

(92) Masuda, J.; Kasimatis, K. G.; Torkelson, J. M. 66th Annual Technical Conference of the Society of Plastics Engineers, Plastics Encounter at ANTEC 2008; Vol. 4, pp 2046-2050.

(93) Walker, A. M.; Tao, Y.; Torkelson, J. M. Society of Plastics Engineers Annual Technical Conference: Plastics Encounter at ANTEC 2007; Vol. 3, pp 1712-1716.

(94) Hubert, P. J. Solid-State Fabrication and Characterization of Polymer-graphite Nanocomposites, Bucknell University, Lewisburg, PA, 2009.

(95) Lebovitz, A. H.; Khait, K.; Torkelson, J. M. *Polymer* **2003**, *44*, 199-206.

(96) Winnik, F. M.; Winnik, M. A.; Tazuke, S. *J. Phys. Chem.* **1987**, *91*, 594-597.

(97) Robello, D. R. *J. Polym. Sci. Part A: Polym. Chem.* **1990**, *28*, 1-13.

(98) Lebovitz, A. H. Intimate Mixing and In Situ Compatibilization of Immiscible Polymer Blends via an Innovative Process: Solid-State Shear Pulverization (SSSP), Northwestern University, Evanston, Illinois, 2003.

(99) Majeste, J.; Montfort, J. -.; Allal, A.; Marin, G. *Rheol. Acta* **1998**, *37*, 486-499.

(100) Fuchs, K.; Friedrich, C.; Weese, J. *Macromolecules* **1996**, *29*, 5893-5901.

(101) Witkin, D. B.; Lavernia, E. J. *Prog. Mat. Sci.* **2006**, *51*, 1-60.

(102) Martin, J. P.; Kander, R. G. *J. Appl. Polym. Sci.* **2003**, *88*, 1196-1202.

(103) Dynisco Plastics Laboratory Mixing Molder Fact Sheet, 2008.

(104) Utracki, L. A.; *Polymer Blends Handbook*. Dordrecht: Kluwer Academic Publishers, 2002.

(105) Mattox, Donald M.; *Handbook of Physical Vapor Deposition (PVD) Processing: Film Formation, Adhesion, Surface Preparation and Contamination Control*. Westwood, N.J.: Noyes Publications, 1998.

(106) Moore, J. C. *J. Polym. Sci. Part A* **1964**, *2*, 835-843.

(107) Crompton, T. R.; *Polymer Reference Book*. Shrewsbury, U.K.: Rapra Technology Limited, 2006.

(108) Lauger, J.; Lay, R.; Gronski, W. *J. Chem. Phys.* **1994**, *101*, 7181-7184.

(109) Crist, B. *Macromolecules* **1996**, *29*, 7276-7279.

(110) Whitwell, J. C.; Wakelin, J. H. *Text. Res. J.* **1958**, *28*, 929-940.

(111) Daniel, C. *Ind. Eng. Chem.* **1963**, *55*, 45-48.

(112) Daniel, C. *Technometrics* **1959**, *1*, 311-341.

(113) Wakabayashi, K.; Pierre, C.; Diking, D. A.; Ruoff, R. S.; Ramanathan, T.; Catherine Brinson, L.; Torkelson, J. M. *Macromolecules* **2008**, *41*, 1905-1908.

(114) Pujari, S.; Ramanathan, T.; Kasimatis, K.; Masuda, J.; Andrews, R.; Torkelson, J. M.; Brinson, L. C.; Burghardt, W. R. *J. Polym. Sci Part B* **2009**, *47*, 1426.

(115) Chuai, C.; Almdal, K.; Lyngaae-Jrgensen, J. *J. Appl. Polym. Sci.* **2004**, *91*, 609-620.

(116) Jana, R. N.; Nando, G. B. *J. Appl. Polym. Sci.* **2003**, *90*, 635-642.

(117) Joshi, J.; Lehman, R.; Hall, G. S. *Appl. Spectrosc.* **2006**, *60*, 483-489.

(118) Tucker, J. D.; Lee, S. Y.; Einsporn, R. L. *Polym. Eng. Sci.* **2000**, *40*, 2577-2589.

(119) Yao, Z.; Yin, Z.; Sun, G.; Liu, C.; Tong, J.; Ren, L.; Yin, J. *J. Appl. Polym. Sci.* **2000**, *75*, 232-238.

(120) Park, S. H.; Lee, G. J.; Im, S. S.; Suh, K. D. *Polym. Eng. Sci.* **1998**, *38*, 1420-1425.

Appendix A. Additional Figures

A.1 Crist Growth Model for Cryogenically Milled PS/HDPE Blends…….. 126
A.2 Two-Stage Crist Growth Model for Cryogenically Milled PS/HDPE Blends…128
A.3 Diameter Histograms for Statically Annealed Cryomilled PS/HDPE Blends…130
A.4 Crist Model and Histograms for PS/HDPE Blends Fabricated via SSSP……...132

A.1 Crist Growth Model for Cryogenically Milled PS/HDPE Blends

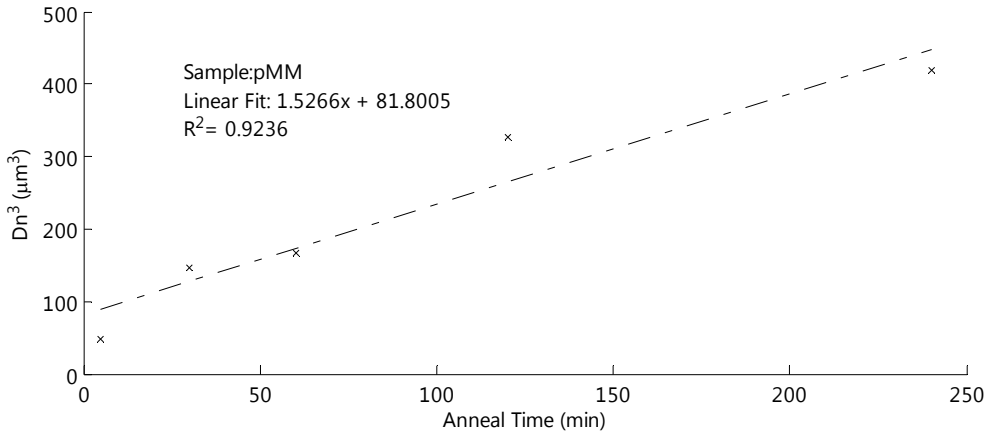

Figure A.1.1. The Crist growth model applied to an pellet melt-mixed PS/HDPE (80/20 wt%) blend

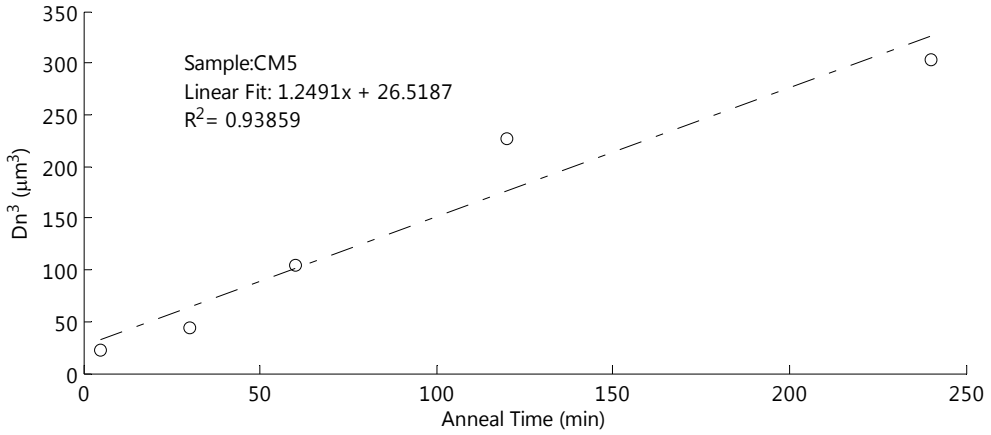

Figure A.1.2. The Crist growth model applied to a 5-cycle cryomilled and melt-mixed PS/HDPE (80/20 wt%) blend

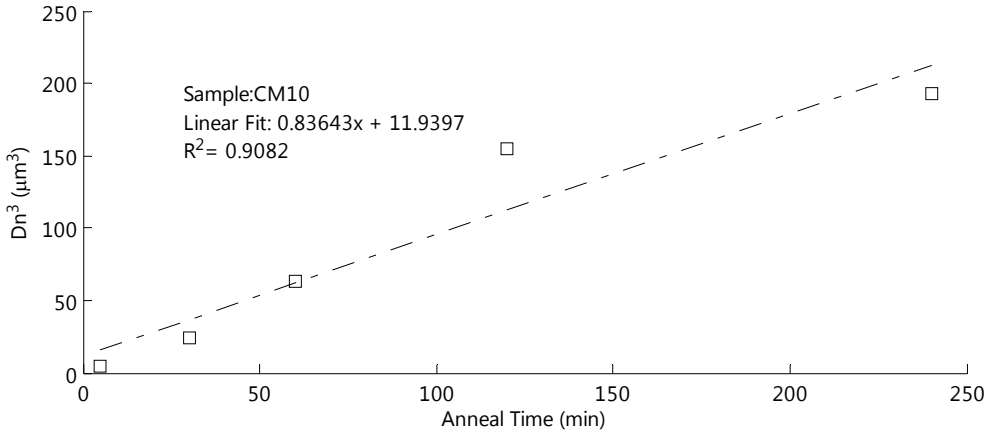

Figure A.1.3. The Crist growth model applied to a 10-cycle cryomilled and melt-mixed PS/HDPE (80/20 wt%) blend

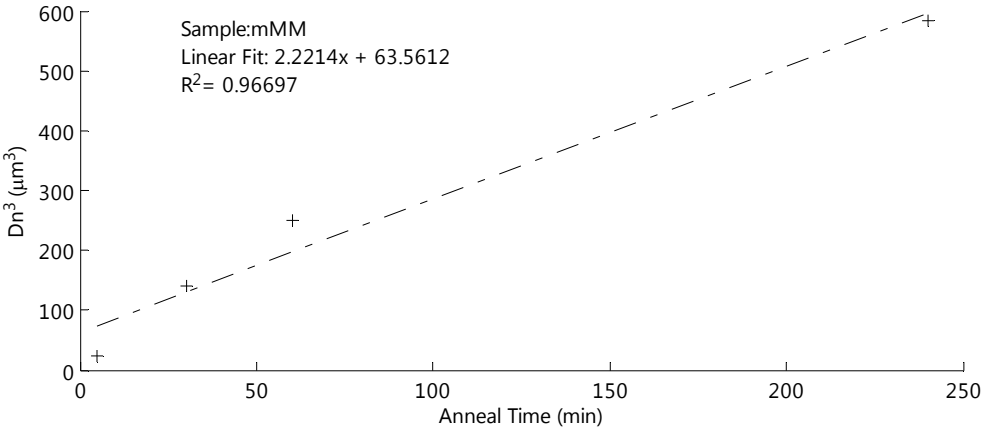

Figure A.1.4. The Crist growth model applied to a melt-mixed PS/HDPE (80/20 wt%) blend whose components were independently cryomilled for 10 cycles

A.2 Two-Stage Crist Growth Model for Cryogenically Milled PS/HDPE Blends

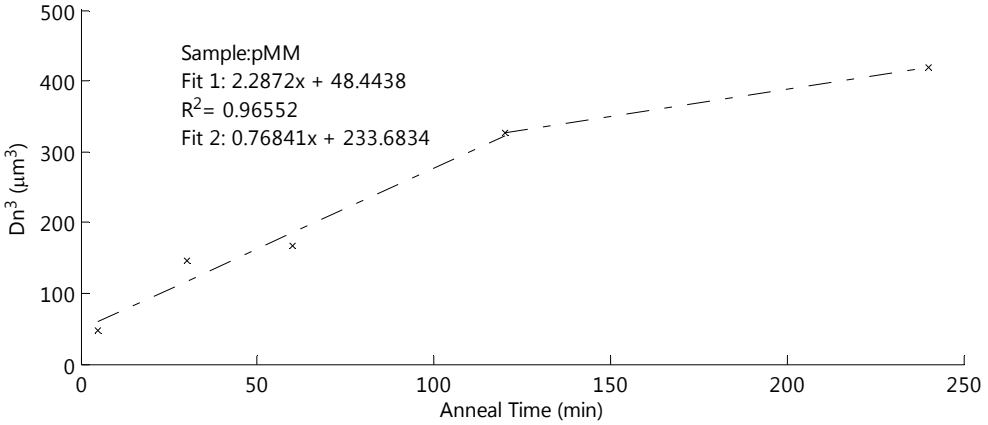

Figure A.2.1. A two-stage Crist growth model applied to a pellet melt-mixed PS/HDPE (80/20 wt%) blend

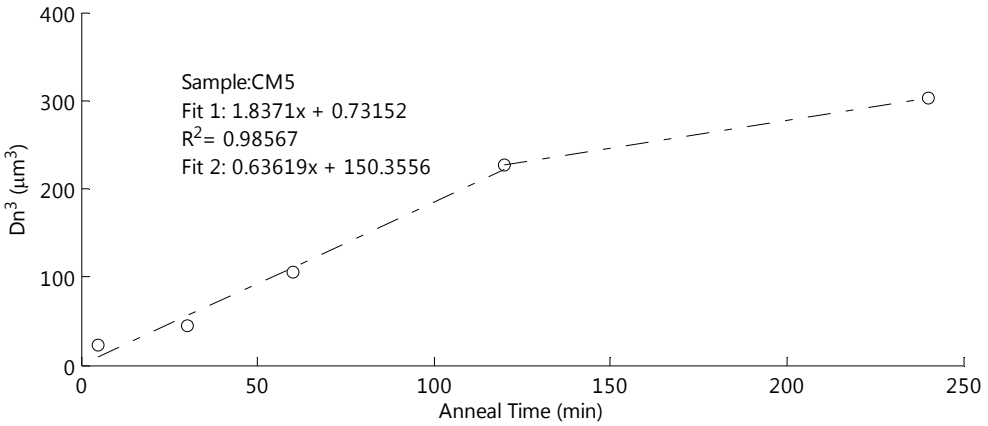

Figure A.2.2. A two-stage Crist growth model applied to a 5-cycle cryomilled and melt-mixed PS/HDPE (80/20 wt%) blend

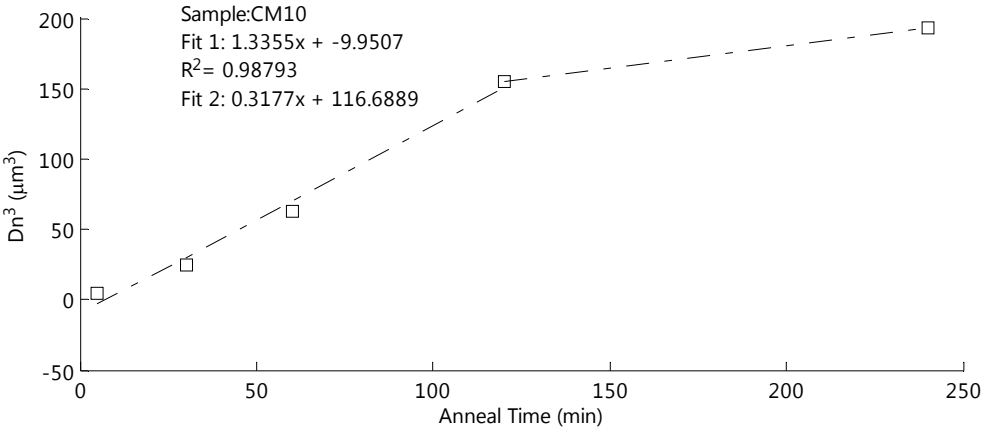

Figure A.2.3. A two-stage Crist growth model applied to a 10-cycle cryomilled and melt-mixed PS/HDPE (80/20 wt%) blend

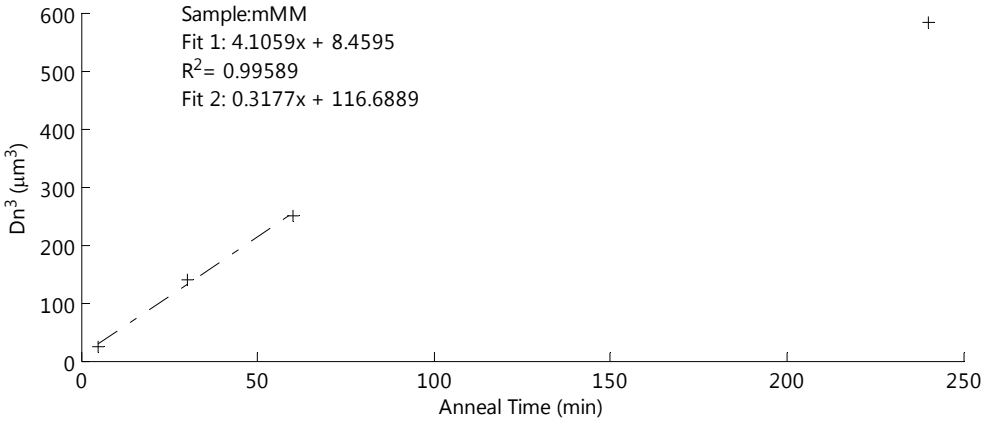

Figure A.2.4. A two-stage Crist growth model applied to a melt-mixed PS/HDPE (80/20 wt%) blend whose components were independently cryomilled for 10 cycles

A.3 Diameter Histograms for Statically Annealed Cryomilled PS/HDPE Blends

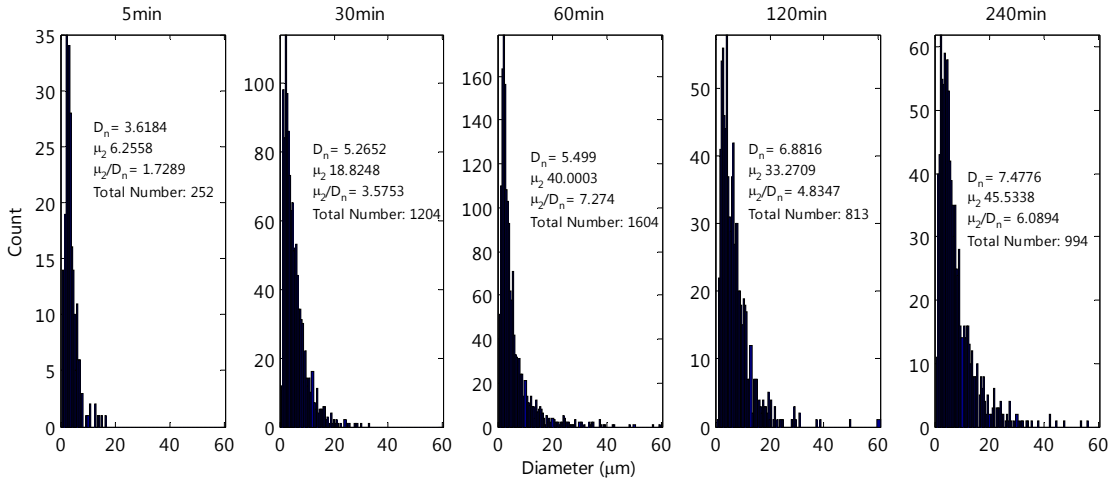

Figure A.3.1. Dispersed phase diameter histograms for a pellet melt-mixed PS/HDPE blend (80/20 wt%) at different anneal times

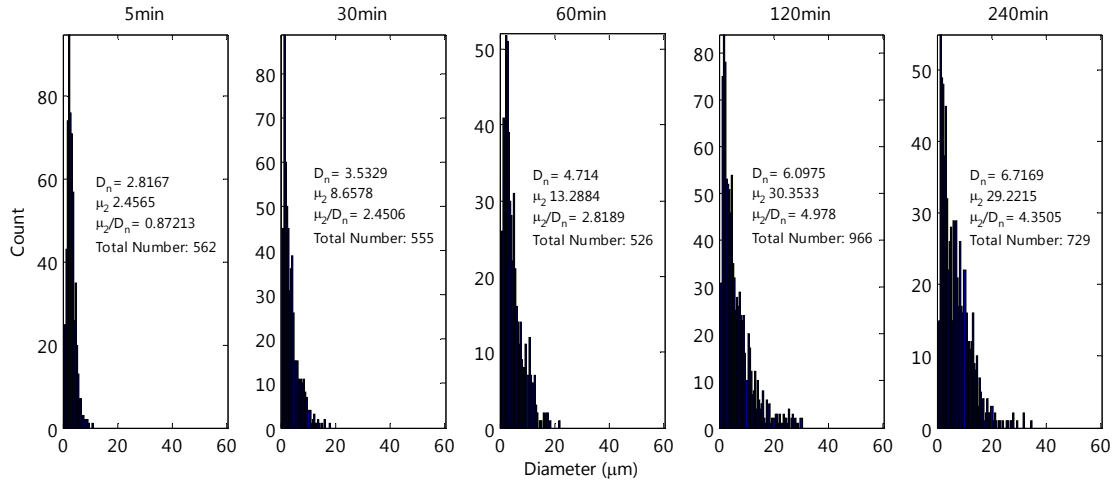

Figure A.3.2. Dispersed phase diameter histograms for a 5-cycle cryomilled and melt-mixed PS/HDPE (80/20 wt%) blend

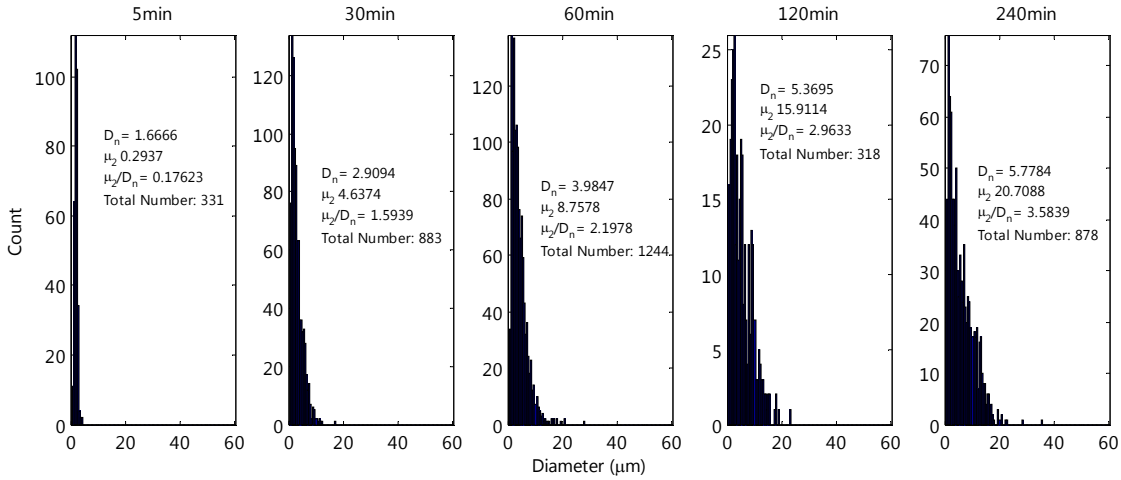

Figure A.3.3. Dispersed phase diameter histograms for a 10-cycle cryomilled and melt-mixed PS/HDPE (80/20 wt%) blend

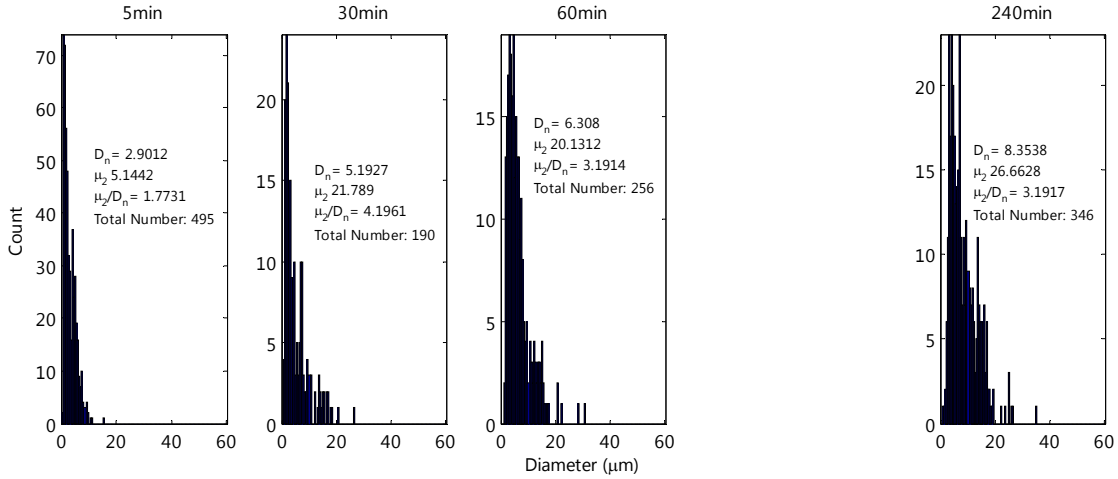

Figure A.3.4. Dispersed phase diameter histograms for a melt-mixed PS/HDPE (80/20 wt%) blend whose components were independently cryomilled for 10 cycles

A.4 Crist Growth Model and Histograms for PS/HDPE Blends Fabricated via SSSP

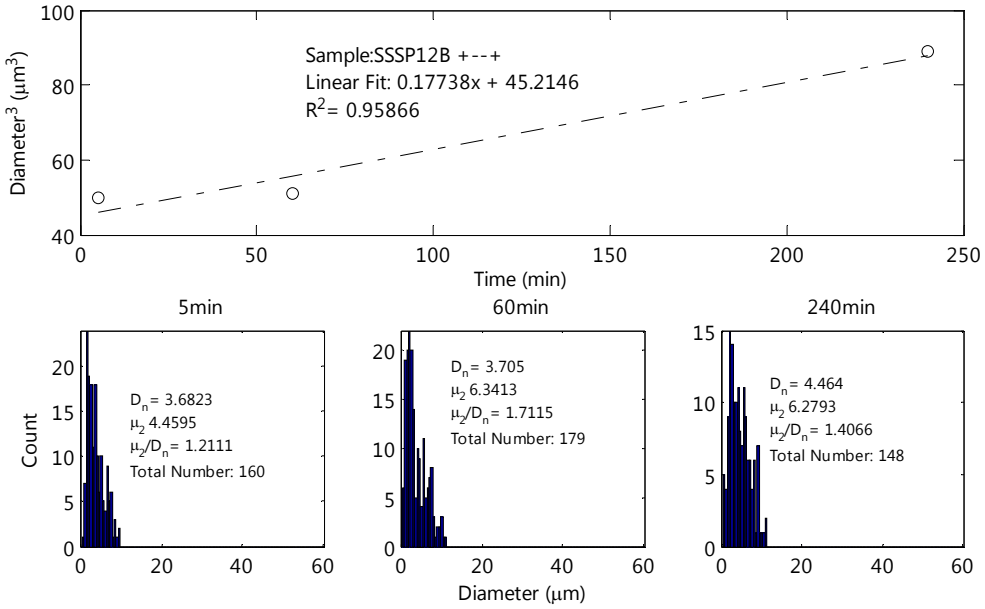

Figure A.4.1. A Crist growth model applied to the "+ - - +" SSSP PS/HDPE blend along with histogram data for each anneal time

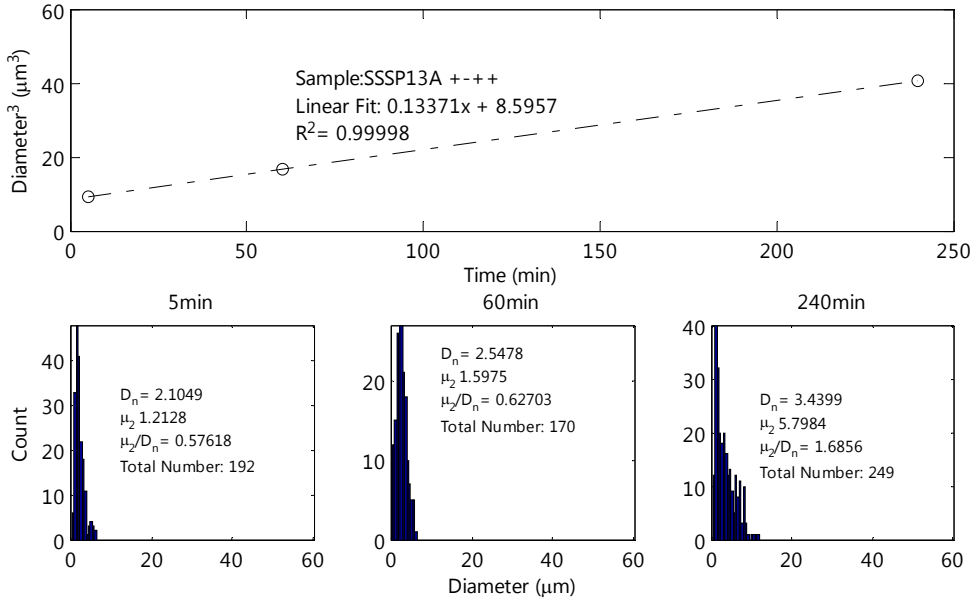

Figure A.4.2. A Crist growth model applied to the "+ - + +" SSSP PS/HDPE blend along with histogram data for each anneal time

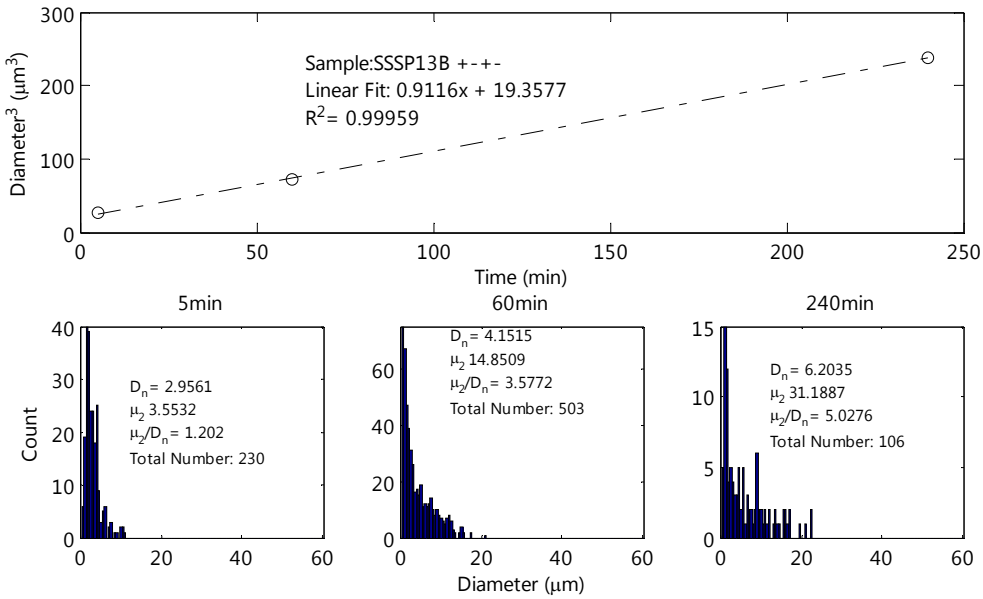

Figure A.4.3. A Crist growth model applied to the "+ - + -" SSSP PS/HDPE blend along with histogram data for each anneal time

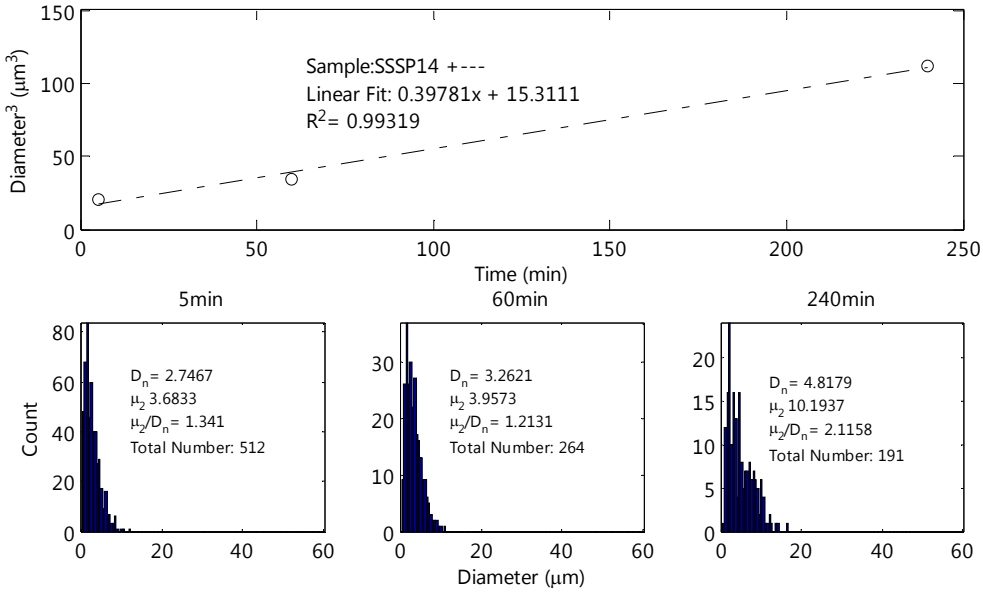

Figure A.4.4. A Crist growth model applied to the "+ - - -" SSSP PS/HDPE blend along with histogram data for each anneal time

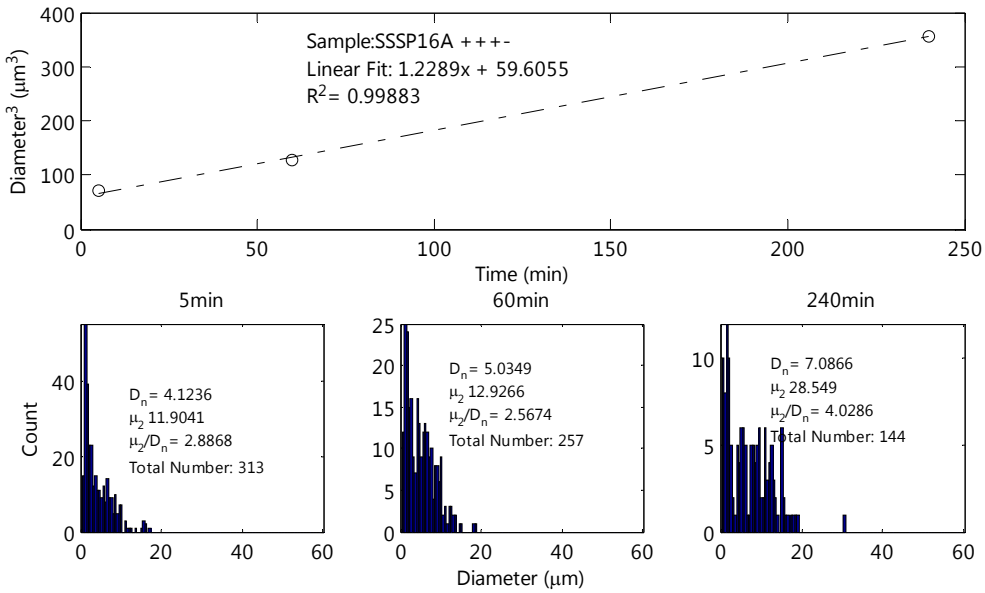

Figure A.4.5. A Crist growth model applied to the "+ + + -" SSSP PS/HDPE blend along with histogram data for each anneal time

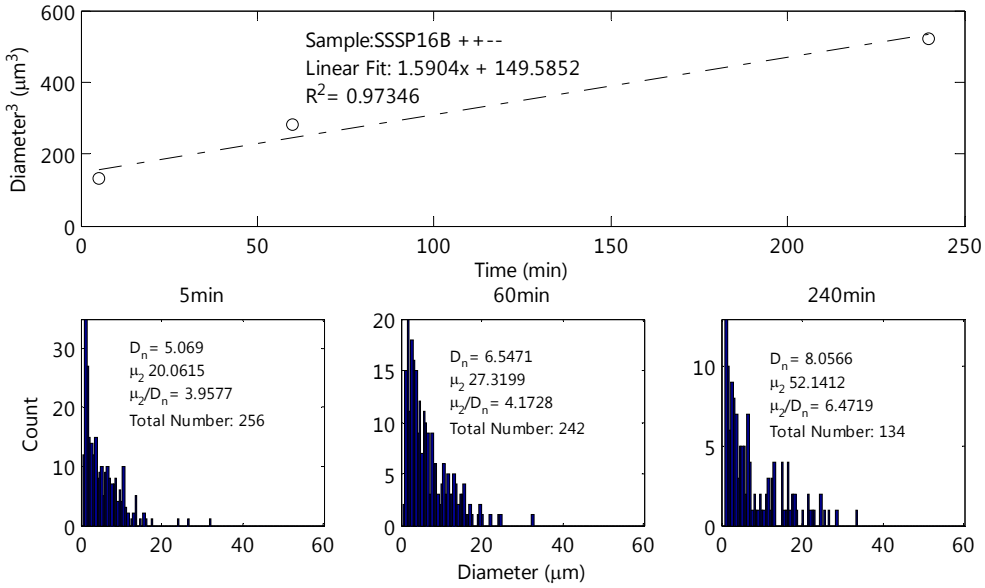

Figure A.4.6. A Crist growth model applied to the "+ + - -" SSSP PS/HDPE blend along with histogram data for each anneal time

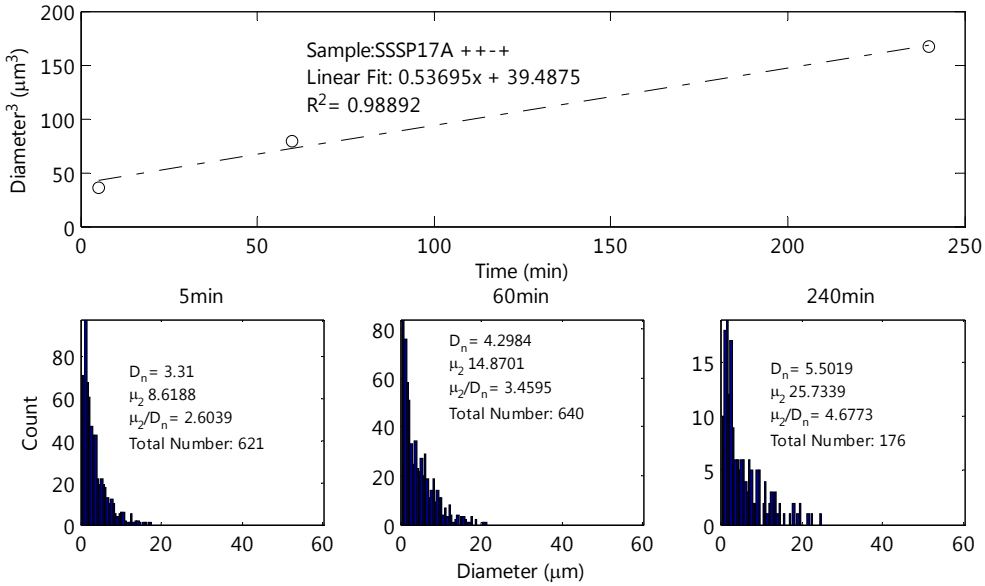

Figure A.4.7. A Crist growth model applied to the "+ + - +" SSSP PS/HDPE blend along with histogram data for each anneal time

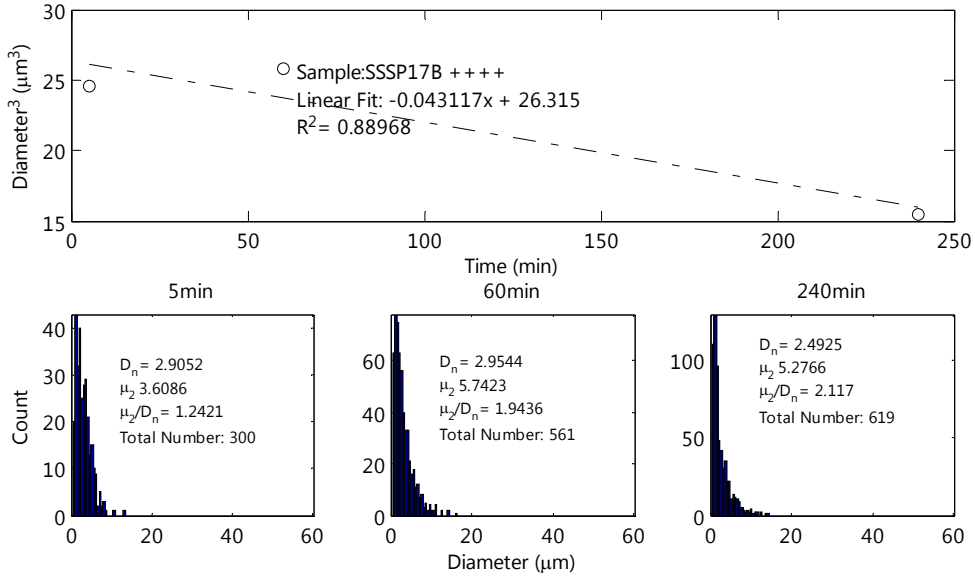

Figure A.4.8. A Crist growth model applied to the "+ + + +" SSSP PS/HDPE blend along with histogram data for each anneal time

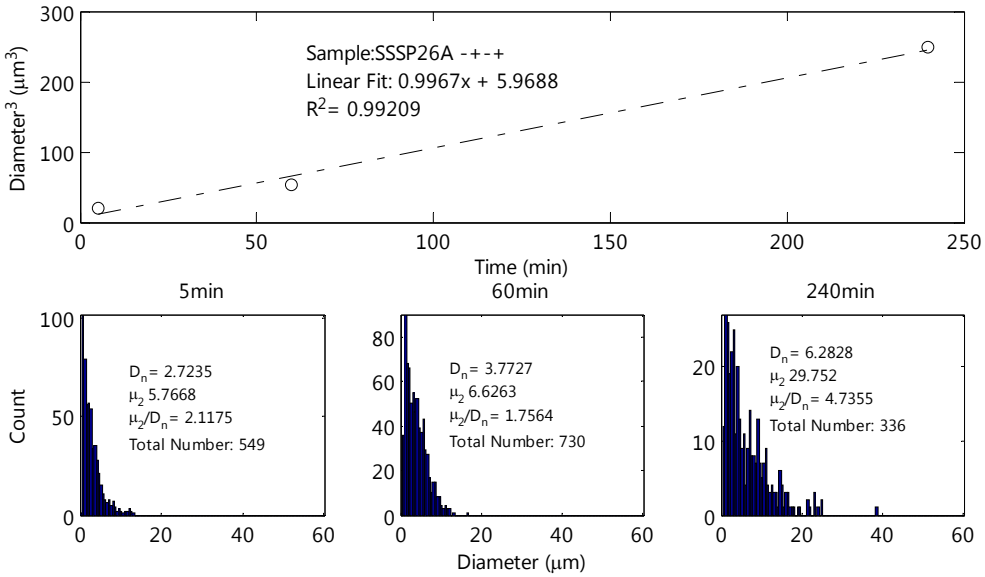

Figure A.4.9. A Crist growth model applied to the "- + - +" SSSP PS/HDPE blend along with histogram data for each anneal time

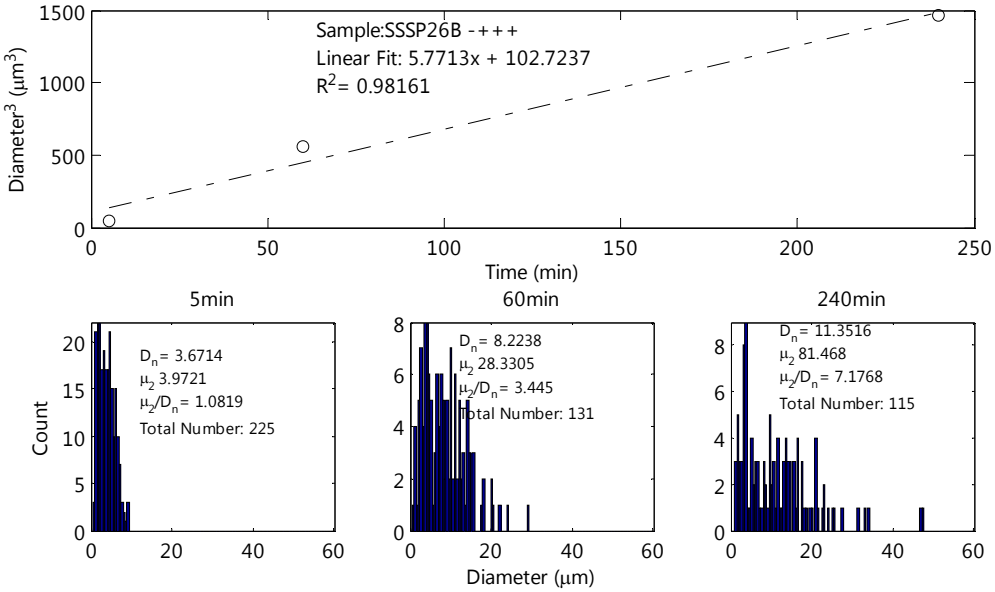

Figure A.4.10. A Crist growth model applied to the "- + + +" SSSP PS/HDPE blend along with histogram data for each anneal time

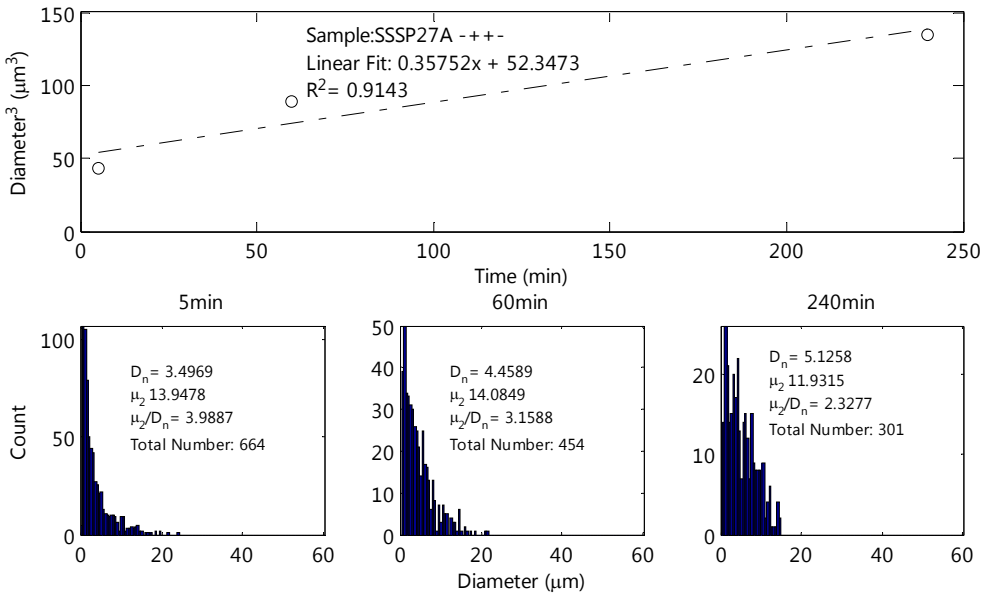

Figure A.4.11. A Crist growth model applied to the "- + + -" SSSP PS/HDPE blend along with histogram data for each anneal time

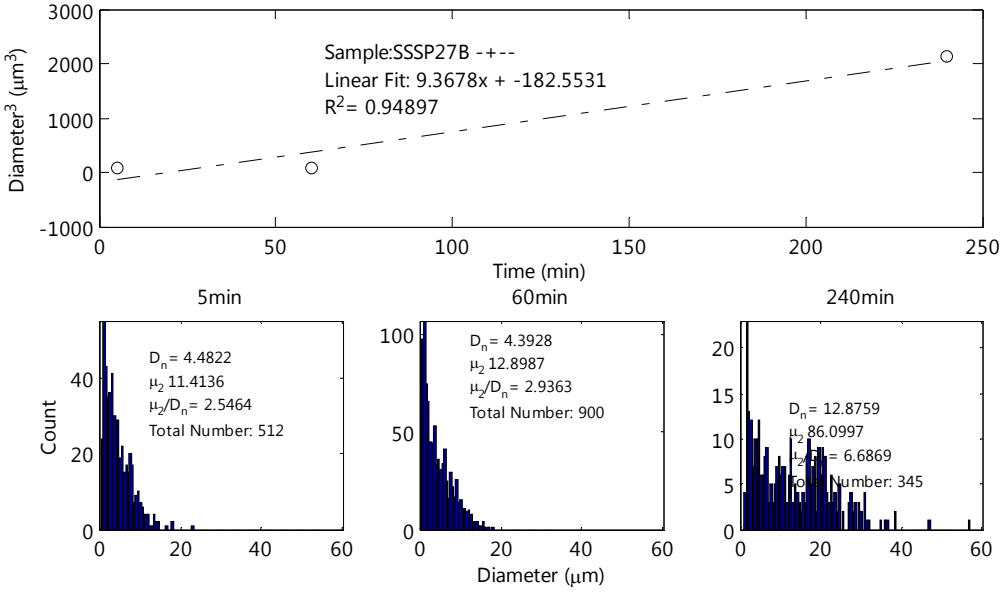

Figure A.4.12. A Crist growth model applied to the "- + - -" SSSP PS/HDPE blend along with histogram data for each anneal time

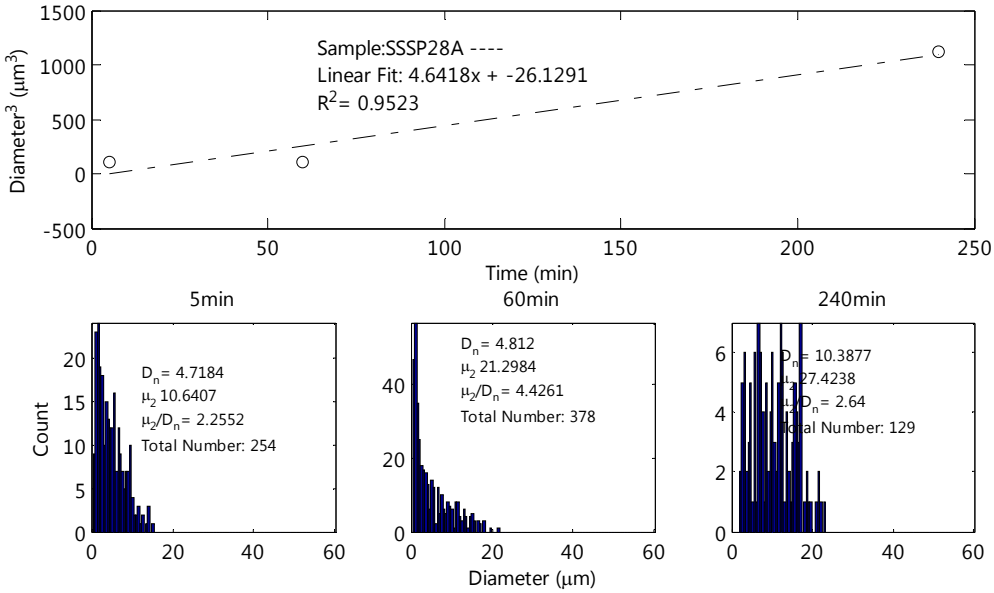

Figure A.4.13. A Crist growth model applied to the "- - - -" SSSP PS/HDPE blend along with histogram data for each anneal time

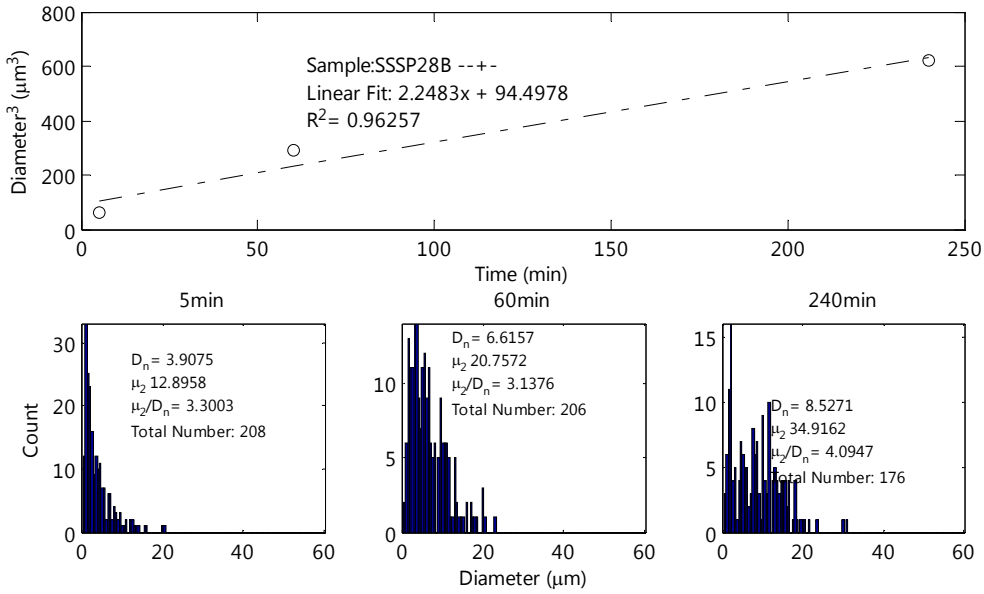

Figure A.4.14. A Crist growth model applied to the "- - + -" SSSP PS/HDPE blend along with histogram data for each anneal time

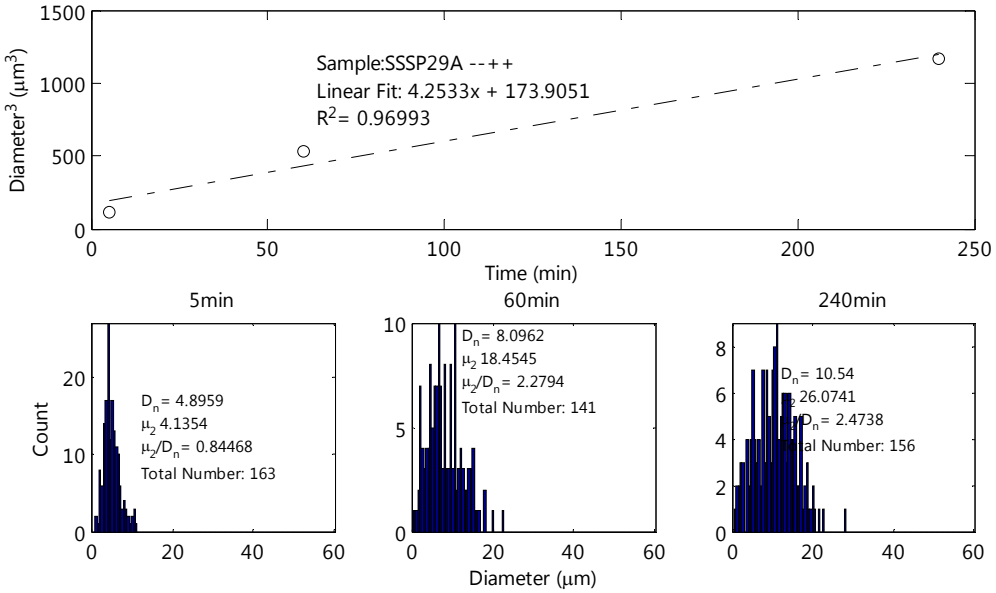

Figure A.4.15. A Crist growth model applied to the "- - + +" SSSP PS/HDPE blend along with histogram data for each anneal time

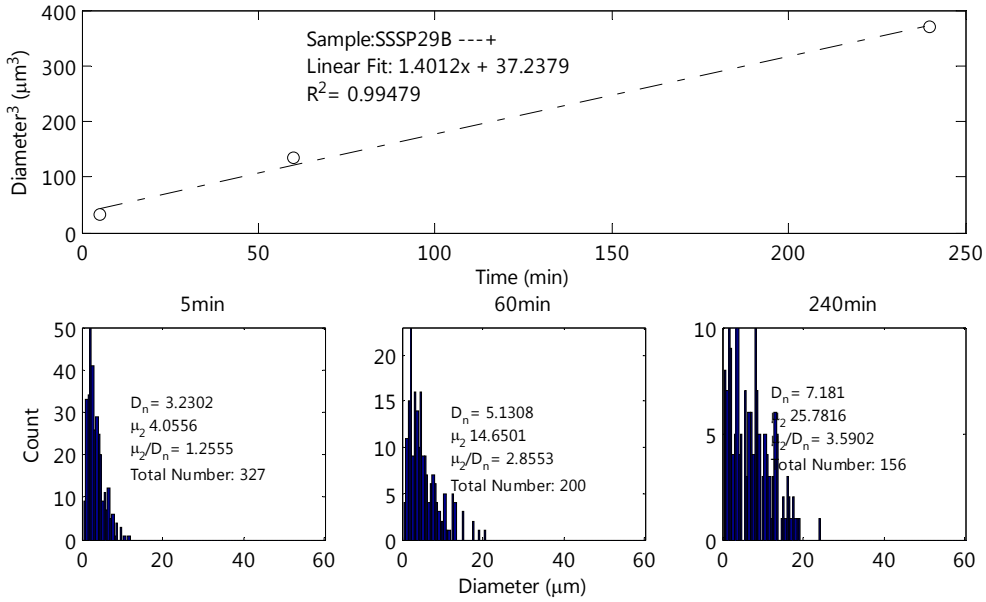

Figure A.4.16. A Crist growth model applied to the "- - - +" SSSP PS/HDPE blend along with histogram data for each anneal time

Appendix B. Software Design, Analysis, and Code

B.1 Tensile Test Analyzer…… 141
B.1.1 Description and Purpose…….. 141
B.1.2 Supported Input Data Format…….……. 141
B.1.3 Typical Usage Case Study……... 142
B.1.4 M-File Code…… 144
B.2 GPC – SEC Analysis……. 150
B.2.1 Description and Purpose……. 150
B.2.2 Supported Input Data Formats…… 151
B.2.3 Typical Usage Case Study…….. 151
B.2.4 M-File Code…… 153
B.3 Particle Size Analyzer……... 163
B.3.1 Description and Purpose……. 163
B.3.2 Supported Input Data Formats…… 163
B.3.3 Typical Usage Case Study…….. 164
B.3.4 M-File Code…… 168
B.4 Statistics…… 176
B.4.1 Description and Purpose……. 176

Throughout this course of study the current means of analyzing data quickly and efficiently were either nonexistent at Bucknell University or severely deficient. To increase productivity in this research, several useful software tools were created in the MATLAB coding environment and are presented to the University for future use. This appendix serves as a design document detailing the proper use and maintenance of these tools.

B.1 Tensile Test Analyzer

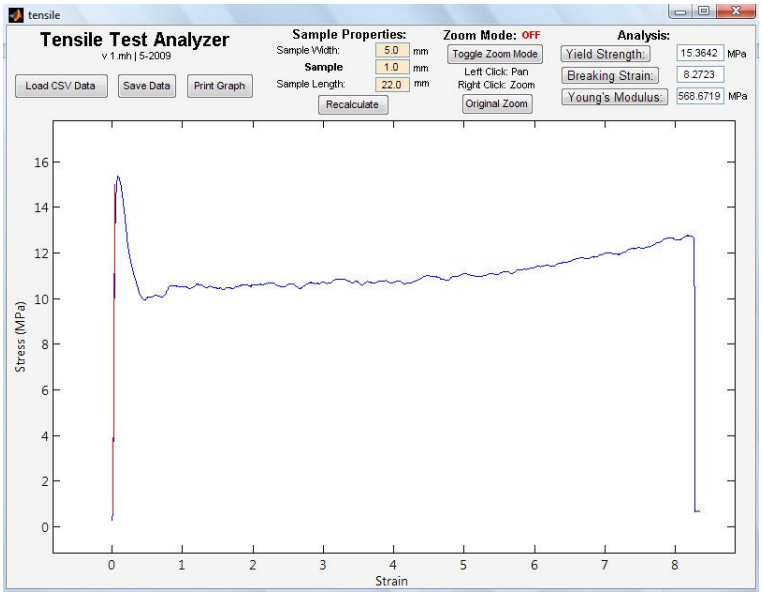

Figure B.1. The Tensile Test Analyzer user interface

B.1.1 Description and Purpose

The Tensile Test Analyzer (TTA) takes raw force and extension data from a Universal Tester, converts these data into SI stress and strain, and performs analysis to calculate yield strength, breaking strain, and Young's modulus. Given dimensions of the sample, the TTA attempts to automatically find yield strength and breaking strain, while requiring the user to define which data should be used to calculate Young's modulus. The TTA allows users to dynamically zoom and scale imported data to focus on any points of interest.

B.1.2 Supported Input Data Format

The TTA imports raw data saved by Bucknell University's custom "Tinius Control" program. The files must be in comma separated value (.csv) format and consist of four columns of data, as seen in Table B.1, with no column headings. As the final two

columns are not used in the TTA, they may be omitted. Extension and force values are expected to initially be zeroed.

Table B.1. Expected data file format for the TTA

Extension (inches)	Force (lbf)	Time (sec) (Not used for Calculations)	Extension Rate (in/min) (Not used for Calculations)

B.1.3 Typical Usage Case Study

This case study follows the steps that a typical user will take when operating the program and details the functions performed with each action.

- **User runs 'tensile.m' file.**
  - *Tensile Test Analyzer GUI is loaded and sets the initial directory.*
- **User clicks "Load CSV Data" button, browses to, and opens a properly formatted .csv data file.**
  - *Zoom mode, if on, is deactivated.*
  - *The data file's directory is made the current directory, the data is loaded, and the current directory is reset to the initial directory.*
    - Note: If the "Select File to Open" dialog box is closed or cancelled, the initial directory will not be reset and the program will stop functioning.
  - *The raw extension (inches) and force (lbf) data is converted to SI stress (MPa) and strain using sample dimensions provided in input boxes.*
  - *The visual plot is updated with the converted stress-strain data.*
  - *The Yield Strength is automatically detected by finding the maximum stress in the first 70% of the converted data and updated.*
    - Note: 70% was arbitrarily chosen to prevent samples with large stresses prior to failure from being detected as the yield strength. For very brittle samples which fail at their yield strength, this might prevent accurate detection.

- *Breaking strain is automatically detected by back-stepping through the converted data and finding a value 1.5 times higher than the sample after it and updated.*
    - Note: The 1.5 value was arbitrarily chosen and performs well for most systems. Systems which exhibit extended failure responses may not be accurately detected.

- **User enters new geometry measurements in the Sample Properties boxes and clicks 'Recalculate'.**
    - *The raw extension (inches) and force (lbf) data is converted to SI stress (MPa) and strain using sample dimensions provided in input boxes.*
    - *The visual plot is updated with the converted stress-strain data.*
    - *The Yield Strength is automatically detected by finding the maximum stress in the first 70% of the converted data and updated.*
        - Note: 70% was arbitrarily chosen to prevent samples with large stresses prior to failure from being detected as the yield strength. For very brittle samples which fail at their yield strength, this might prevent accurate detection.
    - *Breaking strain is automatically detected by back-stepping through the converted data and finding a value 1.5 times higher than the sample after it and updated.*
        - Note: The 1.5 value was arbitrarily chosen and performs well for most systems. Systems which exhibit extended failure responses may not be accurately detected.

- **User clicks on 'Toggle Zoom Mode' and adjusts graph to view linear elastic deformation region.**
    - *The "INTERACTIVEMOUSE" function, retrieved from the MATLAB File Exchange, is activated and Zoom Mode is engaged.*

- **User clicks on Young's Modulus button and selects two points from which to calculate modulus.**
    - *Zoom mode is disabled, if active.*

- *Clicks are sorted to determine which is the beginning and end of selected data.*
- *Linear regression is performed on data between the x-axis values of the two clicks.*
- *The current graph zoom state is saved, the graph is re-plotted with the linear regression represented by a red line from the origin to the Yield Strain, and the zoom state is restored.*

- **User clicks on Yield Strength or Breaking Strain buttons and selects a point on the graph.**
  - *Zoom mode is disabled, if active.*
  - *Data point closest to the user click on the X axis is found*
  - *Desired property is updated.*
- **User clicks on Save Data button and inputs a desired file name and path.**
  - *Current path is changed to the desired save directory.*
  - *The converted stress-strain data is saved to the desired file name in .csv format where the first column is stress and the second is strain.*
  - *The current path is reset to the initial directory.*
- **User clicks on 'Print Graph'**
  - *Standard operating system print dialog is opened allowing printing*
    - Note: Printing prints the graph along with the UI interface, allowing calculated yield strength, breaking strain, and Young's modulus to be saved.

B.1.4 M-File Code

```
function varargout = tensile(varargin)
% TENSILE M-file for tensile.fig
%      TENSILE, by itself, creates a new TENSILE or raises the existing
%      singleton*.

% Edit the above text to modify the response to help tensile

% Last Modified by GUIDE v2.5 19-Mar-2010 13:10:14

% Begin initialization code - DO NOT EDIT
gui_Singleton = 1;
gui_State = struct('gui_Name',       mfilename, ...
                   'gui_Singleton',  gui_Singleton, ...
                   'gui_OpeningFcn', @tensile_OpeningFcn, ...
                   'gui_OutputFcn',  @tensile_OutputFcn, ...
                   'gui_LayoutFcn',  [] , ...
```

```
                    'gui_Callback',   []);
if nargin && ischar(varargin{1})
    gui_State.gui_Callback = str2func(varargin{1});
end

if nargout
    [varargout{1:nargout}] = gui_mainfcn(gui_State, varargin{:});
else
    gui_mainfcn(gui_State, varargin{:});
end
% End initialization code - DO NOT EDIT


% --- Executes just before tensile is made visible.
function tensile_OpeningFcn(hObject, eventdata, handles, varargin)
% This function has no output args, see OutputFcn.
% hObject    handle to figure
% eventdata  reserved - to be defined in a future version of MATLAB
% handles    structure with handles and user data (see GUIDATA)
% varargin   command line arguments to tensile (see VARARGIN)

% Choose default command line output for tensile
handles.output = hObject;

%Set the directory that tensile is running from
handles.homeDir = cd;
handles.pathName = cd;

% Update handles structure
guidata(hObject, handles);

% UIWAIT makes tensile wait for user response (see UIRESUME)
% uiwait(handles.figure1);


% --- Outputs from this function are returned to the command line.
function varargout = tensile_OutputFcn(hObject, eventdata, handles)
% varargout  cell array for returning output args (see VARARGOUT);
% hObject    handle to figure
% eventdata  reserved - to be defined in a future version of MATLAB
% handles    structure with handles and user data (see GUIDATA)

% Get default command line output from handles structure
varargout{1} = handles.output;


function widthInput_Callback(hObject, eventdata, handles)


% --- Executes during object creation, after setting all properties.
function widthInput_CreateFcn(hObject, eventdata, handles)
if ispc && isequal(get(hObject,'BackgroundColor'),
get(0,'defaultUicontrolBackgroundColor'))
    set(hObject,'BackgroundColor','white');
end


function thicknessInput_Callback(hObject, eventdata, handles)

% --- Executes during object creation, after setting all properties.
function thicknessInput_CreateFcn(hObject, eventdata, handles)
if ispc && isequal(get(hObject,'BackgroundColor'),
get(0,'defaultUicontrolBackgroundColor'))
    set(hObject,'BackgroundColor','white');
end


function lengthInput_Callback(hObject, eventdata, handles)
```

```
% --- Executes during object creation, after setting all properties.
function lengthInput_CreateFcn(hObject, eventdata, handles)
if ispc && isequal(get(hObject,'BackgroundColor'),
get(0,'defaultUicontrolBackgroundColor'))
    set(hObject,'BackgroundColor','white');
end


% --- Executes on button press in toggleZoom.
function toggleZoom_Callback(hObject, eventdata, handles)
INTERACTIVEMOUSE
if (strcmp(get(handles.zoomStatus,'String'),'OFF'))
    set(handles.zoomStatus,'String','ON');
    set(handles.zoomStatus,'ForegroundColor',[0 1 0]);
else
    set(handles.zoomStatus,'String','OFF');
    set(handles.zoomStatus,'ForegroundColor',[1 0 0]);
end

% --- Executes on button press in originalZoom.
function originalZoom_Callback(hObject, eventdata, handles)
INTERACTIVEMOUSE RESTORE_ORIG


% --- Executes on button press in loadFile.
function loadFile_Callback(hObject, eventdata, handles)
%Turn off Zoom mode if on
if (strcmp(get(handles.zoomStatus,'String'),'ON'))
    interactivemouse off
    set(handles.zoomStatus,'String','OFF');
    set(handles.zoomStatus,'ForegroundColor',[1 0 0]);
end

cd(handles.pathName)
[handles.fileName,handles.pathName] = uigetfile('*.csv');
cd(handles.pathName)
handles.rawData = load(handles.fileName);
cd(handles.homeDir)

% Update handles structure
guidata(hObject, handles);

%Convert data
convertData(hObject, handles);



%This function will take the raw data and convert from force and extension
%to stress and strain using the values provided in the sample measurement
%boxes
function convertData(hObject, handles)
handles.convertedData = zeros(length(handles.rawData(:,1)),2);

%Conversions
%extension inch->mm
handles.convertedData(:,1) = handles.rawData(:,1)*25.4;
%force lbf->N
handles.convertedData(:,2) = handles.rawData(:,2)*4.44822162;

%Cross-sectional area in mm^2
CSA =
str2double(get(handles.thicknessInput,'String'))*str2double(get(handles.widthInput,'Strin
g'));

%N->MPa (Stress)
handles.convertedData(:,2) = handles.convertedData(:,2) / (CSA * 10^-6) / 10^6;

%mm-> (Strain)
```

```
handles.convertedData(:,1) = handles.convertedData(:,1) /
str2double(get(handles.lengthInput,'String'));

%Update Graph
axes(handles.graph);
plot(handles.convertedData(:,1),handles.convertedData(:,2));
set(get(handles.graph,'YLabel'),'String','Stress (MPa)')
set(get(handles.graph,'XLabel'),'String','Strain')

%Update Yield Strength (scan the first 70% of the data for the maximum -
%tries to cut out any max spikes at the end of the data

set(handles.yieldStrength,'String',num2str(max(handles.convertedData(1:(length(handles.co
nvertedData(:,2)*0.7)),2))));

lastValue = 10;
set(handles.breakingExtension,'String','N/A');
%Find Break Point

for k=length(handles.convertedData(:,2)):-1:1
    if( handles.convertedData(k,2) >= lastValue*1.5 )
        set(handles.breakingExtension,'String',num2str(handles.convertedData(k,1)));
        break;
    else
        lastValue = handles.convertedData(k,2);
    end
end

set(handles.youngsModulus,'String','N/A');

% Update handles structure
guidata(hObject, handles);



% --- Executes on button press in saveFile.
function saveFile_Callback(hObject, eventdata, handles)
cd(handles.pathName);
[handles.fileName,handles.pathName] = uiputfile([handles.fileName '.csv']);
cd(handles.pathName);
%handles.file = load(handles.fileName);
if ~isequal(handles.fileName,0)
    csvwrite(handles.fileName,handles.convertedData);
end
cd(handles.homeDir)

% --- Executes on button press in printGraph.
function printGraph_Callback(hObject, eventdata, handles)
% hObject    handle to printGraph (see GCBO)
% eventdata  reserved - to be defined in a future version of MATLAB
% handles    structure with handles and user data (see GUIDATA)
printdlg()


% --- Executes on button press in recalculateData.
function recalculateData_Callback(hObject, eventdata, handles)
%Convert data
convertData(hObject, handles);



function yieldStrength_Callback(hObject, eventdata, handles)

% --- Executes during object creation, after setting all properties.
function yieldStrength_CreateFcn(hObject, eventdata, handles)
if ispc && isequal(get(hObject,'BackgroundColor'),
get(0,'defaultUicontrolBackgroundColor'))
    set(hObject,'BackgroundColor','white');
end
```

```
function breakingExtension_Callback(hObject, eventdata, handles)


% --- Executes during object creation, after setting all properties.
function breakingExtension_CreateFcn(hObject, eventdata, handles)
if ispc && isequal(get(hObject,'BackgroundColor'),
get(0,'defaultUicontrolBackgroundColor'))
    set(hObject,'BackgroundColor','white');
end


% --- Executes on button press in breakButton.
function breakButton_Callback(hObject, eventdata, handles)
%Turn off Zoom mode if on
if (strcmp(get(handles.zoomStatus,'String'),'ON'))
    interactivemouse off
    set(handles.zoomStatus,'String','OFF');
    set(handles.zoomStatus,'ForegroundColor',[1 0 0]);
end


[newx, newy] = ginput(1);
%Find the data points closest (on the X axis) to the clicks
[lowDiff, lowIndex] = min(abs(handles.convertedData(:,1)-newx));

set(handles.breakingExtension,'String',num2str(handles.convertedData(lowIndex,1)));


% --- Executes on button press in yieldButton.
function yieldButton_Callback(hObject, eventdata, handles)
%Turn off Zoom mode if on
if (strcmp(get(handles.zoomStatus,'String'),'ON'))
    interactivemouse off
    set(handles.zoomStatus,'String','OFF');
    set(handles.zoomStatus,'ForegroundColor',[1 0 0]);
end


[newx, newy] = ginput(1);
%Find the data points closest (on the X axis) to the clicks
[lowDiff, lowIndex] = min(abs(handles.convertedData(:,1)-newx));
set(handles.yieldStrength,'String',num2str(handles.convertedData(lowIndex,2)));



function youngsModulus_Callback(hObject, eventdata, handles)


% --- Executes during object creation, after setting all properties.
function youngsModulus_CreateFcn(hObject, eventdata, handles)
if ispc && isequal(get(hObject,'BackgroundColor'),
get(0,'defaultUicontrolBackgroundColor'))
    set(hObject,'BackgroundColor','white');
end


% --- Executes on button press in youngButton.
function youngButton_Callback(hObject, eventdata, handles)
%Turn off Zoom mode if on
if (strcmp(get(handles.zoomStatus,'String'),'ON'))
    interactivemouse off
    set(handles.zoomStatus,'String','OFF');
    set(handles.zoomStatus,'ForegroundColor',[1 0 0]);
end
```

```
[newx, newy] = ginput(2);
a=handles.convertedData(:,1); b=handles.convertedData(:,2);
if newx(1) < newx(2)
    q = a>newx(1) & a<newx(2);
else
    q = a>newx(2) & a<newx(1);
end
linearData=[a(q),b(q)];

%Linear Regression
p = polyfit(linearData(:,1),linearData(:,2),1);

newx(1)=(-p(2))/p(1);
newx(2)=(str2double(get(handles.yieldStrength,'String'))-p(2))/p(1);
q = a>newx(1) & a<newx(2);
linearData=[a(q),b(q)];
regressionLine = polyval(p,linearData(:,1));

%Update Graph
axes(handles.graph);
interactivemouse on
interactivemouse reset
plot(handles.convertedData(:,1),handles.convertedData(:,2),linearData(:,1),regressionLine
,'r');
%hold on
%plot(linearData(:,1),regressionLine, 'r');
%old off
interactivemouse restore
interactivemouse off


set(get(handles.graph,'YLabel'),'String','Stress (MPa)')
set(get(handles.graph,'XLabel'),'String','Strain')

set(handles.youngsModulus,'String',num2str(p(1)));
```

B.2 GPC – SEC Analysis

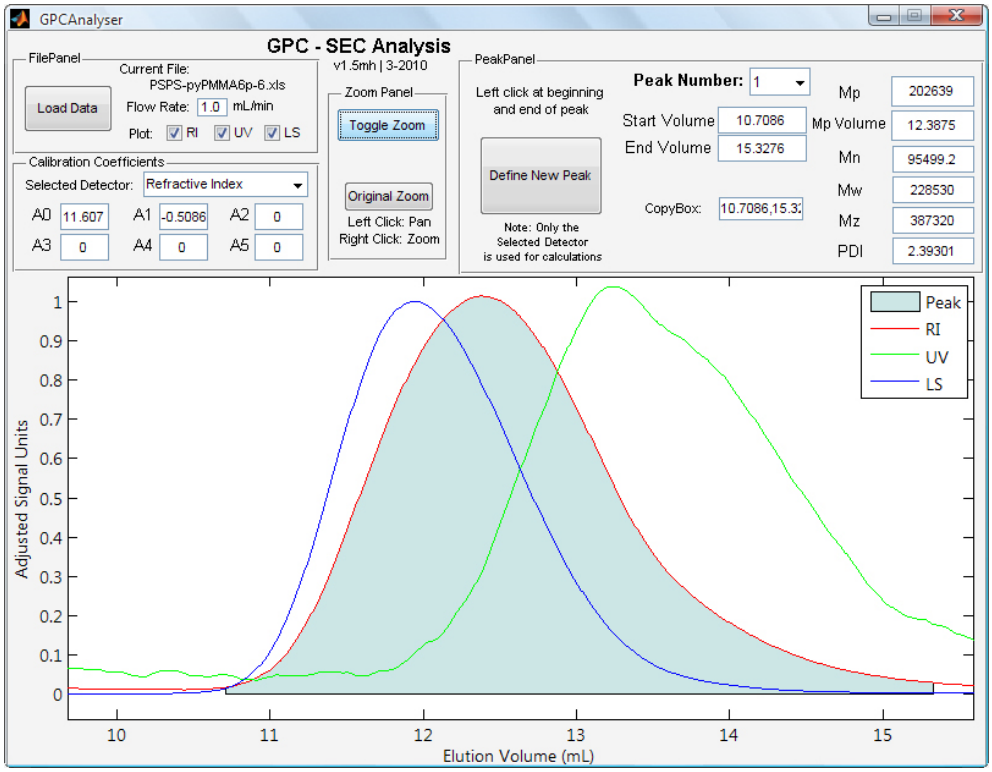

Figure B.2. User interface of the GPC – SEC Analysis program

B.2.1 Description and Purpose

The GPC-SEC Analysis program (GSA) imports pre-baselined refractive index (RI) detection data and allows the user to define peaks to calculate molecular weight information based on a pre-calculated calibration. Mobile phase flow rate must be specified prior to importing data, while the RI Calibration equation must be specified prior to peak definition. Once the beginning and end points of a peak are defined, the GSA automatically calculates the M_n, M_w, M_z, and PDI. An unlimited number of peaks may be defined. Ultraviolet and light scattering data can also be plotted but are not used for calculations.

B.2.2 Supported Input Data Formats

The GSA can accept refractive index data in two different forms. The first is a comma separated value (.csv) file without column headers in which the first column is elution time and the second is RI signal response. The data will automatically be adjusted so the minimum value is set to zero, to prevent errors when integrating. The second supported data format is an Excel (.xls) file exported from the Wyatt ASTRA software package when "Peaks" graph is double-clicked. The expected data structure is shown in Table B.2.

Table B.2 Expected data structure of .XLS files exported from the Wyatt ASTRA Software

LS Detector Time (min)	**Baselined LS Signal**	**UV Detector Time** (min)	**Baselined UV Signal**	**RI Detector Time** (min)	**Baselined RI Signal**

B.2.3 Typical Usage Case Study

This case study follows the steps that a typical user will take when operating the program and details the functions performed with each action.

- **User runs 'GPCAnalyser.m' file.**
  - *GPC-SEC Analysis GUI is loaded and sets the initial directory.*
- **User specifies the flow rate of the data to be loaded, selects which signals to plot, clicks "Load Data" button, browses to, and opens a properly formatted data file.**
  - *Zoom mode, if on, is deactivated.*
  - *The data file's directory is made the current directory, the data is loaded, and the current directory is reset to the initial directory.*
    - Note: If the "Select File to Open" dialog box is closed or cancelled, the initial directory will not be reset and the program will stop functioning.
  - *The format of the data is determined based on file extension*

- *Old peak data, if present, is deleted*
- *If data contains negative values, the each detector signal adjusted to make the most negative value zero to prevent integration errors.*
- *The visual plot is updated with the desired detector signals.*

- **User selects either RI or UV detector for molecular weight characterization and checks the calibration coefficients to ensure they are correct for the current GPC configuration. If not, new numbers are inputted.**
  - *If the detector is changed, the values for the calibration coefficients for the last detector is saved and the coefficients for the new detector are loaded.*
    - Note: Use the MATLAB GUIDE to edit GPCAnalyser.fig to change the default values of the RI Calibration Coefficients, while UV Calibration Coefficients can be changed in GPCAnalyser.m.
- **User clicks on the Toggle Zoom button and adjusts graph to focus on an RI signal peak.**
  - *The "INTERACTIVEMOUSE" function, retrieved from the MATLAB File Exchange, is activated and Zoom Mode is engaged.*
- **User clicks on the Define New Peak button and selects two points to define the edges of a new peak.**
  - *Zoom mode is disabled, if active.*
  - *Clicks are sorted to determine which is the beginning and end of the new peak and data closest to the x-axis value of each click is saved.*
  - *The RI Calibration curve is generated from the given coefficients and used to calculate peak molecular weight (M_p), and number-, weight-, and z-averages (M_n, M_w, and M_z).*
  - *Peak Number is iterated and calculated data populates display boxes.*
  - *Graph is updated with the new peak highlighted*
- **User selects a different peak from the Peak Number dropdown menu.**
  - *Zoom mode is disabled, if active.*
  - *Calculated data for desired peak populates display boxes.*
  - *Graph is updated with the desired peak highlighted*

- **User copies the contents of the CopyBox and pastes into an open Excel spreadsheet.**
  - *No action taken.*
    - Note: The CopyBox is a quick means of getting all calculated peak data out of the GSA. The following values are separated by commas: peak start volume, peak end volume, M_p, M_p volume, M_n, M_w, M_z, and PDI. Excel is capable of converting this structure to cells when pasting.

B.2.4 M-File Code

```
function varargout = GPCAnalyser(varargin)
% GPCANALYSER M-file for GPCAnalyser.fig
%      GPCANALYSER, by itself, creates a new GPCANALYSER or raises the existing
%      singleton*.

% Edit the above text to modify the response to help GPCAnalyser

% Last Modified by GUIDE v2.5 21-Mar-2010 10:45:23

% Begin initialization code - DO NOT EDIT
gui_Singleton = 1;
gui_State = struct('gui_Name',       mfilename, ...
                   'gui_Singleton',  gui_Singleton, ...
                   'gui_OpeningFcn', @GPCAnalyser_OpeningFcn, ...
                   'gui_OutputFcn',  @GPCAnalyser_OutputFcn, ...
                   'gui_LayoutFcn',  [] , ...
                   'gui_Callback',   []);
if nargin && ischar(varargin{1})
    gui_State.gui_Callback = str2func(varargin{1});
end

if nargout
    [varargout{1:nargout}] = gui_mainfcn(gui_State, varargin{:});
else
    gui_mainfcn(gui_State, varargin{:});
end
% End initialization code - DO NOT EDIT


% --- Executes just before GPCAnalyser is made visible.
function GPCAnalyser_OpeningFcn(hObject, eventdata, handles, varargin)
% This function has no output args, see OutputFcn.
% hObject    handle to figure
% eventdata  reserved - to be defined in a future version of MATLAB
% handles    structure with handles and user data (see GUIDATA)
% varargin   command line arguments to GPCAnalyser (see VARARGIN)

% Choose default command line output for GPCAnalyser
handles.output = hObject;

%Set the directory that this program is running from and where to look for
%files
handles.homeDir = cd;
handles.pathName = cd;

%"Global" variables
handles.numPeaks = 0;
handles.curDetect = 1;
```

```
handles.RIA0 = '11.607';
handles.RIA1 = '-0.5086';
handles.RIA2 = '0';
handles.RIA3 = '0';
handles.RIA4 = '0';
handles.RIA5 = '0';
handles.UVA0 = '11.621';
handles.UVA1 = '-0.5079';
handles.UVA2 = '0';
handles.UVA3 = '0';
handles.UVA4 = '0';
handles.UVA5 = '0';

% Update handles structure
guidata(hObject, handles);

% UIWAIT makes GPCAnalyser wait for user response (see UIRESUME)
% uiwait(handles.figure1);


% --- Outputs from this function are returned to the command line.
function varargout = GPCAnalyser_OutputFcn(hObject, eventdata, handles)
% varargout  cell array for returning output args (see VARARGOUT);
% hObject    handle to figure
% eventdata  reserved - to be defined in a future version of MATLAB
% handles    structure with handles and user data (see GUIDATA)

% Get default command line output from handles structure
varargout{1} = handles.output;


% --- Executes on button press in loadDataButton.
function loadDataButton_Callback(hObject, eventdata, handles)
%If zoom mode is on, set off
if (strcmp(get(handles.zoomText,'String'),'ZOOM ON'))
    INTERACTIVEMOUSE
    set(handles.zoomText,'String','');
end


cd(handles.pathName)
[handles.fileName,handles.pathName] = uigetfile({'*.csv;*.xls','XLS or CSV without
headers (*.csv, *.xls)'});
cd(handles.pathName)
if(strfind(handles.fileName,'.csv'))
    handles.rawRIData = load(handles.fileName);
    handles.rawRIData(:,1) =
handles.RIData(:,1)./str2double(get(handles.flowRate,'String'));
else
    fileData = xlsread(handles.fileName);
    handles.rawLSData = [fileData(:,1).*str2double(get(handles.flowRate,'String'))
fileData(:,2)];
    handles.rawUVData = [fileData(:,3).*str2double(get(handles.flowRate,'String'))
fileData(:,4)];
    handles.rawRIData = [fileData(:,5).*str2double(get(handles.flowRate,'String'))
fileData(:,6)];

end

cd(handles.homeDir)
set(handles.currentFileText,'String',handles.fileName);

%clear old data
handles.peaks={};
handles.peakData=[];
handles.numPeaks=0;
strlist{1}='N/A';
set(handles.peakNumberMenu,'String',strlist);
set(handles.peakNumberMenu,'Value',1);
```

```
%Check to see if there are negative RI values and adjust to zero the lowest
if(handles.rawRIData(handles.rawRIData < 0))
    temp = abs(min(handles.rawRIData(:,2)));
    handles.rawRIData(:,2) = handles.rawRIData(:,2) + temp;
end

%Check to see if we have LS and UV data and zero them as well.
if(strfind(handles.fileName,'.xls'))
    if(handles.rawUVData(handles.rawUVData < 0))
        temp = abs(min(handles.rawUVData(:,2)));
        handles.rawUVData(:,2) = handles.rawUVData(:,2) + temp;
    end
    if(handles.rawLSData(handles.rawLSData < 0))
        temp = abs(min(handles.rawLSData(:,2)));
        handles.rawLSData(:,2) = handles.rawLSData(:,2) + temp;
    end
end

%Plot Data
if(strfind(handles.fileName,'.csv'))
    plot(handles.mainAxes,handles.rawRIData(:,1),handles.rawRIData(:,2));
    set(get(handles.mainAxes,'YLabel'),'String','Adjusted RI Units')
    set(get(handles.mainAxes,'XLabel'),'String','Elution Volume (mL)')
else
    legendstr = '';
    hold off
    if(get(handles.RICheck,'Value') == 1)
        plot(handles.mainAxes,handles.rawRIData(:,1),handles.rawRIData(:,2),'r');
        hold on
        legendstr = [legendstr '''RI'','];
    end
    if(get(handles.UVCheck,'Value') == 1)
        plot(handles.mainAxes,handles.rawUVData(:,1),handles.rawUVData(:,2),'g');
        hold on
        legendstr = [legendstr '''UV'','];
    end
    if(get(handles.LSCheck,'Value') == 1)
        plot(handles.mainAxes,handles.rawLSData(:,1),handles.rawLSData(:,2),'b');
        legendstr = [legendstr '''LS'','];
    end
    legendstr = legendstr(1:(end-1));
    eval(['legend(' legendstr ');']);
    set(get(handles.mainAxes,'YLabel'),'String','Adjusted Signal Units')
    set(get(handles.mainAxes,'XLabel'),'String','Elution Volume (mL)')
    hold off
end

% Update handles structure
guidata(hObject, handles);


% --- Executes on selection change in peakNumberMenu.
function peakNumberMenu_Callback(hObject, eventdata, handles)
%If zoom mode is on, set off
if (strcmp(get(handles.zoomText,'String'),'ZOOM ON'))
    INTERACTIVEMOUSE
    set(handles.zoomText,'String','');
end

curPeak = get(handles.peakNumberMenu,'Value');

%Update data boxes
set(handles.peakStart,'String',handles.peakData(curPeak,1));
set(handles.peakEnd,'String',handles.peakData(curPeak,2));
set(handles.mp,'String',handles.peakData(curPeak,3));
set(handles.mpTime,'String',handles.peakData(curPeak,4));
set(handles.mn,'String',handles.peakData(curPeak,5));
set(handles.mw,'String',handles.peakData(curPeak,6));
```

```
set(handles.mz,'String',handles.peakData(curPeak,7));
set(handles.pdi,'String',handles.peakData(curPeak,8));

set(handles.copyBox,'String',[num2str(handles.peakData(curPeak,1)) ','
num2str(handles.peakData(curPeak,2)) ',' num2str(handles.peakData(curPeak,3)) ','
num2str(handles.peakData(curPeak,4)) ',' num2str(handles.peakData(curPeak,5)) ','
num2str(handles.peakData(curPeak,6)) ',' num2str(handles.peakData(curPeak,7)) ','
num2str(handles.peakData(curPeak,8))]);
%get peak data points
x = handles.peaks(curPeak,1);
x = x{1};
y = handles.peaks(curPeak,2);
y = y{1};

%save the Zoom, then replot the graph with selected peak filled
%interactivemouse on;
interactivemouse reset;
%Plot Data
if(strfind(handles.fileName,'.csv'))
    plot(handles.mainAxes,handles.rawRIData(:,1),handles.rawRIData(:,2));
    set(get(handles.mainAxes,'YLabel'),'String','Adjusted RI Units')
    set(get(handles.mainAxes,'XLabel'),'String','Elution Volume (mL)')
    hold on;
    a = area(x,y,'FaceColor',[.1 .3 .8]);
    hold off;
else
    hold off
    area(x,y,'FaceColor',[.8 .9 .9]);
    legendstr = '''Peak'',';
    hold on
    if(get(handles.RICheck,'Value') == 1)
        plot(handles.mainAxes,handles.rawRIData(:,1),handles.rawRIData(:,2),'r');
        hold on
        legendstr = [legendstr '''RI'','];
    end
    if(get(handles.UVCheck,'Value') == 1)
        plot(handles.mainAxes,handles.rawUVData(:,1),handles.rawUVData(:,2),'g');
        hold on
        legendstr = [legendstr '''UV'','];
    end
    if(get(handles.LSCheck,'Value') == 1)
        plot(handles.mainAxes,handles.rawLSData(:,1),handles.rawLSData(:,2),'b');
        legendstr = [legendstr '''LS'','];
    end
    legendstr = legendstr(1:(end-1));
    eval(['legend(' legendstr ');'])
    set(get(handles.mainAxes,'YLabel'),'String','Adjusted Signal Units')
    set(get(handles.mainAxes,'XLabel'),'String','Elution Volume (mL)')
    hold off
end
interactivemouse restore;
%interactivemouse off;


% --- Executes during object creation, after setting all properties.
function peakNumberMenu_CreateFcn(hObject, eventdata, handles)
if ispc && isequal(get(hObject,'BackgroundColor'),
get(0,'defaultUicontrolBackgroundColor'))
    set(hObject,'BackgroundColor','white');
end

function peakStart_Callback(hObject, eventdata, handles)


% --- Executes during object creation, after setting all properties.
function peakStart_CreateFcn(hObject, eventdata, handles)
if ispc && isequal(get(hObject,'BackgroundColor'),
get(0,'defaultUicontrolBackgroundColor'))
    set(hObject,'BackgroundColor','white');
```

```
end

function peakEnd_Callback(hObject, eventdata, handles)

% --- Executes during object creation, after setting all properties.
function peakEnd_CreateFcn(hObject, eventdata, handles)
if ispc && isequal(get(hObject,'BackgroundColor'),
get(0,'defaultUicontrolBackgroundColor'))
    set(hObject,'BackgroundColor','white');
end

function mp_Callback(hObject, eventdata, handles)

% --- Executes during object creation, after setting all properties.
function mp_CreateFcn(hObject, eventdata, handles)
if ispc && isequal(get(hObject,'BackgroundColor'),
get(0,'defaultUicontrolBackgroundColor'))
    set(hObject,'BackgroundColor','white');
end

function mpTime_Callback(hObject, eventdata, handles)

% --- Executes during object creation, after setting all properties.
function mpTime_CreateFcn(hObject, eventdata, handles)
if ispc && isequal(get(hObject,'BackgroundColor'),
get(0,'defaultUicontrolBackgroundColor'))
    set(hObject,'BackgroundColor','white');
end

function mn_Callback(hObject, eventdata, handles)

% --- Executes during object creation, after setting all properties.
function mn_CreateFcn(hObject, eventdata, handles)
if ispc && isequal(get(hObject,'BackgroundColor'),
get(0,'defaultUicontrolBackgroundColor'))
    set(hObject,'BackgroundColor','white');
end

function mw_Callback(hObject, eventdata, handles)

% --- Executes during object creation, after setting all properties.
function mw_CreateFcn(hObject, eventdata, handles)
if ispc && isequal(get(hObject,'BackgroundColor'),
get(0,'defaultUicontrolBackgroundColor'))
    set(hObject,'BackgroundColor','white');
end

function a0_Callback(hObject, eventdata, handles)

% --- Executes during object creation, after setting all properties.
function a0_CreateFcn(hObject, eventdata, handles)
if ispc && isequal(get(hObject,'BackgroundColor'),
get(0,'defaultUicontrolBackgroundColor'))
    set(hObject,'BackgroundColor','white');
end
```

```
function a1_Callback(hObject, eventdata, handles)


% --- Executes during object creation, after setting all properties.
function a1_CreateFcn(hObject, eventdata, handles)
if ispc && isequal(get(hObject,'BackgroundColor'),
get(0,'defaultUicontrolBackgroundColor'))
    set(hObject,'BackgroundColor','white');
end


function a2_Callback(hObject, eventdata, handles)


% --- Executes during object creation, after setting all properties.
function a2_CreateFcn(hObject, eventdata, handles)
if ispc && isequal(get(hObject,'BackgroundColor'),
get(0,'defaultUicontrolBackgroundColor'))
    set(hObject,'BackgroundColor','white');
end


function a5_Callback(hObject, eventdata, handles)


% --- Executes during object creation, after setting all properties.
function a5_CreateFcn(hObject, eventdata, handles)
if ispc && isequal(get(hObject,'BackgroundColor'),
get(0,'defaultUicontrolBackgroundColor'))
    set(hObject,'BackgroundColor','white');
end


function a3_Callback(hObject, eventdata, handles)


% --- Executes during object creation, after setting all properties.
function a3_CreateFcn(hObject, eventdata, handles)
if ispc && isequal(get(hObject,'BackgroundColor'),
get(0,'defaultUicontrolBackgroundColor'))
    set(hObject,'BackgroundColor','white');
end


function a4_Callback(hObject, eventdata, handles)


% --- Executes during object creation, after setting all properties.
function a4_CreateFcn(hObject, eventdata, handles)
if ispc && isequal(get(hObject,'BackgroundColor'),
get(0,'defaultUicontrolBackgroundColor'))
    set(hObject,'BackgroundColor','white');
end



function mz_Callback(hObject, eventdata, handles)


% --- Executes during object creation, after setting all properties.
function mz_CreateFcn(hObject, eventdata, handles)
if ispc && isequal(get(hObject,'BackgroundColor'),
get(0,'defaultUicontrolBackgroundColor'))
    set(hObject,'BackgroundColor','white');
end
```

```
% --- Executes on button press in toggleZoomButton.
function toggleZoomButton_Callback(hObject, eventdata, handles)
INTERACTIVEMOUSE
if (strcmp(get(handles.zoomText,'String'),'ZOOM ON'))
    set(handles.zoomText,'String','');
else
    set(handles.zoomText,'String','ZOOM ON');
end


% --- Executes on button press in originalZoomButton.
function originalZoomButton_Callback(hObject, eventdata, handles)
INTERACTIVEMOUSE RESTORE_ORIG


% --- Executes on button press in newPeakButton.
function newPeakButton_Callback(hObject, eventdata, handles)
%Check for Zoom Mode, off if on
if (strcmp(get(handles.zoomText,'String'),'ZOOM ON'))
    INTERACTIVEMOUSE
    set(handles.zoomText,'String','');
end


%Take in two points to define a new peak & sanitize the X coord to find
%high/low
[newx, newy] = ginput(2);
if newx(1) < newx(2)
    lowX = newx(1);
    highX = newx(2);
else
    lowX = newx(2);
    highX = newx(1);
end

%Get the detector to use and then make it's raw data the working data
if(handles.curDetect == 1) %RI
    workingData = handles.rawRIData;
elseif(handles.curDetect == 2) %UV
    workingData = handles.rawUVData;
else
    error = 'Cannot determine which detector is to be used!'
    return;
end

%Find the data points closest (on the X axis) to the clicks
[lowDiff, lowIndex] = min(abs(workingData(:,1)-lowX));
[highDiff, highIndex] = min(abs(workingData(:,1)-highX));

%Save the data points into the peak array
handles.numPeaks = handles.numPeaks+1;
handles.peaks(handles.numPeaks, 1)= {workingData(lowIndex:highIndex,1)};
handles.peaks(handles.numPeaks, 2)= {workingData(lowIndex:highIndex,2)};

%Make calibration array
detectCalib = [str2double(get(handles.a5,'String')) str2double(get(handles.a4,'String'))
str2double(get(handles.a3,'String')) str2double(get(handles.a2,'String'))
str2double(get(handles.a1,'String')) str2double(get(handles.a0,'String'))];

%calculate the assorted data for the new peak
handles.peakData(handles.numPeaks,1) = workingData(lowIndex,1); %Start Time
handles.peakData(handles.numPeaks,2) = workingData(highIndex,1); %End Time
[MpRI, MpIndex] = max(workingData(lowIndex:highIndex,2)); %Mp RI value and MP max index
MpTime = workingData(MpIndex+lowIndex,1);
handles.peakData(handles.numPeaks,4) = MpTime; %Mp Time
handles.peakData(handles.numPeaks,3) = 10^(polyval(detectCalib, MpTime)); %calculate the
Mp concentration

%Calculate the important concentration and molecular weight data!
```

```
ci=workingData(lowIndex:highIndex,2);
Mi=(10.^polyval(detectCalib,workingData(lowIndex:highIndex,1)));

handles.peakData(handles.numPeaks,5) = sum(ci)/sum(ci./Mi); %Mn
handles.peakData(handles.numPeaks,6) = sum(ci.*Mi)/sum(ci); %Mw
handles.peakData(handles.numPeaks,7) = sum(ci.*Mi.^2)/sum(ci.*Mi); %Mz
handles.peakData(handles.numPeaks,8) =
handles.peakData(handles.numPeaks,6)/handles.peakData(handles.numPeaks,5); %PDI


% Update handles structure
guidata(hObject, handles);

%Update the Peak Number Dropdown menu
updatePeakMenu(handles);

%Updates the number of peaks available in the peak dropdown box
function updatePeakMenu(handles)
if(handles.numPeaks == 0)
    strlist{1}='N/A';
    set(handles.peakNumberMenu,'String',strlist);
    set(handles.peakNumberMenu,'Value',1);

else
    for i=1:handles.numPeaks
        strlist{i} = i;
    end
    curPeak = handles.numPeaks;
    set(handles.peakNumberMenu,'String',strlist);
    set(handles.peakNumberMenu,'Value',curPeak);
    peakNumberMenu_Callback('', '', handles)
end


function pdi_Callback(hObject, eventdata, handles)


% --- Executes during object creation, after setting all properties.
function pdi_CreateFcn(hObject, eventdata, handles)
if ispc && isequal(get(hObject,'BackgroundColor'),
get(0,'defaultUicontrolBackgroundColor'))
    set(hObject,'BackgroundColor','white');
end


function copyBox_Callback(hObject, eventdata, handles)


% --- Executes during object creation, after setting all properties.
function copyBox_CreateFcn(hObject, eventdata, handles)
if ispc && isequal(get(hObject,'BackgroundColor'),
get(0,'defaultUicontrolBackgroundColor'))
    set(hObject,'BackgroundColor','white');
end


function flowRate_Callback(hObject, eventdata, handles)


% --- Executes during object creation, after setting all properties.
function flowRate_CreateFcn(hObject, eventdata, handles)
if ispc && isequal(get(hObject,'BackgroundColor'),
get(0,'defaultUicontrolBackgroundColor'))
    set(hObject,'BackgroundColor','white');
end
```

```
% --- Executes on button press in RICheck.
function RICheck_Callback(hObject, eventdata, handles)


% --- Executes on button press in UVCheck.
function UVCheck_Callback(hObject, eventdata, handles)


% --- Executes on button press in LSCheck.
function LSCheck_Callback(hObject, eventdata, handles)


% --- Executes on selection change in detectorSelector.
function detectorSelector_Callback(hObject, eventdata, handles)
selDetect = get(handles.detectorSelector,'Value')

if(selDetect == 1 && handles.curDetect == 1) %RI is current and then selected again
    handles.RIA0 = get(handles.a0,'String');
    handles.RIA1 = get(handles.a1,'String');
    handles.RIA2 = get(handles.a2,'String');
    handles.RIA3 = get(handles.a3,'String');
    handles.RIA4 = get(handles.a4,'String');
    handles.RIA5 = get(handles.a5,'String');
err = '1'
elseif(selDetect == 2 && handles.curDetect == 2) %UV is current and then selected again
    handles.UVA0 = get(handles.a0,'String');
    handles.UVA1 = get(handles.a1,'String');
    handles.UVA2 = get(handles.a2,'String');
    handles.UVA3 = get(handles.a3,'String');
    handles.UVA4 = get(handles.a4,'String');
    handles.UVA5 = get(handles.a5,'String');
    err = '2'
elseif(selDetect == 2 && handles.curDetect == 1) %RI is current and then UV selected
    handles.RIA0 = get(handles.a0,'String');
    handles.RIA1 = get(handles.a1,'String');
    handles.RIA2 = get(handles.a2,'String');
    handles.RIA3 = get(handles.a3,'String');
    handles.RIA4 = get(handles.a4,'String');
    handles.RIA5 = get(handles.a5,'String');
    set(handles.a0,'String',handles.UVA0);
    set(handles.a1,'String',handles.UVA1);
    set(handles.a2,'String',handles.UVA2);
    set(handles.a3,'String',handles.UVA3);
    set(handles.a4,'String',handles.UVA4);
    set(handles.a5,'String',handles.UVA5);
    err = '3'
elseif(selDetect == 1 && handles.curDetect == 2) %UV is current and then RI selected
    handles.UVA0 = get(handles.a0,'String');
    handles.UVA1 = get(handles.a1,'String');
    handles.UVA2 = get(handles.a2,'String');
    handles.UVA3 = get(handles.a3,'String');
    handles.UVA4 = get(handles.a4,'String');
    handles.UVA5 = get(handles.a5,'String');
    set(handles.a0,'String',handles.RIA0);
    set(handles.a1,'String',handles.RIA1);
    set(handles.a2,'String',handles.RIA2);
    set(handles.a3,'String',handles.RIA3);
    set(handles.a4,'String',handles.RIA4);
    set(handles.a5,'String',handles.RIA5);
    err = '4'
end

handles.curDetect = selDetect;

% Update handles structure
guidata(hObject, handles);


% --- Executes during object creation, after setting all properties.
```

```
function detectorSelector_CreateFcn(hObject, eventdata, handles)
if ispc && isequal(get(hObject,'BackgroundColor'),
get(0,'defaultUicontrolBackgroundColor'))
    set(hObject,'BackgroundColor','white');
end
```

B.3 Particle Size Analyzer

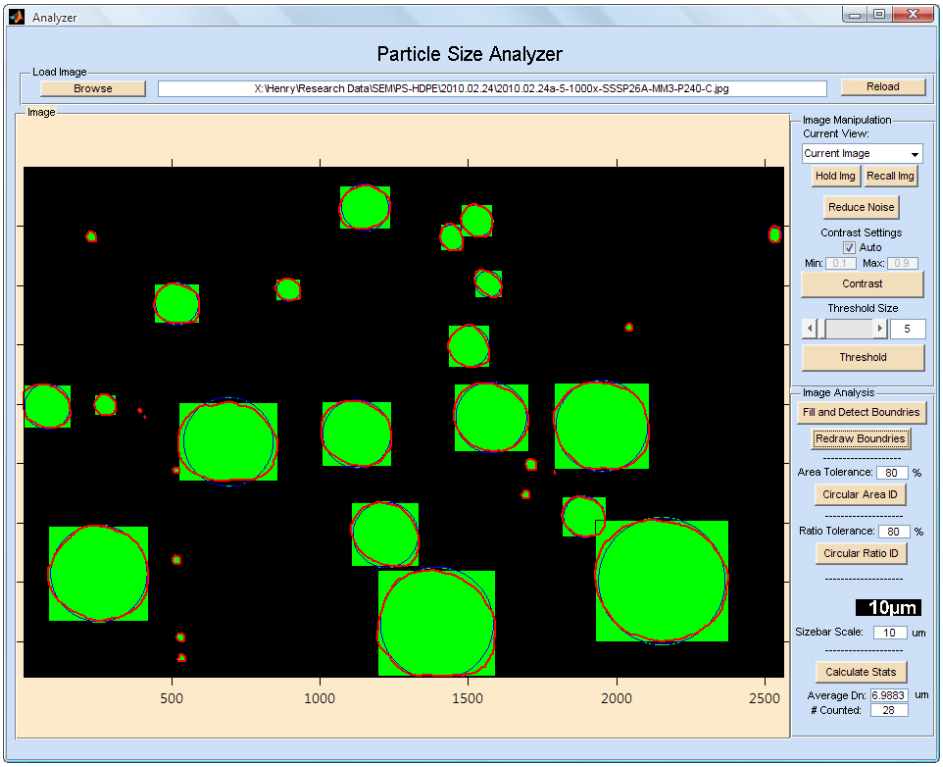

Figure B.3. User interface of the Particle Size Analyzer program

B.3.1 Description and Purpose

The Particle Size Analyzer program (PSA) loads digital micrographs saved from the JOEL SEM Control software, detects objects within the image, and calculates the idealized diameter of each object based on area and the image size bar. The output is the total number of objects counted, the average diameter for counted objects, and a comma separated value (.csv) file containing the calculated diameter for each object.

B.3.2 Supported Input Data Formats

The PSA can import any JPEG (.jpg) file, but is streamlined to anticipate an image produced by the JOEL SEM Control software. These images can vary in resolution depending on magnification, capture time, and quality but the positions and

dimensions of the image elements remains constant. To allow any image size to be imported, the PSA segments imported images into the regions indicated in Figure B.4. As long as the size bar is the only detectable object within the "Size Bar" region and the scale is clearly indicated within the "Size Bar Scale" region, the "Micrograph" region may be modified in the source image to accent objects or completely replaced with another image for analysis.

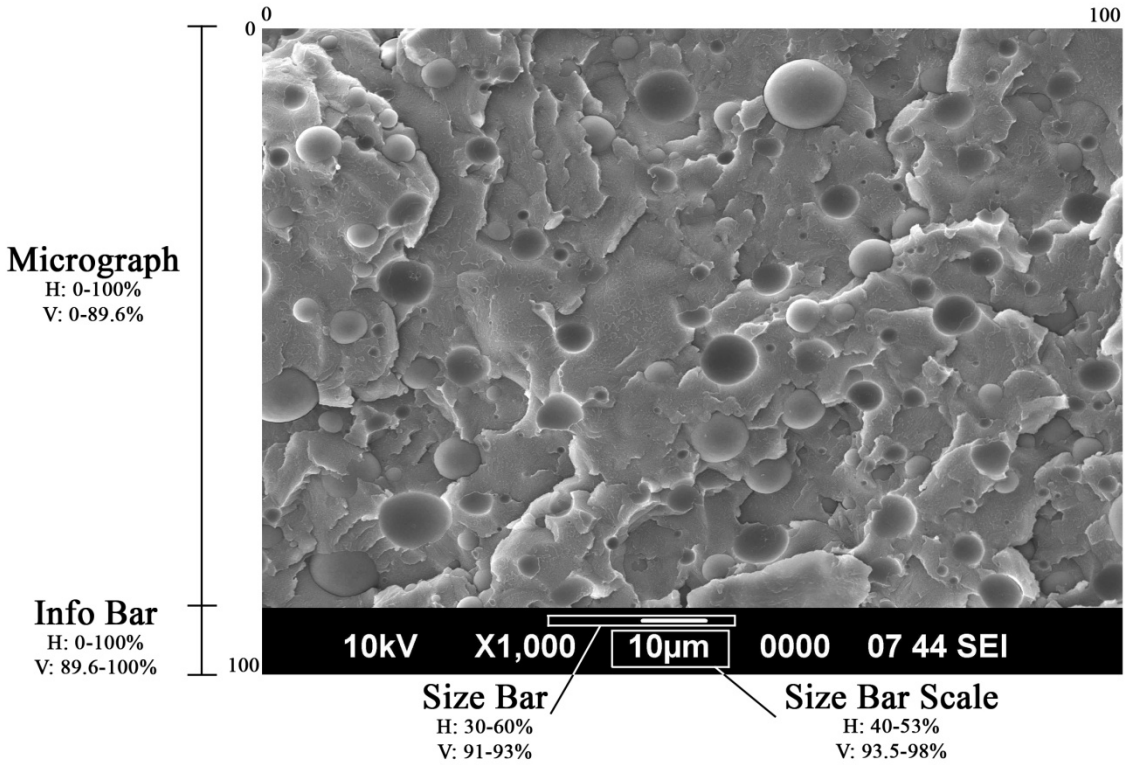

Figure B.4. Required dimensions and configurations of images to be imported into the PSA. Note that the top left corner is used as the image origin.

B.3.3 Typical Usage Case Study

This case study follows the steps that a typical user will take when operating the program and details the functions performed with each action.

- **User runs 'Analyzer.m' file.**
  - *Particle Size Analyzer GUI is loaded and sets the initial directory.*

- **User clicks on the Browse button and selects an image file to open.**
    - *The data file's directory is made the current directory, the image is loaded into memory, and the current directory is reset to the initial directory.*
        - Note: If the "Select File to Open" dialog box is closed or cancelled, the initial directory will not be reset and the program will stop functioning.
    - *The image is segmented into the different regions as described in Figure B.4. The Micrograph region is displayed in the primary view while the Size Bar Scale region is displayed in the secondary size bar view.*
    - *The Size Bar region is analyzed to determine the length of the size bar in units of pixels*
- **User clicks on the Reload button.**
    - *The image file listed to the left of the Reload button is loaded as the current image.*
    - *The listed directory is made the current directory, the image is loaded into memory, and the current directory is reset to the initial directory.*
    - *The image is segmented into the different regions as described in Figure B.4. The Micrograph region is displayed in the primary view while the Size Bar Scale region is displayed in the secondary size bar view.*
    - *The Size Bar region is analyzed to determine the length of the size bar in units of pixels*

The following four steps assume the user is working with a raw image with decent contrast between the objects to be counted and the background. If a pre-masked or thresholded image is being used, they may be skipped.

- **User clicks on the Hold Img button.**
    - *The current image is temporarily saved.*
        - Note: The Hold/Recall functions can be used to save the User's progress when processing an image before a potentially destructive transformation is done on the current image.
- **User clicks on the Recall Img button.**

- *The image previously saved using Hold Img is made the current image and displayed in the primary view.*
    - Note: The Hold/Recall functions can be used to save the User's progress when processing an image before a potentially destructive transformation is done on the current image.

- **User clicks on the Reduce Noise button.**
    - *The current image is processed with a pixelwise adaptive Wiener filter to reduce digital noise.*
    - *The noise-reduced image is made the current image and displayed in the primary view.*
- **User clicks on the Contrast button, selecting automatic contrast or specifying the contrast amount until desired contrast level is reached**
    - *If automatic contrast is used, the current image will be adjusted so that 1% of the image will be fully saturated white and fully saturated black. Successive runs of automatic contrast yield no change, as the conditions are satisfied after the initial run.*
    - *Specifying MIN and MAX values will adjust image contrast to take the pixels with the lowest MIN% saturation (whiter pixels) and fully saturate them light, while taking the darkest (1-MAX)% units and saturating them dark. Specified contrast adjustments can be repeated.*
    - *The contrast adjusted image is set to the current image and the primary view is updated.*
- **User specifies the minimum number of pixels a detectable object should have under Threshold Size and clicks the Threshold button.**
    - *The current image is converted into a black and white image using a global Otsu intensity threshold.*
    - *The black and white image is scanned for continuous white regions smaller than the specified Threshold Size and, if found, deletes them.*
    - *The resulting black and white image is made the current image and displayed in the primary view.*

- **User clicks on the Fill and Detect Boundaries button.**
  - *Black regions fully enclosed by a larger white area are filled in.*
  - *All white regions are counted and have their boundaries traced.*
  - *Boundaries are plotted on the current image in a red line.*
- **User specifies a tolerance for finding circular objects (default: 80% circular) and clicks either the Circular Area ID or Circular Ratio ID buttons.**
  - *All previously accepted boundaries are cleared.*
  - *Circular Area ID calculates the actual area of each boundary and then compares it to the area of a circle with a diameter of the average of the maximum width and height of the boundary. If the actual area is between AreaTolerance×CircularArea and (2-AreaTolerance)×CircularArea, the boundary is considered circular and accepted.*
  - *Circular Ratio ID estimates the value of π by finding the circumference of each boundary and dividing by the idealized diameter of each boundary found using the boundary area. This estimated value of π is compared to the true value of π. If the estimated π is between RatioTolerance× π and (2-RatioTolerance)× π, the boundary is considered circular and accepted.*
    - Note: Circular Area ID is more effective than Circular Ratio ID when white domains have large perimeters which 'double back' on themselves significantly. Circular Ratio ID is stricter in its acceptance of circular objects which exhibit large concavities.
  - *All accepted boundaries are covered with a green rectangle while rejected boundaries are covered with a yellow rectangle in the primary display. These blocks are not incorporated into the Current Image permanently.*
- **User inputs the size bar scale seen in the secondary display into the Sizebar Scale box and clicks the Calculate Stats button.**
  - *The area of each accepted boundary is used to calculate an idealized diameter which is converted from pixels to μm using the scaling determined from the size bar and the inputted size bar scale.*

- *The number of accepted boundaries and the average idealized diameter are calculated and reported in their respective display boxes.*
- *A histogram of the accepted domain diameters is created.*
- *A comma separated value (.csv) file of the sizes of each accepted boundary is created using the same folder and name as the source image file.*

B.3.4 M-File Code

```
function varargout = Analyzer(varargin)
% ANALYZER M-file for Analyzer.fig
%      ANALYZER, by itself, creates a new ANALYZER or raises the existing
%      singleton*.

% Edit the above text to modify the response to help Analyzer

% Last Modified by GUIDE v2.5 20-Mar-2010 15:52:42

% Begin initialization code - DO NOT EDIT
gui_Singleton = 1;
gui_State = struct('gui_Name',       mfilename, ...
                   'gui_Singleton',  gui_Singleton, ...
                   'gui_OpeningFcn', @Analyzer_OpeningFcn, ...
                   'gui_OutputFcn',  @Analyzer_OutputFcn, ...
                   'gui_LayoutFcn',  [] , ...
                   'gui_Callback',   []);
if nargin && ischar(varargin{1})
    gui_State.gui_Callback = str2func(varargin{1});
end

if nargout
    [varargout{1:nargout}] = gui_mainfcn(gui_State, varargin{:});
else
    gui_mainfcn(gui_State, varargin{:});
end
% End initialization code - DO NOT EDIT


% --- Executes just before Analyzer is made visible.
function Analyzer_OpeningFcn(hObject, eventdata, handles, varargin)
% This function has no output args, see OutputFcn.
% hObject    handle to figure
% eventdata  reserved - to be defined in a future version of MATLAB
% handles    structure with handles and user data (see GUIDATA)
% varargin   command line arguments to Analyzer (see VARARGIN)

% Choose default command line output for Analyzer
handles.output = hObject;

%Set default paths
handles.HomePath = cd;
handles.RecentPath = cd;

% Update handles structure
guidata(hObject, handles);

% UIWAIT makes Analyzer wait for user response (see UIRESUME)
% uiwait(handles.figure1);


% --- Outputs from this function are returned to the command line.
function varargout = Analyzer_OutputFcn(hObject, eventdata, handles)
% varargout  cell array for returning output args (see VARARGOUT);
```

```
% hObject    handle to figure
% eventdata  reserved - to be defined in a future version of MATLAB
% handles    structure with handles and user data (see GUIDATA)

% Get default command line output from handles structure
varargout{1} = handles.output;

%------------------------- NON-GUI FUNCTIONS ------------------------%

function DrawBoundries(handles)
%This function will go through the 'boundries' array and draw a boarder
%around each object
hold on
for k=1:size(handles.boundaries)
   b = handles.boundaries{k};
   plot(b(:,2),b(:,1),'r','LineWidth',2);
end
hold off

function findSizeBarSize(hObject,handles)
%This function will take the size bar and find how many pixels long it is
level = graythresh(handles.IsizeBar);
bw = im2bw(handles.IsizeBar,level);
threshold = round(10);
bw = bwareaopen(bw, threshold);
handles.IsizeBar = bw;
Ifill = imfill(handles.IsizeBar,'holes');
sizeBoundaries = bwboundaries(Ifill);
b = sizeBoundaries{1};
handles.sizeLength = max(b(:,2)) - min(b(:,2));

guidata(hObject,handles);

function altCalcs(handles)
for k=1:size(handles.boundaries)
   b = handles.boundaries{k};
   x = b(:,2);
   y = b(:,1);
   perimeter = length(x);
   area = polyarea(x,y);
   sizebarScale = str2num(get(handles.SizebarScale,'String'));
   sizePerPixel = sizebarScale/handles.sizeLength;

   Q(k) = (perimeter/area) / sizePerPixel;
end
avgQ=mean(Q)

function H=circle(center,radius,NOP,style)
%-----------------------------------------------------------------------------------------
-----
% H=CIRCLE(CENTER,RADIUS,NOP,STYLE)
% This routine draws a circle with center defined as
% a vector CENTER, radius as a scaler RADIS. NOP is
% the number of points on the circle. As to STYLE,
% use it the same way as you use the rountine PLOT.
% Since the handle of the object is returned, you
% use routine SET to get the best result.
%
%   Usage Examples,
%
%   circle([1,3],3,1000,':');
%   circle([2,4],2,1000,'--');
%
%   Zhenhai Wang <zhenhai@ieee.org>
%   Version 1.00
%   December, 2002
%-----------------------------------------------------------------------------------------
-----
```

```
if (nargin <3),
 error('Please see help for INPUT DATA.');
elseif (nargin==3)
    style='b-';
end;
THETA=linspace(0,2*pi,NOP);
RHO=ones(1,NOP)*radius;
[X,Y] = pol2cart(THETA,RHO);
X=X+center(1);
Y=Y+center(2);
H=plot(X,Y,style);



%------------------------END NON-GUI FUNCTIONS----------------------%

% --- Executes on button press in Browse.
function Browse_Callback(hObject, eventdata, handles)
cd(handles.RecentPath)
[handles.FileName,handles.RecentPath] = uigetfile('*.jpg','Select the SEM JPG');
cd(handles.HomePath);

set(handles.FilePath,'String',[handles.RecentPath handles.FileName]);


LoadButton_Callback(hObject, eventdata, handles);



function FilePath_Callback(hObject, eventdata, handles)


% --- Executes during object creation, after setting all properties.
function FilePath_CreateFcn(hObject, eventdata, handles)
if ispc && isequal(get(hObject,'BackgroundColor'),
get(0,'defaultUicontrolBackgroundColor'))
    set(hObject,'BackgroundColor','white');
end


% --- Executes on button press in LoadButton.
function LoadButton_Callback(hObject, eventdata, handles)

handles.I = imread(get(handles.FilePath,'String'));
Isize = size(handles.I);
handles.IsansInfoBar = handles.I(1:Isize(1)*(1-0.104166),1:Isize(2));
guidata(handles.title1,handles.IsansInfoBar);
handles.IsizeBar = handles.I(Isize(1)*.91:Isize(1)*.93,Isize(2)*.3:Isize(2)*.6);
handles.IsizeText = handles.I(Isize(1)*.935:Isize(1)*.98,Isize(2)*.4:Isize(2)*.53);
handles.IinfoBar = handles.I(Isize(1)*(1-0.104166):Isize(1),1:Isize(2));
handles.Icurrent = handles.IsansInfoBar;
imshow(handles.IsizeText,'Parent',handles.sizeTextAxes);
axis(handles.sizeTextAxes, 'off');
imshow(handles.Icurrent,'Parent',handles.ImageAxes);
set(gcf,'CurrentAxes',handles.ImageAxes)
guidata(hObject,handles);

findSizeBarSize(hObject,handles);



% --- Executes on button press in ThresholdButton.
function ThresholdButton_Callback(hObject, eventdata, handles)
level = graythresh(handles.Icurrent);
bw = im2bw(handles.Icurrent,level);
threshold = round(get(handles.ThresholdSlider,'Value'));
bw = bwareaopen(bw, threshold);
imshow(bw,'Parent',handles.ImageAxes);
```

```
handles.Icurrent = bw;
guidata(hObject,handles);

% --- Executes on button press in ContrastButton.
function ContrastButton_Callback(hObject, eventdata, handles)

%Get current image
if handles.AutoContrast == 0
    low = str2double(get(handles.ContrastMin,'String'));
    high = str2double(get(handles.ContrastMax,'String'));
    Icontrast = imadjust(handles.Icurrent,[low high]);
else
    Icontrast = imadjust(handles.Icurrent);
end
imshow(Icontrast,'Parent',handles.ImageAxes);
handles.Icurrent = Icontrast;
guidata(hObject,handles);


% --- Executes on selection change in SelectView.
function SelectView_Callback(hObject, eventdata, handles)
contents = get(hObject,'Value');
switch(contents)
    case 2
        imshow(handles.IsansInfoBar,'Parent',handles.ImageAxes);
    case 3
        imshow(handles.I,'Parent',handles.ImageAxes);
    case 1
        imshow(handles.Icurrent,'Parent',handles.ImageAxes);
    case 4
        imshow(handles.Itemp1,'Parent',handles.ImageAxes);
    case 5
        imshow(handles.Itemp2,'Parent',handles.ImageAxes);

end

% --- Executes during object creation, after setting all properties.
function SelectView_CreateFcn(hObject, eventdata, handles)
if ispc && isequal(get(hObject,'BackgroundColor'),
get(0,'defaultUicontrolBackgroundColor'))
    set(hObject,'BackgroundColor','white');
end


% --- Executes on slider movement.
function ThresholdSlider_Callback(hObject, eventdata, handles)
value = get(hObject,'Value');
value =round(value);
set(handles.ThresholdValue,'String',num2str(value));


% --- Executes during object creation, after setting all properties.
function ThresholdSlider_CreateFcn(hObject, eventdata, handles)
if isequal(get(hObject,'BackgroundColor'), get(0,'defaultUicontrolBackgroundColor'))
    set(hObject,'BackgroundColor',[.9 .9 .9]);
end



function ThresholdValue_Callback(hObject, eventdata, handles)
value = str2double(get(hObject,'String'));
set(handles.ThresholdSlider,'Value',value);


% --- Executes during object creation, after setting all properties.
function ThresholdValue_CreateFcn(hObject, eventdata, handles)
if ispc && isequal(get(hObject,'BackgroundColor'),
get(0,'defaultUicontrolBackgroundColor'))
    set(hObject,'BackgroundColor','white');
```

```
end


% --- Executes on button press in holdImgButton.
function holdImgButton_Callback(hObject, eventdata, handles)
handles.Itemp1 = handles.Icurrent;
guidata(hObject,handles);


% --- Executes on button press in recallImgButton.
function recallImgButton_Callback(hObject, eventdata, handles)
handles.Icurrent = handles.Itemp1;
imshow(handles.Icurrent,'Parent',handles.ImageAxes);
guidata(hObject,handles);


function ContrastMin_Callback(hObject, eventdata, handles)


% --- Executes during object creation, after setting all properties.
function ContrastMin_CreateFcn(hObject, eventdata, handles)
if ispc && isequal(get(hObject,'BackgroundColor'),
get(0,'defaultUicontrolBackgroundColor'))
    set(hObject,'BackgroundColor','white');
end


function ContrastMax_Callback(hObject, eventdata, handles)


% --- Executes during object creation, after setting all properties.
function ContrastMax_CreateFcn(hObject, eventdata, handles)
if ispc && isequal(get(hObject,'BackgroundColor'),
get(0,'defaultUicontrolBackgroundColor'))
    set(hObject,'BackgroundColor','white');
end
handles.AutoContrast = 1;
guidata(hObject,handles);


% --- Executes on button press in ContrastAuto.
function ContrastAuto_Callback(hObject, eventdata, handles)
onoff = get(hObject,'Value');
if onoff == 1.0
    handles.AutoContrast = 1;
    set(handles.ContrastMin,'Enable','off');
    set(handles.ContrastMax,'Enable','off');
else
    handles.AutoContrast = 0;
    set(handles.ContrastMin,'Enable','on');
    set(handles.ContrastMax,'Enable','on');
end
guidata(hObject,handles);



% --- Executes on button press in FillButton.
function FillButton_Callback(hObject, eventdata, handles)

%figure, imshow(mat2gray(entropyfilt(handles.Icurrent)));
%figure, imshow(edge(handles.Icurrent,'canny'));
% Ifill = mat2gray(entropyfilt(handles.Icurrent));
% imshow(Ifill,'Parent',handles.ImageAxes);

Ifill = imfill(handles.Icurrent,'holes');
imshow(Ifill,'Parent',handles.ImageAxes);
handles.boundaries = bwboundaries(Ifill);
DrawBoundries(handles)
handles.Icurrent = Ifill;
```

```
guidata(hObject,handles);


% --- Executes on button press in NoiseButton.
function NoiseButton_Callback(hObject, eventdata, handles)
Inoise = wiener2(handles.Icurrent, [5 5]);
imshow(Inoise,'Parent',handles.ImageAxes);
handles.Icurrent = Inoise;
guidata(hObject,handles);


function AreaTolerance_Callback(hObject, eventdata, handles)


% --- Executes during object creation, after setting all properties.
function AreaTolerance_CreateFcn(hObject, eventdata, handles)
if ispc && isequal(get(hObject,'BackgroundColor'),
get(0,'defaultUicontrolBackgroundColor'))
    set(hObject,'BackgroundColor','white');
end


% --- Executes on button press in AreaAnalysis.
function AreaAnalysis_Callback(hObject, eventdata, handles)
)
tolerance = str2num(get(handles.AreaTolerance,'String'))/100;
handles.acceptedDiameters = [];
handles.acceptedCount = 0;
%handles.acceptedDiameters(:) = [];
for k=1:size(handles.boundaries)
   b = handles.boundaries{k};
   x = b(:,2);
   y = b(:,1);
   lengthX = max(x)-min(x);
   lengthY = max(y)-min(y);
   radius = (lengthX + lengthY)/4;

   area = polyarea(x,y);
   reverseRadius = sqrt(area/pi());
   circleArea = pi()*radius^2;
   hold on

   maxX = max(x); minX = min(x);
   maxY = max(y); minY = min(y);
   %If the calculated area is within the tolerance from a circle's area
   if ((circleArea * tolerance <= area) && (circleArea * (2-tolerance) >= area))
       handles.acceptedCount = handles.acceptedCount + 1;
       handles.acceptedObjects{handles.acceptedCount,:,1} = y;
       handles.acceptedObjects{handles.acceptedCount,:,2} = x;
       handles.acceptedDiameters(handles.acceptedCount) = reverseRadius*2;
       circle([min(x)+lengthX/2,min(y)+lengthY/2], radius, 1000, 'g');
       rectangle('Position', [minX, minY, maxX-minX, maxY-minY],'FaceColor','g');
   else
       circle([min(x)+lengthX/2,min(y)+lengthY/2], radius, 1000, 'r');
       rectangle('Position', [minX, minY, maxX-minX, maxY-minY],'FaceColor','y');
   end

   circle([min(x)+lengthX/2,min(y)+lengthY/2], reverseRadius, 1000);

   hold off

end

guidata(hObject,handles);

% --- Executes on button press in RedrawBoundries.
function RedrawBoundries_Callback(hObject, eventdata, handles)
DrawBoundries(handles);
```

```
function RatioTolerance_Callback(hObject, eventdata, handles)


% --- Executes during object creation, after setting all properties.
function RatioTolerance_CreateFcn(hObject, eventdata, handles)
if ispc && isequal(get(hObject,'BackgroundColor'),
get(0,'defaultUicontrolBackgroundColor'))
    set(hObject,'BackgroundColor','white');
end


% --- Executes on button press in RatioAnalysis.
function RatioAnalysis_Callback(hObject, eventdata, handles)
tolerance = str2num(get(handles.RatioTolerance,'String'))/100;
handles.acceptedDiameters = [];
handles.acceptedCount = 0;
%handles.acceptedDiameters(:) = [];
for k=1:size(handles.boundaries)
   b = handles.boundaries{k};
   x = b(:,2);
   y = b(:,1);
   maxX = max(x); minX = min(x);
   maxY = max(y); minY = min(y);


   %calculate diameter
   area = polyarea(x,y);
   reverseDiameter = sqrt(area/pi())*2;

   %calculate circumfrence
   circum = length(x)*1.12;

   calculatedPi = circum/reverseDiameter;

   hold on

   %If the calculated area is within the tolerance from a circle's area
   if ((calculatedPi * tolerance <= pi()) && (calculatedPi * (2-tolerance) >= pi()))
       handles.acceptedCount = handles.acceptedCount + 1;
       handles.acceptedObjects{handles.acceptedCount,:,1} = y;
       handles.acceptedObjects{handles.acceptedCount,:,2} = x;
       handles.acceptedDiameters(handles.acceptedCount) = reverseDiameter;
       rectangle('Position', [minX, minY, maxX-minX, maxY-minY],'FaceColor','g');
   else
       rectangle('Position', [minX, minY, maxX-minX, maxY-minY],'FaceColor','y');
   end

   hold off

end
altCalcs(handles);
guidata(hObject,handles);


function SizebarScale_Callback(hObject, eventdata, handles)


% --- Executes during object creation, after setting all properties.
function SizebarScale_CreateFcn(hObject, eventdata, handles)
if ispc && isequal(get(hObject,'BackgroundColor'),
get(0,'defaultUicontrolBackgroundColor'))
    set(hObject,'BackgroundColor','white');
end


% --- Executes on button press in Statistics.
function Statistics_Callback(hObject, eventdata, handles)
```

```
sizebarScale = str2num(get(handles.SizebarScale,'String'));
sizePerPixel = sizebarScale/handles.sizeLength;

%Size the already calculated diameters in terms of the sizebar units, not
%pixels
for k=1:length(handles.acceptedDiameters)
   handles.acceptedDiameters(k) = handles.acceptedDiameters(k) * sizePerPixel;
end
set(handles.dN, 'String', num2str(mean(handles.acceptedDiameters)));
set(handles.objectsCounted, 'String', num2str(length(handles.acceptedDiameters)));
figure;
hist(handles.acceptedDiameters,75);

cd(handles.RecentPath)
csvwrite(strrep(handles.FileName,'.jpg','.csv'),(handles.acceptedDiameters)');
cd(handles.HomePath)



function dN_Callback(hObject, eventdata, handles)


% --- Executes during object creation, after setting all properties.
function dN_CreateFcn(hObject, eventdata, handles)
if ispc && isequal(get(hObject,'BackgroundColor'),
get(0,'defaultUicontrolBackgroundColor'))
    set(hObject,'BackgroundColor','white');
end


function objectsCounted_Callback(hObject, eventdata, handles)

function objectsCounted_CreateFcn(hObject, eventdata, handles)
if ispc && isequal(get(hObject,'BackgroundColor'),
get(0,'defaultUicontrolBackgroundColor'))
    set(hObject,'BackgroundColor','white');
end
```

B.4 Statistics

B.4.1 Description and Purpose

An additional, non-GUI program, Statistics, was created during the course of study to calculate the values of each factorial effect and develop every plot used in this thesis. While not explored in depth due to its limited user input and statistical focus, it is worth mentioning due to its high-level code design. The factorial analysis and plotting utilized in this study can be applied to any dataset with only limited modifications to the current code base. This tool will prove useful to others when analyzing full-factorial experiments of any size and power.

Appendix C. Standard Operation Manuals

C.1 Gel Permeation Chromatography Manual……. 178
C.2 Solid-State Shear Pulverizer Manual…… 185
C.3 Ultraviolet Spectraphotometry (UV-Spec) …….. 194

Several new pieces of equipment where utilized which were not previously documented in the Polymer Hybrid Nanotechnology Research Group Archive. This section is a collection of standard operations manuals which were created to accelerate the adoption of these technologies to future members of the research group. Unless otherwise noted, a user should be able to operate the equipment with only the manual for assistance.

C.1 Gel Permeation Chromatography Manual

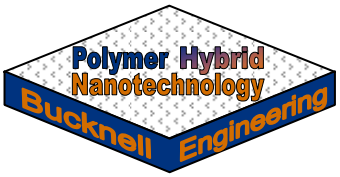

Equipment Manual: Gel Permeation Chromatography (GPC)

Ver 1.0 (03/2010) Marc Henry

Basic Information

Location: Dana 239A (Analytical Lab)

Equipment:
Hewlett-Packard 1090 Liquid Chromatograph
Linear UVIS-205 Ultraviolet Absorbance Detector
Wyatt miniDAWN Treos
Hewlett-Packard 1037A Refractive Index Detector

Tools and Materials:

Sample Preparation:
- 2× 20 mL foil-topped disposable vials
- 6 mL disposable syringe (no rubber stopper)
- Whatman Anotop 25 0.02 µm Filter
- 5 mL glass pipette and bulb

Running GPC:
- 250 µL glass syringe

Refilling THF Reservoir:
- 1 L Nuclepore vacuum Earlenmyer flask
- Nuclepore attachment
- Nuclepore Reservoir
- Nuclepore Clamp
- Gelman Sciences Polypropylene 0.2 µm Membrane Filter
- Vacuum tube
- Ring stand

Procedure

Sample Preparation:

1. Measure 0.01-0.05 g of sample into a disposable vial on an analytical balance. Record actual mass.
2. Pipette 10 mL of fresh THF into vial, cap, and shake until sample is fully dissolved. This may require heating or extended agitation.

   Note: Be sure to use a glass pipette when transferring THF. Disposable polystyrene pipets will dissolve, contaminating

the sample and the bulk THF!

3. Use disposable syringe to remove solution from vial, attach Whatman filter onto the syringe, and filter into the second sample vial. Remove the filter and repeat until all fluid has been filtered and transferred. Cap filtered vial.
4. Label top of vial with sample information and concentration! (1-5 mg/mL)

Equipment Preparation:

1. Ensure GPC pumps have been running (on Recycle) for at least an hour before starting equipment preparations. If GPC is off contact Diane Hall.
2. Check THF reservoir (Reservoir B) to make sure there is sufficient THF for your runs. If less than a quarter full, see "Refilling the THF Reservoir" section.
3. Check to make sure network cable (has a label tape flag) is connected to Dell computer to right of GPC.
4. Log onto the Dell computer. Turn on the monitor to the old, IBM computer.
5. Once logged-in, disconnect the network cable from the Dell computer.

   Note: You will lose access to the internet and network! Be sure to save any files you will need during GPC onto the local hard drive.
6. On GPC, turn Pumps off.
7. On IBM computer, click on the middle drop-down menu (which should currently read "GPCRECYC.M") and select "GPCWTHF.M".

   → Ensure that under "LC1090 Status", B is set to 100% while A and C are at 0%.
8. Change tubing on Outlet of the RI Detector from metal recycle mode tube to polypropylene GPC Run mode tube.
9. On other side of island, open helium gas tank and open cap seal on the THF waste jar. Open the jar by hold onto the cap and rotating the jar itself as to not break the silicone seal. Leave cap on jar to waste THF drips inside.
10. Turn GPC Pumps on.
11. Optional – Injecting a high-concentration (~10 mg/mL) PS solution after turning on the fresh THF flow can help bring detectors to steady state slightly quicker. See steps #-# under "Running GPC" for injection instructions.
12. Check the Wavelength (λ) on the UV Detector is set to the correct setting for your sample: Styrenes and generic polymers – 245 nm, Pyrene-labeled polymers – 343 nm, Ester-bond containing polymers – 224 nm. To change wavelength, push the down arrow twice, then

use the left/right arrows and +/- buttons to change. Press Enter, then Status.

→ To find maximum absorbance wavelength for your sample, obtain a UV spectra of your sample using the SpectraMax M5 UV-Spectrophotometer in Dana 141.

13. On RI Detector, quickly switch the Reference Valve lever from Measurement to Flush. Count to ten. Quickly return lever to Measurement. RI signal on miniDAWN (blue line) should have fallen dramatically.
14. Start ASTRA software on Dell computer. Click File→New→Experiment from template. Select "Bucknell online UV-LS-RI-PS-THF". Push the "Run Experiment" button at the top of the screen and click OK on the popup window.
15. Allow RI and UV detectors to stabilize over a period of 20-35 minutes. See Figure 50 for a reference to stable and unstable detector slopes.

Running GPC:

1. Once detector signals have stabilized, on the Dell computer click the "Stop Experiment" button at the top of the screen. This data can be discarded without saving.
2. Open a new experiment file using the same template. Push the "Run Experiment" button, but do **not** click OK on the popup yet.
3. Rinse the 250 µL glass syringe two times with your sample solution. Discard the waste.
4. Pull 75-125 µL of your sample into syringe. Hold tip vertical and flick until the air bubble dislodges and travels up to the needle. Stick needle under a paper towel and push plunger slightly to remove bubble from syringe.
5. Place syringe into Injection Loop port and quickly rotate lever from "Inject" to "Load". Push in syringe plunger. You should see fluid dripping into the waste vial to the right.
6. Stand in front of the detectors with your left hand on the GPC Injection Loop lever and right hand above the Dell computer keyboard. Simultaneously rotate the lever from "Load" to "Inject" while hitting the space bar to start data collection. Blue, green, and red dots should appear in the ASTRA software, indicating data collection.
7. A typical GPC run with two PL-gel columns takes 20 minutes. Go find something productive to do for this time.
8. Either right before or following the atmospheric contaminate peaks elude (see Figure 51), press the "Stop Experiment" button.
9. Save the raw data to the C:/Light Scattering Experiments/Student Data/ folder on the local hard drive.

10. Repeat with any additional samples.

Exporting Data:

1. If not open already, open the ASTRA software and load a previously run experiment you would like to analyze.
2. In left frame, double click on “Basic Collection” under “Procedure”. Click on the “Run Experiment” button at the top of the screen.
3. In the left frame, double click on “Baselines”. Go through each detector signal (using the checkboxes above the graph) and drag the baseline points to make a straight line between the bottoms of your desired peak(s). Click “OK” at the bottom of the screen when complete.
4. In the left frame, double click on “Peaks”. Press the Delete key to clear the automatically placed peak region. Double click on the graph. Click on the “Export” tab at the top of the window which appears. Click on the “Data” sub-tab. Select the “Excel” radio button and click “Save”.
5. Save and close the experiment. Repeat as needed.
6. Reconnect the network cable to the Dell computer

   Note: Once you connect the network cable, you will lose communications to the detectors! Do not reconnect the cable until all experiments have been completed.
7. Transfer the .vaf experiment files and .xls data files to the /RESEARCH/ folder.

Shutting GPC Down:

1. Ensure the negative contaminates peaks from the last run have eluded through the detectors.
2. Turn off GPC pumps.
3. On the IBM computer, click on Run→Stop Injection/Run Sequence.
4. Change the tubing on the outlet of the RI Detector from the polypropylene waste tube to the metallic recycle tube.

   Note: The waste tube will drain when the seal is broken at the RI output. Be sure to wear gloves and have a napkin handy.
5. On the IBM computer, change the middle drop-down menu from “GPCWTHF.M” to “GPCRECYC.M”.
6. Wait for the “LC1090 Status” to change to A-0% B-0% C-100%.
7. Turn GPC pumps on.
8. On other side of the island, close helium tank and close cap on the waste THF jar by holding the cap and twisting the jar.
9. Turn off monitor of IBM computer. Log off Dell computer.

Data Analysis:

1. Open the GPC-SEC Analysis MATLAB program (GPCAnalyser.m)
2. Input the mobile phase flow rate used (default: 1.0 mL/min) and check the signals that you would like to see plotted.

3. Click on the Load Data button and open the .xls file exported from the ASTRA software.
4. Select the detector you would like to use for molecular weight calculations and check to make sure the calibration coefficients are correct for the GPC column configuration used.
5. Turn on Zoom Mode and focus onto your desired peak(s).
6. Click the Define New Peak button and click on the two points which represent the beginning and end of the desired peak.
7. Continue re-zooming and defining peaks until all desired peaks are analyzed.
8. Go through defined peaks using the Peak Number drop down menu and copy desired values to Excel. For quick copying of all data, copy the contents of the CopyBox and paste into Excel, which has an import function to split comma separated values into columns.

Refilling the THF Reservoir:

1. If you haven't refilled the reservoir before, contact someone who has or Diane Hall first for a personal walk-through.
2. Assemble the glassware in a hood as seen in Figure 52. Remember to place a polypropylene filter between the Nuclepore attachment and reservoir.
3. Turn on low vacuum to apparatus.
4. Pour THF into Nuclepore reservoir and allow to drain. Try to estimate how much solvent is needed.
5. Turn off vacuum and disassemble glassware. Let sit in hood to remove any residual solvent.
6. Ensure that GPC pumps are currently drawing from Reservoir C or are off.
7. At GPC, hold bottom of Reservoir B and pull the black lever out. Remove reservoir while taking care not to excessively bend the pump tubes.
8. Fill Reservoir B in the hood and replace. Slide pump tubes back into reservoir, and visually confirm good contact between the top of the glass and the gasket. Push black lever in to secure reservoir in place.
9. Replace Nuclepore glassware to proper drawer.

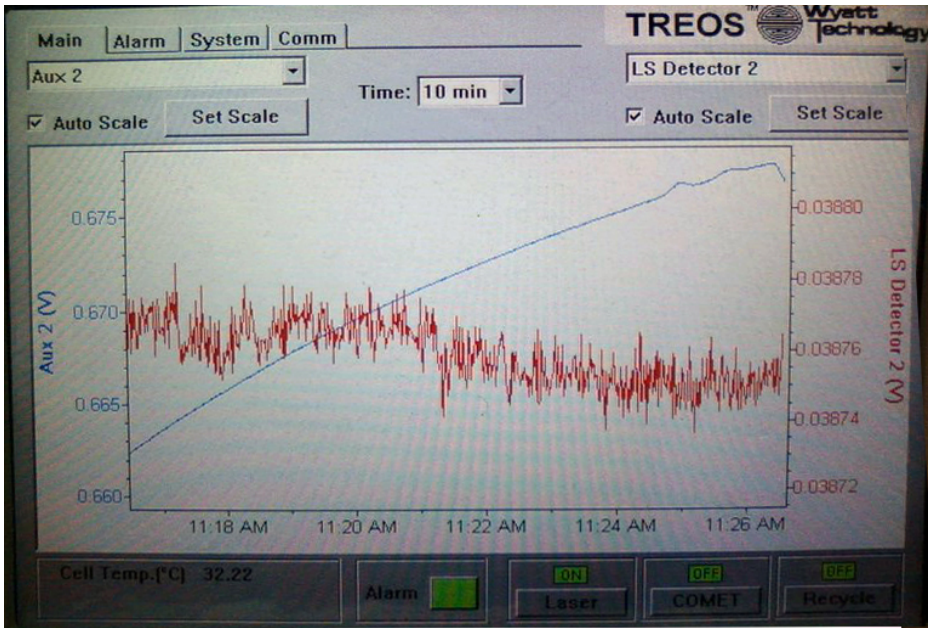

Figure 50. Screen of the miniDAWN. Note the slope of the blue line on the left compared to the middle-to-right. The left slope is not yet stabilized, while the nearly linear slope on the right has stabilized (disregard the peaks). Similar slopes can be seen in the ASTRA software window.

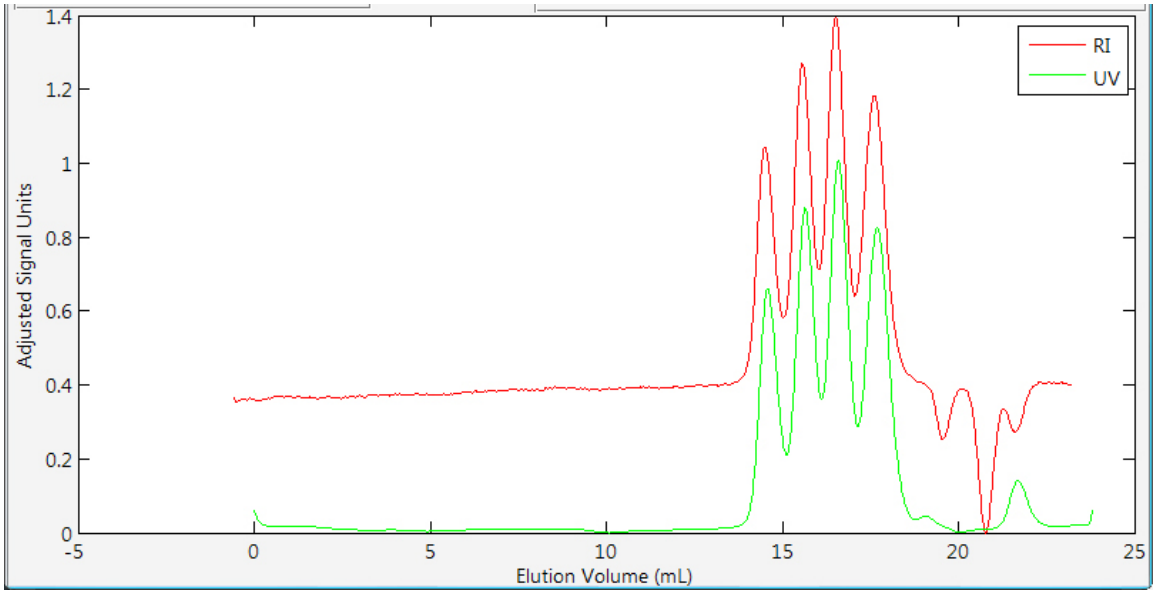

Figure 51. Example GPC run with a four-species standard solution. Note that the three negative peaks shown ~20 minutes are atmospheric contaminates (water, gases, etc) and indicate the end of the run.

Figure 52. The assembled and secured Nuclepore HPLC solvent filtering apparatus.

C.2 Solid-State Shear Pulverizer Manual

Equipment Manual: Solid-State Shear Pulverizer

Ver. 1.0 (11/2009) Marc Henry
Ver. 1.1 (03/2010) Marc Henry

Contents

Basic Information 185
Screw Design Considerations 185
Changing Screw Design 186
Startup Preparation 187
Startup and Sample Collection 188
Shutdown and Cleaning 189
Recovering from a Melt During SSSP 190
Troubleshooting 191

Basic Information

Location: Breakiron B64

Equipment: Berstorff ZE 25A x 34D UTX
Budzar BWA-AC-10 Chiller

Tools and Materials:
- Air gun
- Brass tools
- Metric Allen wrenches (#2,8)
- Rubber mallet
- Gladware trays or metal bowls for sample collection

Safety Equipment
- Safety Glasses
- Earplugs
- Mask

Screw Design Considerations

General: 1. The larger 31.25 mm screw elements should be used in the Feed and

Zone 1 regions to fracture the large pellets into smaller particles. A transition (Mx) element should **always** be placed following the 31.25 mm elements when transitioning to 25 mm elements.

2. Kneading blocks should not be placed in the first or last 12.5 mm of any Zone. These areas are parts of the zone unions and are not in immediate contact with coolant. Placing a kneading block within these regions will result in excessive heat generation.
3. The open-barrel section of Zone 5 is not in direct contact with coolant. Avoid placing kneading blocks within this section.
4. The presence of reverse-driving kneading blocks has been shown to: increase zone temperature by ~5ºC compared to a neutral kneading block, not significantly alter M_n, significantly reduce M_w by ~1,250 g/mol, and significantly decrease the static growth coefficient in polymer blends.
5. Distributing kneading blocks between conveying elements has been shown not to decrease operating temperature or significantly alter the: M_n, M_w, or average dispersed domain of blends.

<u>Changing Screw Design</u>

Tools and Materials:

- Air gun
- Brass tools
- 10 mm wrench
- Rubber mallet
- Desk vice (with brass attachments)
- Bolt gripper (if dissembling TSE screws)
- Anti-seize paste
- Loose element cart

Procedure:

1. Print out most recent screw design list from /RESEARCH/MANUALS AND CALIBRATIONS/SSSP Screw Designs/
2. Use vice and wrench/bold gripper to loosen the bolt at the end of the screw.
3. Dissemble one screw at a time, placing elements on the rods of the loose element cart.

   **Note: If elements have become stuck due to molten polymer penetration, use vice, brass tools, and rubber hammer to force element down screw core. Afterwards, be sure to re-apply anti-seize paste.*
4. When assembling a new screw, elements should freely slide up and down the screw core. If not, add anti-seize paste at the top and slide an element down and up to spread evenly.
5. Screw elements DO have a proper direction! There is an ‘R’ stamped on the down-barrel side of each element. Ensure that each element is

placed with the R facing down the barrel. See Figure 53.

6. Always leave one element at the tip of the screw to ensure elements are added positioned correctly.
7. When fully assembled, use vice to fully tighten end bolt.
   **Note: Failure to tighten end bolt sufficiently will lead to polymer penetrating between and under elements should a melt be created*
8. When both screws are assembled, roll together across a flat surface to ensure proper element placement and positioning.
9. Insert screws into end of SSSP barrel, taking care not to be pinched. The penultimate screw element should align with the end of the sixth barrel zone
10. Screw in the set screws in the screw-gearbox unions. (Metric #2 Allen wrench)

<u>Startup Preparation</u>:

Procedure:

5. Turn on room ventilation system (by door).
6. Turn on SSSP via breaker on controller's side of the machine.
   **Note: Buzzer will sound. Simply push "Silence Alarm" once software loads*
7. On Chiller, ensure "Pump" and "Compressor" toggles are off and then turn the red power switch clockwise to "ON".
8. Set Chiller's setpoint using electronic controller (hold top left button while increasing/decreasing using the arrows) to 25ºF.
9. Turn on "Pump" toggle and then "Compressor" toggle.
10. Allow Chiller to cool working fluid to 25ºF before changing setpoint to operating temperature (typically 11ºF).
    **Note: Failure to do so will result in Low Pressure Alarm being tripped*
11. On SSSP, open "Recipe" menu. Triple press the Recipe Title box in upper left of screen (says "Product 1" by default) and select "SSSP" from the dropdown list that appears. Push the "Restore" button. Push the "Accept Recipe" button.
12. Open "Layout" menu. Ensure all Zone setpoints (in yellow) are at 1ºF. On right of screen, push "Master Heat" to turn on coolant.
    **Note: Allow SSSP to cool to desired operating temperature. Initial cooling typically takes ~30 minutes.*
13. Ensure proper screw design is installed. If changing screw design, see *Changing Screw Design* (p. 2). If screws are already installed and bearing zone segment attached, skip to *Startup and Sample Collection* (p. 188).
14. Make sure screw-side set screws on gearbox unions are unscrewed (metric Allen #2)
15. Slide screws down barrels. May have to rotate screws slightly to align teeth to enter gearbox unions. Screws should insert as far as the second to last screw element.

**Note: If screws give resistance when trying to insert into barrels check to make sure all screw elements are properly aligned and there is no residual polymer blocking barrel or on screws*

16. Screw in gearbox union set screws (metric Allen #2).
17. Attach the ball bearing zone. When attaching zone clamps, take care holding the bottom one in place, it is heavy and apt to fall. There should be one convex and one concave washer on both sides of the two tightening screws. When tightening, try to ensure open space between the clamps is even on both sides (metric Allen #8).
18. Rotate screws manually (via clutch) at least one rotation to be sure screws are properly installed and drive will not disengage due to high initial torque.
19. Allow screws to cool inside SSSP prior to initiating run.

<u>Startup and Sample Collection</u>

Equipment: Brabender DS28-10 Pellet Feeder
Brabender DD-SR12-1 Powder Feeder
Team Grande Sacs Ultra-Low-Rate Powder Feeder

Tools and Materials:
- Gladware trays or metal bowls
- Stopwatch

Procedure:

1. Ensure screws are properly inserted, bearing zone attached, and set screws are tightened. (See Startup Preparation)
2. On SSSP, open "Extruder Main Control" menu and ensure that the RPM Setpoint is 0.
3. Pull green "Start/Stop" button to start drive.
4. In increments of ~75 RPM, bring drive up to desired speed.
5. Start feeders at desired feed rate. See individual feeder calibrations for settings.

   **Note: SSSP will squeak slightly for a few seconds following starting pellet feeder*

6. While SSSP reaches steady state (~10-15 min) watch temperature trends to ensure no zone melting. To see trends: Open "Trends" menu, selecting Zones 2-9. Double click the legend on left of screen. Switch the green "On" fields for Zones 9-7 to a red "Off". "Accept/OK". Double click on the vertical axis labels. Select all Pens to be drawn on the same axis, and to Auto-scale Axis. "Accept/OK". Graph should now be legible and properly scaled.

   **Note: Zone 2 should have the highest temperature, followed by Zone 6 and/or any zones with reverse-driving elements. Melting can be detected by a rapid, convex increase in zone temperature. Also, product will appear rough and jagged instead of powdery upon melt. Initial product will appear course.*

7. When temperatures equilibrate and reach steady state, use stopwatch

to confirm feed rate.

8. Complete SSSP Log Sheet detailing temperatures, operating conditions, and observations.

   **Note: Keep an eye on the Trends temperatures, as a sinusoidal temperature pattern will develop upon steady state. This action has been shown to grow/induce melts over long run times.*

Shutdown and Cleaning

Tools and Materials:

- Air gun
- Brass tools
- Metric Allen wrenches (#2,8)
- Rubber hammer
- Copper mesh-wrapped rod
- Brass brushes

Procedure:

1. Stop feeding polymer pellets and powder.
2. Wait for product to stop exiting the barrel.
3. Slow drive down to 100 RPM or lower, watching the set screws on the gearbox unions rotate. Push the green "Start/Stop" button just before the set screws are visible to stop the drive and position the set screws for easy access.
4. Unscrew set screws on screw side. Remove ball bearing zone (will need brass tools to separate zone clamps). Grab end of screws and pull with entire body. Screws should slide out easily. If not, see Recovering from a Melt During SSSP (p. 190).
5. Change "Recipe" from "SSSP" to "Dry Cycle". As ice buildup melts, use air gun to blow pooling water off zones and coolant lines.
6. On Chiller, turn off "Compressor" and "Pump" toggles and then turn red power switch to "OFF".
7. Use air gun to blow most polymer residues from screws. Use brass brushes on any melted or stuck pieces.
8. Blow air gun down barrel starting from the beginning of the barrel (through the bearing holes at the gearbox unions), then the feed hopper, then finally down the barrel from the end.

   **Note: Be sure no one is standing in front of the barrel when blowing air down it. Loose powder and pellets exit with significant velocity.*

9. Take copper mesh-covered rod, hold the mesh at the end, and insert into barrel. Scrub barrel walls to remove any melted polymer. Blow with air gun again.
10. Unscrew barrel on pellet feeder and pour excess pellets into storage bag.
11. Clean powder feeders, if used.
12. When barrel segments are dry, use SSSP power breaker to turn

machine off.

Recovering from a Melt During SSSP

Tools and Materials:

- Air gun
- Brass tools
- Metric Allen wrenches (#2,8)
- Rubber hammer
- Copper mesh-wrapped rod
- Shop vacuum

Decision Time: You will most likely have to shut down, remove, and clean the screws in order to recover from a melt. In some instances, melts have been overcome while remaining on-line, but the recovery process was initiated moments after the melt started by watching the temperature trends. If the melt has affected product already: it's too late, skip to Shutdown Melt Recovery section. If zone temperatures just started elevating, you can try Online Melt Recovery.

Shutdown Melt Recovery:

1. Stop feeding polymer pellets and powder.
2. Wait for product to stop exiting the barrel.
3. On the "Extruder Layout" menu, use the "Loop On/Off" button to turn off coolant to the zone in question.
4. Slow the drive and then stop the drive so that the set screws are accessible. Take note that as the screws slow, the melted section of the barrel will cool rapidly, form a plug, and then pop the clutch. This is not desirable as you won't be able to control where the set screws are. If you stop the drive and the set screws are not accessible, quickly re-start the drive and raise the RPMs very high.
5. If you successfully stopped the drive with the set screws accessible, skip to next number. If set screws are not accessible and the clutch has popped/screws seized, manually rock clutch in clockwise (reverse) direction. It will take about 15 minutes of hard rocking to move set screws into accessible region. If screws cannot be rotated to gain access to set screws, set melted and/or all zones to 400ºF and heat barrel. When heated, clutch can be re-engaged and motor can be used to rotate screws to proper position.
6. Unscrew set screws on screw side. Remove ball bearing zone (will need brass tools to separate zone clamps). Grab end of screws, place foot on the white base of the SSSP to the right of barrel, tighten arms, and then use legs/body to pull screws out. Screws will likely get stuck, so take rubber hammer, hit screws back in ~2 inches, and then repeat.
7. Use brass tools to chop melted polymer off of screws, vacuum any extra powder or pellets off of screw's initial and final zones.

8. Re-insert screws into SSSP, allowing warm segments to cool before re-starting.
9. Re-start coolant flow to melted zones.
10. Bring drive up to speed, and start feeding pellets/powder.
11. Watch the temperature trends! The screws will be at elevated temperatures and more apt for additional melting.

Online Melt Recovery:

1. Stop feeding polymer pellets and powder.
2. Lower RPM to 250-300. Carefully watch Temperature Trends. The goal of the Online Melt Recovery is to bring the small amount of melted polymer very close to its glass transition temperature (without it solidifying and seizing the screw) and then flood the extruder with lots of fresh polymer. When melted zone appears to be getting close to its critical temperature, raise RPMs to 450 and restart pellet feeder.
3. Continue switching between low and high RPMs to try to just start creating a plug and then raising the RPMs to remove the material from the screw surface.
4. If you can lower the zone temperature to below its transition temperature, congratulations, you've recovered from the melt. Note that the screws are still at elevated temperatures and will be much more susceptible to melts until fully cooled again. If not, move on to the Shutdown Melt Recovery.

Troubleshooting

Drive Clutch Disengages:

1. Solve problem which generated enough torque to disengage clutch.
2. Re-align clutch using either blue/red lines or finding the one larger "tooth".
3. Insert red clutch engagement tool on either side of disengaged clutch and pull back towards drive. Clutch will click when re-engaged. If clutch does not re-engage, check alignment or try rotating the engagement tool 180º.

SSSP is Squeaking Loudly:

1. Ensure set screws are properly inserted and tightened
2. Screw rotation speed is too great and melting/degrading polymer pellets upon insertion. Reduce RPM.
3. Screw elements have been placed on the screw shafts facing the wrong direction. Stop the SSSP and re-assemble each screw to ensure proper alignment.

Chiller "Low Pressure

1. Turn off "Pump" and "Compressor" toggle switches.
2. Turn red power switch to "OFF".
3. Allow three to five minutes to pass for refrigerant temperature to rise.

Alarm" Goes Off

4. Open lower access panel on Chiller.
5. See Figure 54. While avoiding the hot refrigerant line, reach into the machine towards the front of the low pressure transducer and push the reset switch. It should click once and not click upon repeated pushes. If it continues to click, refrigerant temperature is still too low, wait longer.
6. Raise Chiller set point temperature.

   **Note: Did you remember to set the set point to 25ºF for the initial cool-down?*

SSSP Continues to Form a Melt

1. Reduce pellet feed rate. Lower feed rates have been shown to reduce operating temperatures.
2. Increase RPM. Increased screw rotation rates have been shown to reduce operating temperatures.
3. Alter screw design. Remove any reverse-driving kneading elements. Then remove any neutral-driving kneading elements.

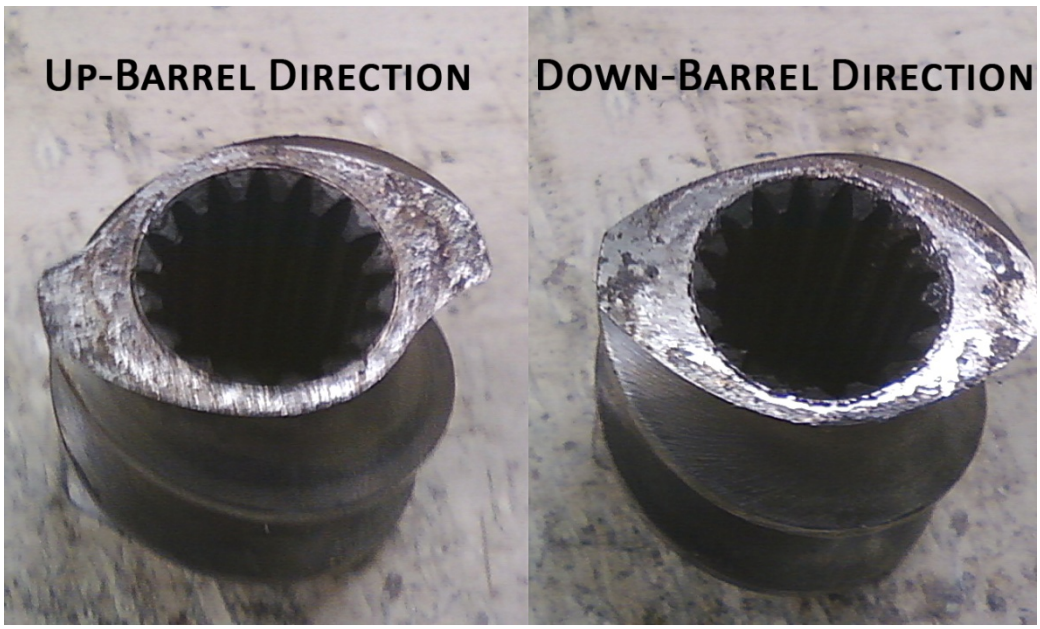

Figure 53. Example of how screw elements have proper up- and down-barrel directions. This is the transition conveying element. Note the difference in channel flights.

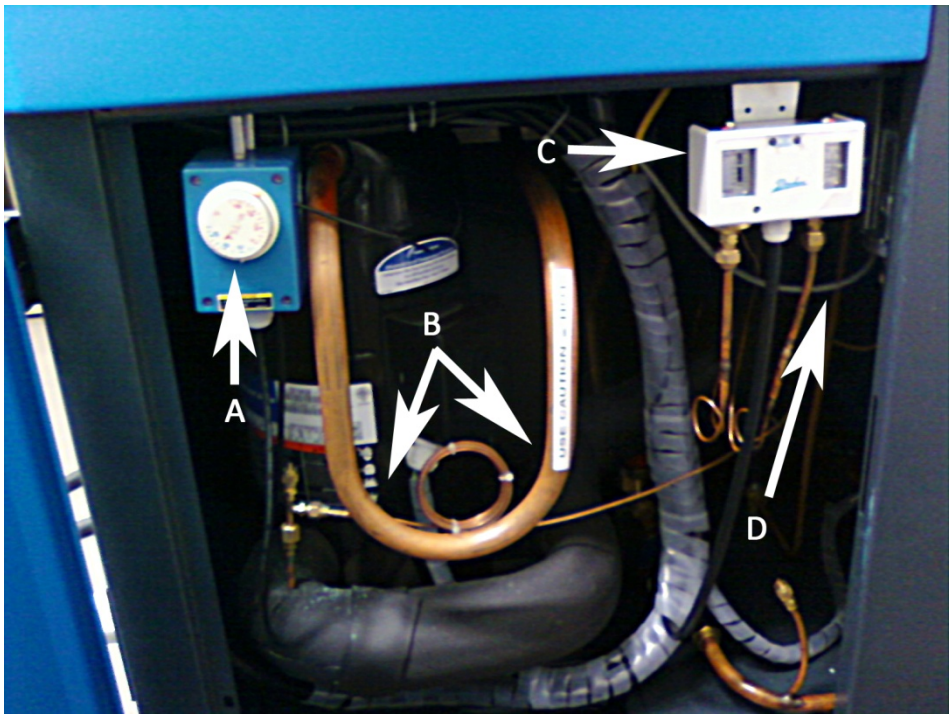

Figure 54. Internals of the lower Chiller access door. A – Emergency temperature shut-off. B – Refrigerant out of compressor to radiator. VERY HOT! USE CAUTION! C – High refrigerant pressure alarm. D – Reach back into here to find the silver Low refrigerant pressure alarm box and reset button.

C.3 Ultraviolet Spectraphotometry (UV-Spec)

Equipment Manual: Ultraviolet Spectraphotometry (UV-Spec)

Ver 1.0 (03/2010) Marc Henry

Basic Information

Location: Dana 141

Equipment: Molecular Devices SpectraMax M5

Tools and Materials:
- SpectraMax Cuvettes
- Fresh Solvent

Procedure

Preparation:
1. Create an ultra-low concentration solution of sample (< 1 mg/mL). If a GPC solution has already been made, try diluting an aliquot of it.
2. Turn on SpectraMax M5 and log onto computer. Run the SoftMax Pro 5.2 software on the desktop.
3. If it reads "No Port Selected" under the "File" menu, double click and select "COM1" for the Connection. Click "OK"
4. If multiple samples are being run, click the "Template" button beside the "CuvetteSet#1" section of the window. Click in the A1 box and drag to the right to make a block for each sample. Click the "Assign" button and then "OK".
5. Click the "Settings" button beside the "CuvetteSet#1" section of the window. Click on the "Spectrum" image on the top of the new window. Then enter the desired span of wavelengths to scan. As starting point, scan from 200-400 nm with a step of 5 nm.

Generating Spectra:
1. Once the M5 has booted, push the black "Drawer" button on the machine to close the side sample drawer.
2. Fill a cuvette about half full with fresh solvent for a reference. Open the hinge to the right of the black "Drawer" button and insert reference cuvette into the slot. The clear faces should point East/West

while the frosted faces point North/South.

Note: Always handle cuvettes with gloves on and only handle using the frosted sides. Wipe cuvettes down with a Kimwipe prior to inserting into the M5.

3. On computer, click on the "A1" box under the "CuvetteSet#1" section to highlight it. Then click on the "Ref." button at the top of the screen. The M5 will start determining the baseline absorbance of the solvent.
4. Once the reference reading is complete, remove the reference cuvette and replace it with one containing the sample. Click on the "A1" box again and then the "Read" button at the top of the screen. Double-clicking on the A1 box will allow spectra to be seen as it is generated.

   Note: If spectra does not seem to appear, click on the "Scale to Data" button. If Absorbance signals above 1.0 are obtained, the sample is too concentrated. Add more solvent.
5. If there are multiple samples, click on "A2" and repeat procedure.
6. Export data for further analysis via "File→Import/Export→Export…"